SYNTHESIS AND STUDY OF SULFONAMIDE CONTAINING ORGANOMETALLIC COMPLEXES AS INHIBITORS FOR INFECTIOUS DISEASES

By

Timothy John Kotzé

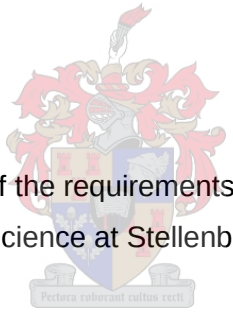

Thesis presented in partial fulfilment of the requirements for the degree of Master of Science in the Faculty of Science at Stellenbosch University.

Supervisor: Dr Prinessa Chellan

Co-supervisor: Prof Gregory S. Smith

December 2019

Declaration

By submitting this thesis electronically, I declare that the entirety of the work contained therein is my own, original work, that I am the sole author thereof (save to the extent explicitly otherwise stated), that reproduction and publication thereof by Stellenbosch University will not infringe any third party rights and that I have not previously in its entirety or in part submitted it for obtaining any qualification.

Timothy John Kotzé December 2019

Abstract

Six imino sulfadoxine derivatised iridium complexes (**C1** - **C6**), previously synthesized in literature, were investigated for drug like character by accessing their aqueous solubility through a turbidimetric assay and probing the potential active species by means of aquation experiments. The complexes **C3**, **C5** and **C6** had solubilities ranging between 20 µM and 160 µM, while **C1**, **C2** and **C4** had solubilities greater than 160 µM. Solubility was found to decrease with increasing addition of hydrophobic groups to the half-sandwich moiety coordinating via a centroidal bond to the iridium metal centre. Ease of hydrolysis of the chlorido ligand was found to decrease as the steric bulk around the metal centre was increased to the point that the chlorido of **C3** remained in-tact under mild conditions in the presence of silver nitrate. This likely means the active species is the, as synthesized, chlorido complex. New synthetic methods were developed for the synthesis of the Schiff base ligands of these complexes to achieve a more efficient synthesis and obtain pure samples for testing. Though pure samples were not obtained, the efficiency of the synthesis was improved.

Six new amido sulfadoxine derivatised iridium complexes (**C7** – **C12**), were synthesized in moderate to good yields of 56% – 84% as yellow powders. Their ligands were synthesized through in situ generation of an acid chloride and subsequent quenching with sulfadoxine. A crystal structure was obtained for the pyridyl amido sulfadoxine ligand which crystallised in the triclinic, $P\bar{1}$, space group as transparent needle like crystals. The drug-like character was also investigated for this series of complexes and their solubilities of **C9**, **C11** and **C12** were between 20 µM and 60 µM, while **C7**, **C8** and **C10** were greater than 160 µM. The same results were obtained for the aquation experiments as for **C1** – **C6**.

All complexes were tested against *Mycobacterium tuberculosis* (*Mtb*) strain H37Rv and *Plasmodium falciparum* strains, 3D7, Dd2 and HB3. Complex **C6** was only tested against *Mtb*. The imino complexes were more active in general, with a MIC_{90} of 2.78 µM for **C6** against strain H37Rv after 7 days and an IC_{50} of 13.8 µM for **C5** against strain 3D7. Although the amido complexes exhibited promising activity against *P. falciparum* with **C12** having an IC_{50} of 0.975 µM against strain 3D7 and IC_{50} of 0.766 µM against multidrug resistant strain Dd2. The activity was generally seen to increase as the solubility decreased with the addition of hydrophobic groups to the complexes.

Opsomming

Ses imino sulfadoksien-afgeleide iridium komplekse (**C1** - **C6**), wat voorheen in die literatuur gesintetiseer is, is ondersoek vir dwelmagtige karakter deur hul wateroplosbaarheid deur middel van 'n turbidimetriese toetsing te verkry, sowel as die potensiële aktiewe spesie deur middel van hidrolise van die chloriedligand te ondersoek. Die komplekse **C3**, **C5** en **C6** het oplosbaarheid tussen 20 µM en 160 µM getoon, terwyl **C1**, **C2** en **C4** oplosbaarheid groter as 160 µM getoon het. Oplosbaarheid is gevind om af te neem met toevoeging van hidrofobiese groepe tot die 'half-sandwich' groep wat koördineer *via* 'n sentroïedebinding na die iridium metaal sentrum. Die gemak waarmee die chloriedligand gehidroliseer het, het afgeneem soos die steriese massa rondom die metaalsentrum verhoog is tot en met die punt dat die chloriedligand van **C3** onder matige toestande in die teenwoordigheid van silwernitraat onverander gebly het. Dit beteken waarskynlik dat die aktiewe spesie die onveranderde chloriedkompleks is. Nuwe sintetiese metodes is ontwikkel vir die sintese van die Schiff-basisligande van hierdie komplekse om 'n meer doeltreffende sintese te ontdek en suiwer monsters vir biologiese toetse te verkry. Alhoewel suiwer monsters nie verkry is nie, is die doeltreffendheid van die sintese verbeter.

'n Tweede stel van ses amido sulfadoksien afgeleide iridium komplekse (**C7** - **C12**), wat nie voorheen gemaak is nie, is met goeie opbrengste van 56% - 84% as geel poeiers gesintetiseer. Hul ligande is gesintetiseer deur *in situ* generasie van 'n suurchloried en daaropvolgende substitusie met sulfadoksien. 'n Kristalstruktuur is verkry vir die piridielamido-sulfadoksienligand wat in die $P\overline{1}$ ruimtegroep as deursigtige naaldagtige kristalle gekristalliseer het. Die dwelmagtige karakter is ook ondersoek vir hierdie reeks komplekse en die oplosbaarheid van **C9**, **C11** en **C12** was tussen 20 µM en 60 µM, terwyl **C7**, **C8** en **C10** oplosbaarheid groter as 160 µM getoon het. Dieselfde resultate is verkry vir die hidrolise van die chloriedligand van **C7** – **C12** as die van **C1** - **C6**.

Alle komplekse is getoets teen *Mycobacterium tuberculosis* (*Mtb*) stam H37Rv en *Plasmodium falciparum* stamme, 3D7, Dd2 en HB3. Kompleks **C6** is slegs teen *Mtb* getoets. Oor die algemeen was die imino-komplekse meer aktief as die amido komplekse, met 'n MIK_{90} na sewe dae van 2.78 µM vir **C6** teen stam H37Rv en 'n IK_{50} van 13.8 µM vir **C5** teen stam 3D7. Die amido-komplekse het wel belowende aktiwiteit teen *P. falciparum* vertoon met **C12** wat 'n IK_{50} waarde van 0.975 µM teen stam 3D7 en 'n IK_{50} waarde van 0.766 µM teen die multidwelmweerstandige stam Dd2 betoon het. Dit is waargeneem dat die toename van die aktiwiteit oor die algemeen gepaardgaande gegaan het met die afname van die oplosbaarheid, soos wat hidrofobiese groepe aan die komplekse bygevoeg is.

Acknowledgements

Thank you to my supervisor Dr Prinessa Chellan for her time, training and availability throughout my MSc. Thank you also to my co-supervisor, Prof Gregory S. Smith, for his input during the project and the writing of the thesis.

Thanks to Elsa Malherbe and Dr Jaco Brand at CAF for their advice regarding analysis and training on the NMR spectroscopy equipment and software. To Dr Marietjie Stander for the analysis of the ESI-MS data. To Dr Leigh Loots for analysis of the crystals obtained and providing the crystal structure. To Dr Paul Verhoeven for assistance in obtaining the Far-IR spectra. To Dr Katherine De Villiers for the use of her lab and equipment to obtain assay data. To the NRF and Stellenbosch University for funding. To Prof Vicky Avery and Sandra Duffy for testing of the compounds against *Plasmodium falciparum* malarial parasite strains 3D7, Dd2 and HB3. To Prof Digby Warner and Audrey Jordaan for testing of the compounds against the *Mycobacterium tuberculosis* strain H37Rv.

Thank you also to the Group of Medicinal and Organic Chemistry (GOMOC) and the Inorganic Chemistry group in SU for advice and guidance and equipment use in the lab. To the technical staff of the De Beers building, Raymond Willemse, Debora Isaacs, Maxwell Wakens and Noluntu Ntwana for all their assistance. To Luke Hodson and Alet Van der Westhuyzen for their support and advice. To the dark side office and Chellan research group for great discussions and fun times. To my sister Talitha Kotzé, and good friend Andrew Way for being the final proof-readers.

Finally, thank you to all my friends and family, who are too many to mention, for their support, love and prayers along the way. Especially my mother for her all-encompassing love and late father who always wanted to inspire growth, character and faith within us.

Abbreviations and Symbols

3D7	Standard genomic, chloroquine sensitive, *P. falciparum* reference strain
%	Percent
°C	Degrees Celsius
Å	Angstrom
ADMET	Absorption, distribution, metabolism, excretion and toxicity
ADC	Albumin-dextrose-catalase enrichment
ATR	Attenuated total reflection (infrared spectroscopy)
CAS	Casitone
cm^{-1}	Reciprocal centimetres
Cp*	1,2,3,4,5-pentamethylcyclopentadienyl
d	Doublet
DAPI	4',6-Diamidino-2-phenylindole
DCM	Dichloromethane
Dd2	Multidrug resistant *P. falciparum* strain
DFT	Density functional theory
DMF	Dimethylformamide
DMSO	Dimethylsulfoxide
DTA	Differential thermal analysis
ESI	Electro-spray ionisation
EPR	Electron paramagnetic resonance
FTIR	Fourier transform infrared
g	Grams
GLU	Glucose
HB3	Gametocyte forming pyrimethamine resistant and chloroquine sensitive *P. falciparum* strain
HEK	Human epidermal keratinocytes
HEPES	4-(2-Hydroxyethyl)-1-piperazineethane sulfonic acid
HOMO	Highest occupied molecular orbital
H37Rv	Most studied strain of *Mtb*
Hz	Hertz
LUMO	Lowest unoccupied molecular orbital
MCF-7	Breast cancer cell line
$IC/MIC_{50/90}$	Minimum inhibitory concentration of test compound to induce 50%/90% inhibition of cell growth
Mtb	*Mycobacterium tuberculosis*
IR	Infrared

J	Coupling constant
m	Multiplet (NMR)
MDR	Multiple drug resistant
Me	methyl
MHz	Megahertz
mL	Millilitre
mM	Millimolar
MS	Mass spectrometry
m/z	Mass-charge ratio (MS)
NMR	Nuclear magnetic resonance spectroscopy
PBS	Phosphate buffered saline
PPh_3	Triphenylphosphine
ppm	Parts per million
q	Quartet (NMR)
rt	Room temperature
s	Singlet (NMR)
t	Triplet (NMR)
TB	Tuberculosis
THF	Tetrahydrofuran
TG/DTG	Thermogravimetric analysis/differential thermogravimetric analysis
TMS	Tetramethylsilane
Tw	Surfactant tween 80
Tx	Surfactant tyloxapol
UV	Ultraviolet
vis	Visible
WHO	World health organisation
XDR	Extensively drug resistant
XRD	X-ray diffraction
µg	Microgram
µL	Microlitre
µM	Micromolar

Table of Contents

Chapter 1
Tuberculosis, Malaria and Sulfonamide Metal Complexes – A Review

1.1 Introduction

The field of drug discovery has come a long way and developed into an intricate and complicated science requiring multiple steps and a host of information before drug candidates are identified.[1] Vital in the process of drug discovery is the investigation of the various properties of potential drug candidates such as aqueous solubility, cell membrane permeability, and solution stability.[1] These factors end up being nearly as important as the biological activity of the drug when evaluating whether it can be used as an effective treatment. One method of finding drug candidates is to start from known clinical drugs, since it can be beneficial to start with known drugs that have already reached the market, due to the simplification of much of the safety research that is required in later stages of drug development.[1]

Despite the streamlining of drug discovery and the new high throughput screening methods being employed for faster active pharmacophore identification, there is an ever-increasing need for more information and research as drug resistance in treatable diseases continues to rise worldwide.[2–4] As we understand the mechanism of disease better, so we can further research more effective treatments and begin to target both specific and multiple aspects of disease thus limiting the rise of resistance against developed treatments.

This review will focus on the use and discovery of sulfonamides and their metal conjugates as chemotherapeutic agents in medicine with a specific application to *Mycobacterium tuberculosis* and *Plasmodium* parasites.

1.2 Tuberculosis

Tuberculosis is an infectious disease caused by *Mycobacterium tuberculosis (Mtb)* which is a bacterium that most often infects the lungs, although other areas of the body may also be infected. The disease has plagued humanity for many years and its causative agent was first discovered and isolated by German doctor Robert Koch, in 1882.[5,6] It is spread primarily through the air by infected individuals when they either sneeze or cough.

Approximately 23% of the world's population (1.7 billion people) are infected with latent *Mtb*, however only 5% - 10% of these individuals end up developing the disease in their lifetime.[7] Despite this there were still 10 million new active infections worldwide in 2017, of which South Africa contributes a major portion, being one of 8 countries responsible for two thirds of these cases.[7] Decline of infection rates per year are currently close to 2%, which is still far too little. If definitive progress towards the eradication of this epidemic is to be made then this percentage needs to be increased nearly three-

fold.[7] To further illustrate the importance of research in this field it is to be noted that *Mtb* remains one of the top ten causes of death worldwide; this is despite a 42% decrease in mortality rate between 2000 and 2017.[7]

Many of the problems result partly from the resurgence of *Mtb* deaths due to increasing development of drug resistance.[2] Multiple drug resistant *Mtb* (MDR-TB) is defined by the WHO as a strain that is resistant to at least two core drugs prescribed for standard treatment, whereas extensively drug resistant *Mtb* (XDR-TB) is a strain that is resistant to at least four of the core drugs.[7] With the rise of MDR-TB and XDR-TB, treatment has greatly been complicated, with the latest reports showing a success rate of only 55% for MDR-TB and merely 34% for XDR-TB.[7] This becomes an even larger problem in immune compromised individuals such as those suffering from HIV.[7] This is of particular importance in South Africa with its large burden of TB-HIV comorbidity. Much is being done to spread awareness of this problem, for example a documented HIV test result was available for 82% of patients in the African region in 2015.[7] Moreover, drug treatments have been significantly shortened, some from 20 months to 6 months, in the hope of decreasing the incidence of drug resistant strains.[7]

A combination of four antimicrobial drugs (Figure 1.1) are currently recommended for drug sensitive *Mtb* (isoniazid, rifampicin, ethambutol and pyrazinamide) with several second line drugs reserved for MDR and XDR-TB, although these are much more toxic and treatment is required for an extended period.[7]

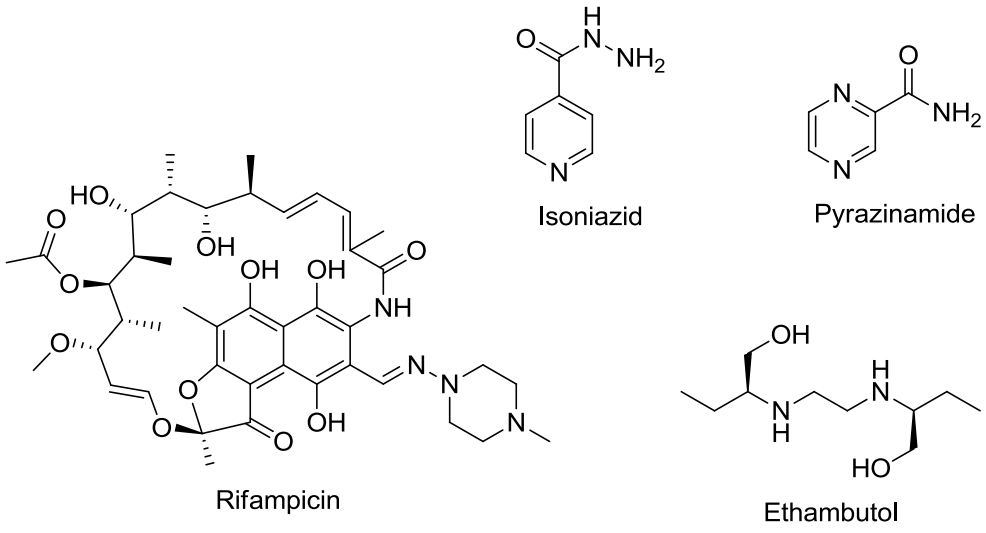

Figure 1.1 - Standard drugs, employed in combination, recommended by the WHO for drug sensitive Mtb.

1.3 Malaria

Plasmodium parasites are the causative agents of malaria, which is a life-threatening infectious disease that is both curable and preventable.[8] The disease is spread by infected female *Anopheles* mosquitoes known as malaria vectors. *P. falciparum* and *P. vivax* are the two species that are the most dangerous, with *P. falciparum* causing 99.7% of all malaria cases in the WHO African Region and most cases in the Eastern Mediterranean, Western Pacific and South-East Asian regions.[8,9]

Although great progress was made in reducing the number of cases worldwide up until 2015, no significant progress has been made since then.[9] Children under the age of five are the most vulnerable group and account for 61% of the 435 000 deaths in 2017, of which 11 countries account for nearly 70% , all but 1 being in Africa.[9]

There are three major stages to the lifecycle of the parasite, namely, the mosquito stage, the blood stage and the liver stage.[10] Considering this, there are several approaches to targeting the parasite and preventing its spread. Firstly, one of the easiest is malaria vector control, which consists of preventing infection by long lasting insecticidal mosquito nets and indoor residual spraying of insecticides.[8,9] These measures are both recommended by the WHO and if applied thoroughly across a wide enough area they can be very effective.[8,9]

Secondly, and by far the most common of targets, is the intraerythrocytic blood stage. While the parasite is busy changing and breaking down the host's erythrocytes it is also digesting a large amount of the haemoglobin, which results in the release of iron(II) protoporphyrin IX.[11–13] This oxidises to the toxic iron(III) compound which the parasite then stores in microcrystalline form as non-toxic haemozoin.[13–15] Many antimalarials target this process to prevent the formation of haemozoin, causing the parasite to die. Chloroquine (Figure 1.2) was one of the first and most effective synthetic antimalarial drugs and functions in this fashion. Unfortunately, resistance soon developed against it, requiring the ongoing search for new therapies.[11,16,17]

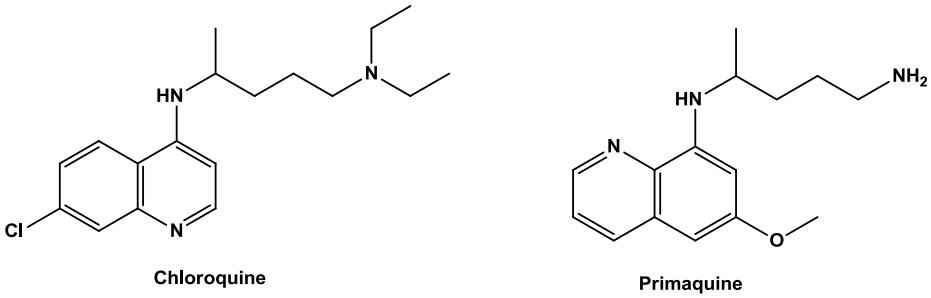

Figure 1.2 – Structures of two antimalarial drugs chloroquine and primaquine that are active against the blood and liver stages, respectively.

Another approach is to prevent the invasion of new erythrocytes. It is during this stage that the parasite is exposed to the immune system, albeit for a very brief duration.[10] The asexual blood stage infection is responsible for the disease pathology, since it is the remodelling and rupturing of the erythrocytes of the host which causes symptoms - and often complications such as anemia due to erythrocyte rupturing, and cerebral malaria, as the parasite filled erythrocytes block blood vessels to the brain. As such, much effort has been put into developing an effective blood stage vaccine.[9,10] Unfortunately, no success has been achieved yet due to the antigenic diversity and complexity that the malarial parasite has developed.[10] Furthermore, the lack of understanding of the protective host immune response towards these antigens has also hindered research efforts.

Finally, the liver stage of the parasite lifecycle may also be targeted, although primaquine (Figure 1.2), which also prevents reinfection, is currently the only marketable drug available for this stage.[11,18] These factors, along with cases of resistance against most of the current antimalarials including the WHO recommended artemisinin-based combination therapy, illustrate the dire need for development of new effective treatments.[19,20]

1.4 Sulfonamides

Sulfonamide-containing drugs have been in use as antimicrobials since the early 20th century and were some of the first chemotherapeutics to be systematically employed.[21,22] They are still prevalent in the pharmaceutical industry and are used for a wide range of treatments.[23] Given their continued prevalence in the industry many different methods have been developed for their synthesis. One of the most common methods involves formation of the required sulfonyl chloride derivative, which is then followed by a nucleophilic substitution of the required amine.[23] This is generally one of the most efficient ways of obtaining sulfonamides, even though the method suffers from requiring the handling of toxic chlorinating agents to produce the desired sulfonyl chloride.[23] The sulfonyl chlorides can be obtained from either the respective thiols[24] or the sulfonic acids.[25] They can also be obtained by oxidation of their sulfenamide or sulfinamide analogues.[26] Furthermore, there are a wide variety of transition metal catalysts which may be employed in their synthesis, primarily in N-arylation of the sulfonamide, with the foremost being palladium[27], ruthenium[28] and copper[29] catalysts.[23] Finally, an oxidative coupling of sodium sulfinates and amines via copper bromide can also provide a range of sulfonamides.[30]

They are generally believed to function by preventing the synthesis of tetrahydrofolic acid (Figure 1.3), which is an important cofactor in the synthesis of DNA. This occurs through competitive inhibition of dihydropteroate synthase, a bacterial enzyme higher up in the pathway that produces the precursors for tetrahydrofolic acid from para-aminobenzoic acid (Figure 1.3).[31]

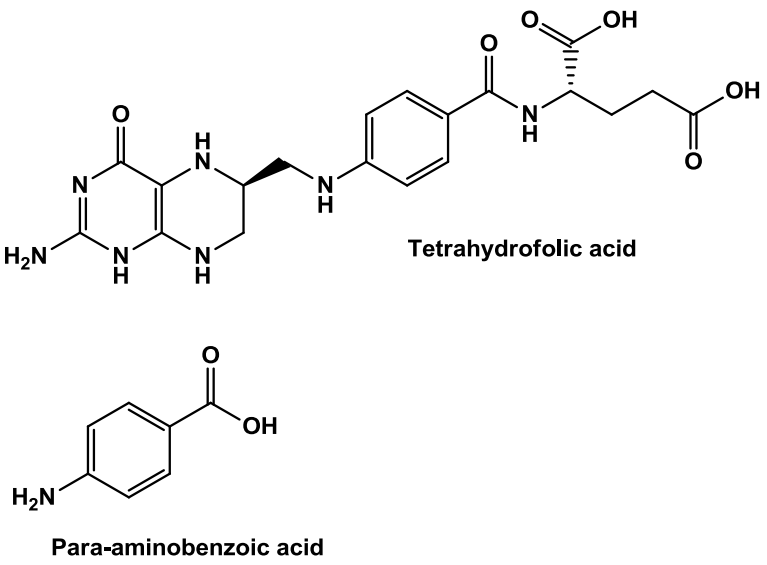

Figure 1.3 - Tetrahydrofolic acid and its precursor para-aminobenzoic acid.

The low toxicity and affordability of sulfonamides make them very attractive candidates for drug research. They have been found to be effective for a wide variety of treatments, having been employed as antibacterial, antiviral, antitumour and antifungal agents, to name but a few.[22,31–37] Regarding malaria, they are no longer commonly used, but a sulfonamide combination therapy of sulfadoxine and pyrimethamine (Figure 1.4) is still used as a preventative treatment in pregnant women and for certain cases of malaria in combination with artesunate (Figure 1.4).[9]

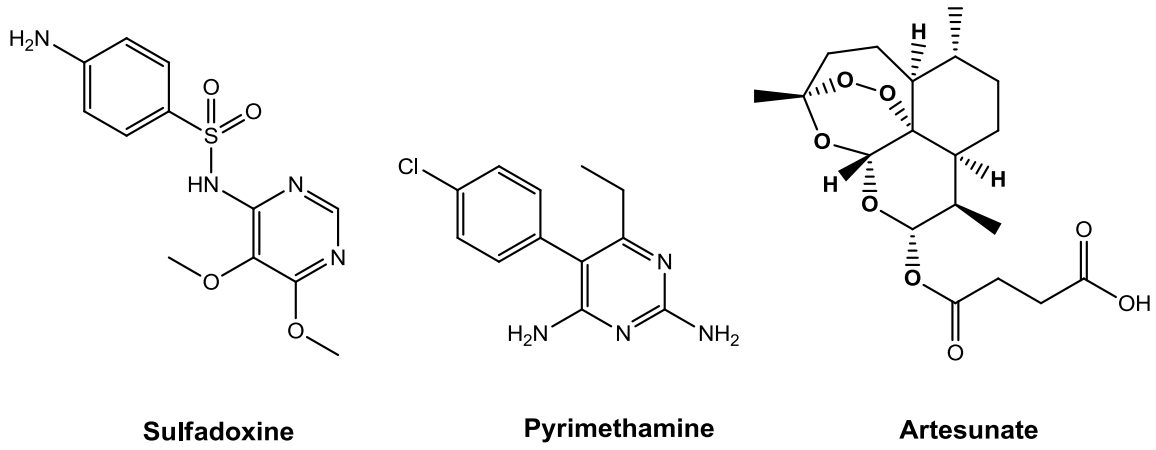

Figure 1.4 – Structures of sulfadoxine, pyrimethamine and artesunate which are used in combination therapies as antimalarials.

They were initially employed as antitubercular drugs, but with the discovery of isoniazid, rifampicin and streptomycin, were largely made obsolete due to their lower efficacy.[38] With the rise of drug resistance against current therapies and the trend of repurposing, it could prove beneficial to once again look to these pharmacophores for answers.Two cases illustrating how derivatisation of the parent sulfonamide alone can influence the activity and properties are discussed below.

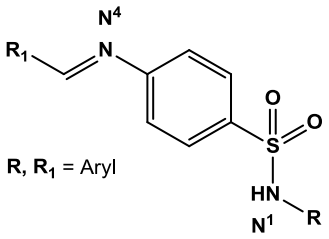

Figure 1.5 - General structure of the sulfanilamide derivatives investigated by Kolloff and Hunter.[39]

Kolloff and Hunter[39] performed a study on a range of N^4 and N^1 substituted aryl benzylidene sulfonamides to investigate the effect that substituting the N^4 position would have on their activity against pneumonococcal and streptococcal bacteria. These positions are shown in Figure 1.5 and are used in sulfanilamide derivatives as a convenient naming method to distinguish which nitrogen is being modified. The derivatives containing a phenyl ring on both N^4 and N^1 positions were particularly unstable and susceptible to hydrolysis, and purification was complicated for all the derivatives. The activity was seen to decrease slightly with substitution of a phenyl ring, while the toxicity decreased significantly. This illustrates that some activity can be sacrificed to decrease the general toxicity of these systems and make them more viable for use.

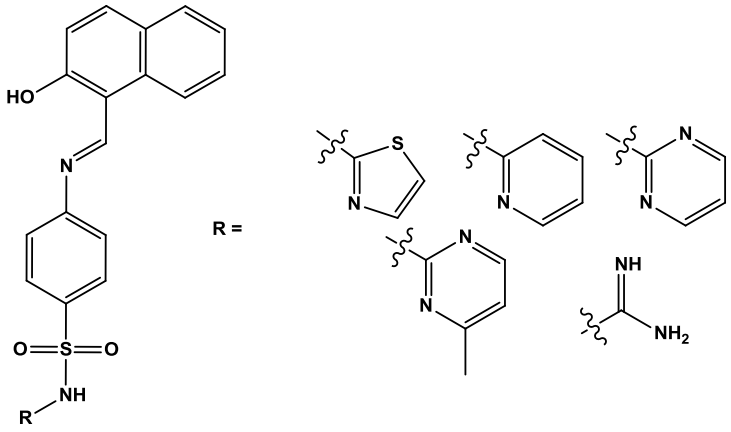

Figure 1.6 - Structure of the sulfonamide Schiff bases investigated by Mondal et al.[40]

Mondal et al.[40] investigated a series of Schiff bases for antimicrobial activity and drug-like potential. These drug candidates were derived from 2-hydroxynaphthaldehyde and the sulfonamides: sulfathiazole, sulfapyridine, sulfadiazine, sulfamerazine, and sulfaguanidine. They are shown in Figure 1.6. These sulfonamide-Schiff bases showed a significant increase in activity towards both gram-positive and gram-negative microbial strains that are resistant to their parent sulfonamides, with similar activity to sensitive strains. Additionally, the cytotoxicity was above that of the minimum inhibitory concentrations for the drug candidates and haemolysis assays indicated that 90% of blood cells remained viable. The ligands were also optimised via DFT calculations and used in docking studies with the enzyme dihydropteroate synthase, through which various hydrogen bonding interactions were observed. Complex energies with the enzyme were very similar, paralleling the

MIC data obtained, which ranged between 32 µg/ml - 128 µg/ml across the various drug candidates and microbial strains.

1.5 Metals in medicine

The use of metals in medicine has been practiced since the age of antiquity with ancient civilisations using copper, gold and iron for a great variety of therapies.[41] More recently, syphilis was being treated with mercury salts, during which there was the very real risk of the patient dying of mercury poisoning, before Paul Ehrlich discovered Arsphenamine (an organoarsenic compound) which was much less toxic and more effective.[21,42] Since then, with the discovery of cisplatin by Rosenberg and the use of bismuth for the treatment of syphilis and gastrointestinal disorders, bioinorganic chemistry has rapidly expanded and become increasingly more applicable in treatments.[43,44]

This utility is due to the incredible versatility that can be achieved through metal complexes, which differ in oxidation state, coordination number, geometries, electronic properties and stability. Furthermore, each of these can be adjusted and modified by selecting the appropriate ligands and using various synthetic methods, allowing for an incredible variety of possibilities in design.[21,45,46] This in turn allows very specific targets to be chosen. Additionally, the careful choice of ligand can control the reactivity and toxicity of the metal complex and determine the secondary coordination sphere interactions, including which biological sites will be targeted specifically.[46]

It is important to consider all the properties of the complex if it is to be biologically relevant. Both its stability and solubility must be carefully designed for the specific purpose to which it is intended. Though the potential for such specific design exists, and metal complexes have already found a great variety of applications in medicine as treatments for syphilis, arthritis, cancer, inflammation, as diagnostic and imaging agents and as antibacterials, it is still difficult to achieve and continued research is necessary to broaden our knowledge and available technology.[21,45–50]

More recently there has been a surge of research into metal complexes of drugs that have already been used in treatments and their direct repurposing or derivatisation for other therapies. In cases where resistance has appeared to the original therapy, the metal complex may be active and function via a different mode of action against the disease. [21,46,51–53]

1.6 Sulfonamide metal complexes as antimicrobials

There are several articles that have been published reporting an increase in activity when the ligand or parent drug is administered in the form of a metal complex, which is especially advantageous against drug resistant variants of diseases.[21,51,54–58] This increase in activity, especially as antimicrobials, has been well documented for sulfonamides and depends on the metal ion used, and a vast range of different sulfonamide metal complexes have been developed over recent years.[54,59,60] They have been tested for a multitude of diseases and applications, some of which include cancer,[61,62] antimicrobials and antifungals[63,64] and carbonic anhydrase inhibitors (which have application to a variety of conditions and diseases).[65–68] Given the large number of heteroatoms

contained in especially heterocyclic sulfonamides and the various ways in which coordination can occur, the scope of activity and application is broad, as is illustrated by some of the most recent cases discussed hereafter.

Kremer et al.[54] decided to pursue this versatility with the incorporation of copper and investigated a series of copper complexes based on sulfonamides incorporating nitrogen containing heterocycles. Figure 1.7 shows the wide range of sulfonamides used in their study.

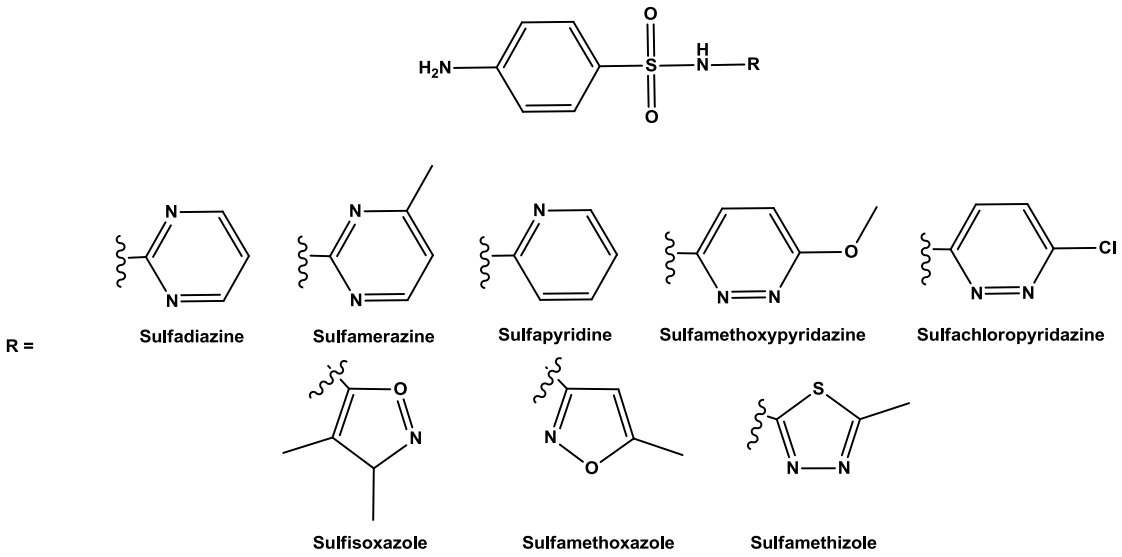

Figure 1.7 – Range of sulfonamides used by Kremer et al.[54]

Note that each of the respective ligands are clinical drugs and thus this work also focusses on the repurposing of current therapies. The complexes were formed by deprotonation of the sulfonamide in an aqueous solution followed by addition of the hydrated copper salt. This resulted in the targeted complexes precipitating out of solution. Seven of the complexes showed coordination through multiple sites on the ligand, where two ligands coordinated through the free amine, one in a bidentate fashion through the sulfonamide and heterocyclic nitrogen, and the last one through another heterocyclic atom. This resulted in four ligands coordinating to one metal ion. The other ligands coordinated in a monodentate fashion through one of the heterocyclic heteroatoms in 2:1 ligand to metal ratio, with the remaining positions taken up by water and hydroxide. Biological evaluation of these complexes showed variable activity against *Staphylococcus aureus* (4 µg/mL – 128 µg/mL) and *Escherichia coli* (2 µg/mL – 128 µg/mL). In both strains in the lab and strains isolated from patients, sulfonamides containing five-membered heterocycles were the most active. Sulfadiazine, sulfamerazine and sulfapyridine complexes are all less active than the native sulfonamides. The authors proposed that this could be due to the specific coordination of these ligands through the free amine.

Mansour and Abdel Ghani[69] investigated the various computational and physical properties of a sulfamethazine-salicylaldehyde Schiff base by density functional theory (Figure 1.8). These included

natural bond orbital analysis, mulliken atomic charges and non-linear effects arising from electromagnetic fields, amongst others. The difference in biological activity between the parent sulfonamide and the resulting Schiff base is proposed to be affected by the ability to penetrate the membrane of the target cells. This is directly influenced by the lipophilicity of the compounds. Mansour[70] then went on to investigate the influence on biological activity of this sulfamethazine Schiff base against strains of *S. aureus* and *E. coli* along with three copper(II) complexes of this ligand (Figure 1.8). Both ligands and complexes were prepared via a one-pot synthesis in water by using the amine salt and were obtained without significant difficulty.

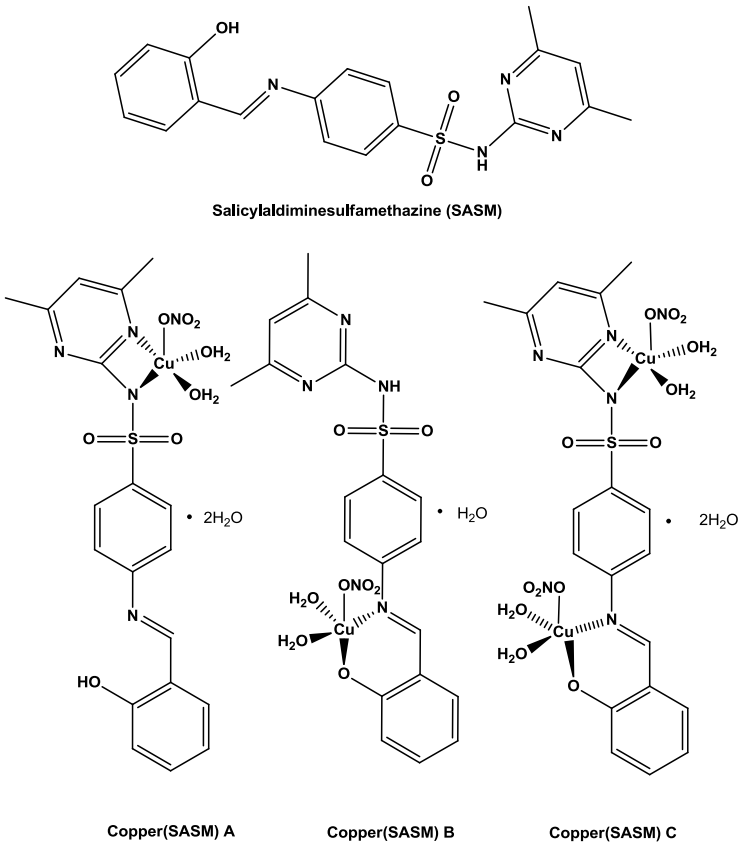

Figure 1.8 - The salicylaldehyde-sulfamethazine Schiff base investigated by Mansour and Abdel Ghani[69], and its copper complexes.[70]

For all complexes the S-N stretch, disappearance of N-H and phenolate ion stretch are used to identify coordination with the copper. EPR was used to determine if there was any magnetic coupling between copper centres of the dinuclear complex (Figure 1.8); none was found. Antibacterial activity (IC_{50}) of the ligand (120 µM) was much less than the free sulfonamide, with the incorporation of the metal reducing activity even further. The IC_{50} for both copper(SASM) A and B was 270 µM while it was 620 µM for copper(SASM) C, as measured against S*. aureus.* Higher activity was seen for gram positive bacteria than gram negative bacteria.

These two studies illustrate that although the general trend of incorporating a metal centre is an increase in activity, this is not always the case and the results depend on the metal used as well as

where it is incorporated. Unlike the hypothesis presented, the activity is not totally dependent upon the lipophilicity of the drug candidates, even though this has often been shown to be the case.

Nakahata et al.[71] prepared an aqueous dimeric silver sulfameter complex, which was shown to coordinate through the oxygen and nitrogen of the sulfonamide group and one of the heterocyclic nitrogens of the pyrimidine ring (Figure 1.9, left). A range of spectroscopic data was obtained to confirm this along with a crystal structure. Antibacterial testing against both gram positive and gram negative strains showed that sulfameter was inactive, the complex was mildly active against *E. coli* and *P. aeruginosa* strains with a MIC (inhibition of visible growth) of 40.9 µM and silver nitrate was the most active with sub micro molar activity. The activity is attributed to the release of silver ions, which are well known for their antimicrobial activity, where the complex is slow to release these ions. The cytotoxicity of the compounds was not tested but it is likely that the silver nitrate would be significantly more cytotoxic than the complexes incorporating the ligands, as it is believed that the toxicity of metal complexes are modulated by the ligands. This is especially in light of a solution of silver nitrate applied as a topical application being regarded as toxic to the tissues affected if it is concentrated enough.[72]

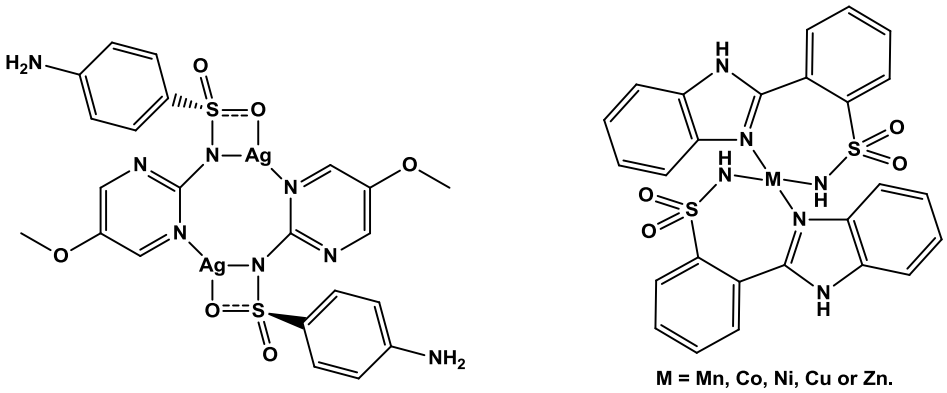

Figure 1.9 - Dimeric silver-sulfameter complex obtained by Nakahata et al.[71] (Left) and the general structure of the complexes synthesized by Ashraf et al.[73] (Right) The Mn complex had an additional two H_2O molecules coordinated to it.

Ashraf et al.[73] synthesized a series of benzimidazole-sulfonamide hybrid metal complexes with the divalent transition metal ions Mn, Co, Ni, Cu and Zn (Figure 1.9, right). The antimicrobial efficacy was evaluated via the agar disc diffusion method and compared to the clinical drugs cefixime and roxithromycin. The bacterial strains used were *Micrococcus luteus, Bordetella bronchiseptica, Salmonella typhi, S. aureus, Enterobacter aerogens* and *E. coli.* The fungal species were *Mucor* species*, Aspergillus niger, Aspergillus flavus, Aspergillus fumigatus, Alternaria* species and *Fusarium solani.* None of the complexes were found to inhibit fungal growth and the only significant inhibition of bacterial strains were shown by the Co and Zn complexes, with the cobalt complex exhibiting a comparable inhibition zone to cefixime for two of the bacterial strains, namely, *M. luteus* and *S. aureus*. Coordination takes place primarily through the nitrogen of the benzimidazole and that of the sulfonamide (Figure 1.9, right).

Alaghaz et al.[74] synthesized a sulfanilamide azo dye and prepared its chromium(III), manganese(II), cobalt(II), nickel(II), copper(II) and cadmium(II) complexes (Figure 1.10, left). The authors did a detailed spectroscopic analysis of the various properties of the compounds, looking at electronic spectra, magnetic moment and a variety of other parameters. The structures of the complexes were determined through a combination of NMR (for non-paramagnetic samples) and IR spectroscopy which was supported by a range of other techniques.

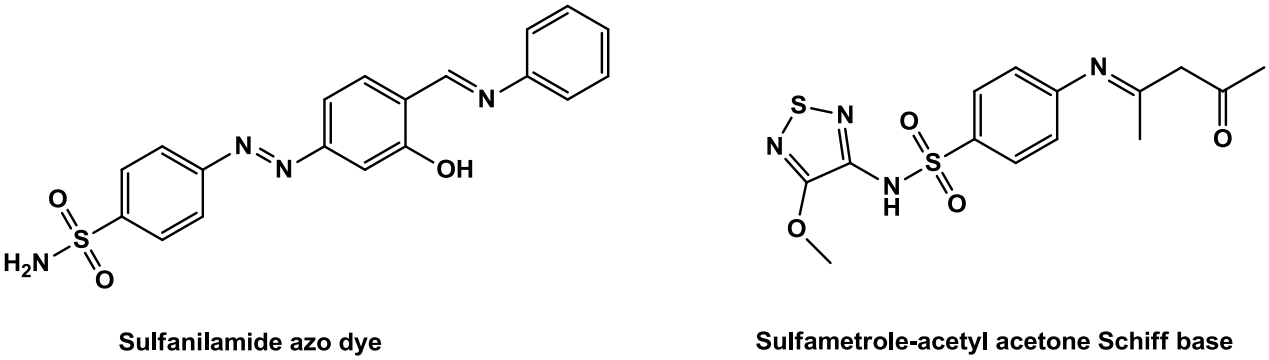

Figure 1.10 – The sulfanilamide azo dye investigated by Alaghaz et al.[74] (Left) and the Schiff base ligand derived from sulfametrole and acetyl acetone used by Sharaby et al.[55] (Right).

Coordination was proposed to occur through the hydroxyl and imine functional groups with coordinated water and acetate molecules to fill the remaining spaces which results in the proposed octahedral geometry. The biological activity was evaluated by means of the agar disc diffusion method which showed some inhibition against *S. aureus, Staphylococcus epidermidis, Klebsiella pneumonia, Shigella flexneri, A. fumigatus, Aspergillus clavatus,* and *Candida albicans* sensitive strains. Inhibition was generally weaker than that of the standards used.

Sharaby et al.[55] synthesized a Schiff base ligand derived from the clinical sulfa drug sulfametrole and acetyl acetone (Figure 1.10, right). Purity was confirmed through various characterisation techniques (IR, ^{1}H NMR, MS, elemental analysis and UV-vis) and a sharp melting point (155 °C). Complexes were then formed by reacting with copper, zinc, cadmium, ferric chloride and ferrous sulphate. Mixed ligand complexes were formed by introducing glycine as a secondary ligand with the metals copper, zinc and cadmium chloride. The following range of techniques were employed for the analysis of the various complexes: elemental analyses (C, H, N, S and Cl), IR, ^{1}H NMR, molar conductance, magnetic moment studies and thermal analyses (TG and DTA). Molar conductance tests provide insight into the potential ways in which compounds can interact under physiological conditions and can be combined with information on lipophilicity and solubility to solidify hypotheses on drug interactions. Results from the molar conductance studies indicate these complexes are not strong electrolytes. Furthermore, IR of the mixed complexes show a shift in the C-O stretch of the carboxylate group of glycine indicating coordination through this group to the metal. Thermal analysis on the copper and cadmium Schiff base complexes showed that water coordinates to the metal through the inner coordination sphere, whereas this is not the case for the mixed ligand complexes.

Antimicrobial activity was tested against a variety of gram-positive (*S. aureus* and *Bacillus subtilis*) and gram-negative bacteria (*Salmonella typhimurium* and *E. coli*) along with some fungal species (*C. albicans* and *A. fumigatus*). The complexes were also tested for anticancer activity against the breast cancer cell line MCF-7. Biological activity against bacteria, yeast and fungi was determined by means of inhibition zones. The complexes showed good antimicrobial activity against the bacteria and yeast but were not very effective against the fungus. The anticancer activity displayed was good for all except the iron complexes, with IC_{50} values ranging between 1.8 and 11.1 µg/ml. The mixed ligand complexes were more active than the standard complexes, and the cadmium complexes were generally the most active for both the cancer and the bacterial testing, with the zinc complexes displaying moderate activity.

Ebrahimi et al.[75] aimed to investigate sulfonamide Schiff base metal complexes along with their beta lactam derivatives as both these moieties have shown considerable biological potential. The respective Schiff bases were synthesized by reacting sulfamethoxazole and sulfathiazole with o-vanillin, from which the beta lactam derivatives could then be made by reacting the Schiff bases with triethylamine and chloroacetyl chloride. Complexes of the two groups of ligands were made with copper and zinc. All compounds were characterised through a wide range of techniques (IR, ^{1}H and ^{13}C NMR, MS, TG/DTG). The ligands are shown in Figure 1.11. The agar disc diffusion method was used to determine the biological activity of the compounds. All the compounds were found to have biological activity against *E. coli, P. aeruginosa, Proteus* species and *S. aureus*. Additionally, enhanced activity was observed once the ligands had been complexed with the metals. This is proposed to be due to the increased hydrophobicity which allows for easier transfer across bacterial membranes. There was no significant difference in activity between the beta lactam ligands and the standard sulfonamide ligands. Furthermore, a brief computational study was also performed using DFT, investigating the HOMO and LUMO orbitals of the ligands.

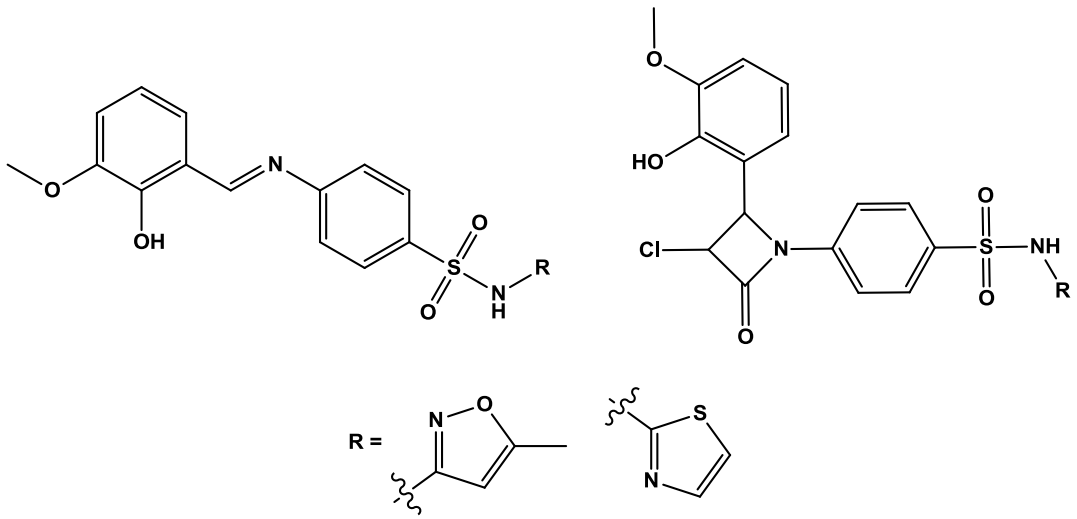

Figure 1.11 - Beta lactams and Schiff bases used as ligands for copper and zinc complexes by Ebrahimi et al.[75]

Although much of their work focusses on carbonic anhydrases,[76] Supuran and co-workers have worked on a range of sulfonamides, including their cobalt, nickel, copper and zinc metal complexes with application to their biological activity as antimicrobials.[64,77–82] The compounds were tested against both gram-positive and gram-negative bacterial strains, various fungal strains and several cancer cell lines. It was generally found that activity of the compounds was increased upon metalation as has been discussed previously, and that the antimicrobial activity was moderate to good. Chohan and co-workers have also done several studies in the same field and obtained similar results for their complexes.[63,83]

1.7 Sulfonamide metal complexes targeting *Mtb*

Despite this multitude of research on sulfonamide metal complexes as general antibacterials and antifungals, very little research has investigated the application of these complexes on malaria and tuberculosis specifically. Three more recent examples are discussed below that focus on targeting mycobacteria.

Mondelli et al.[84] were prompted to investigate cobalt sulfonamide complexes of sulfapyridine, sulfadimethoxine, sulfamethazine, sulfamerazine, sulfamethoxazole and sulfamethizole (Figure 1.12).

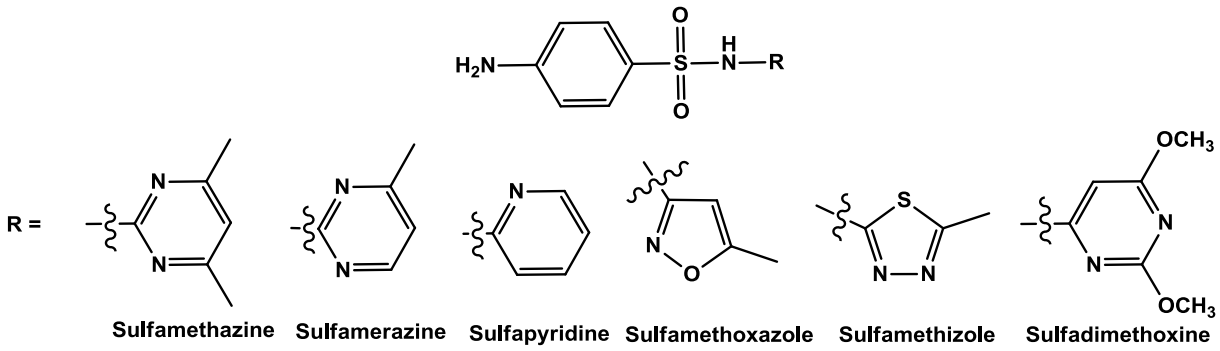

Figure 1.12 - Sulfonamides used by Mondelli et al.[84]

They investigated the various means of coordination that sulfonamides display along with the cytotoxicity and the activity against *Mtb*. From the shifts in the infrared spectrum, especially those of the N-heterocyclic and aryl amines, they were able to tentatively determine that these complexes coordinated primarily through the free amine and the heterocyclic nitrogen groups to the cobalt ion (Figure 1.13). A crystal structure of the sulfamethoxazole complex was obtained and showed that the coordination occurs through the ligand acting in a bridging fashion between two metal centres through the groups previously mentioned. It is postulated that the sulfapyridine complex coordinates in a similar fashion, although crystal structures were not obtained for it. The complexes generally showed comparable activity to that of the free ligands. The exception being sulfapyridine which had the greatest activity among all compounds tested, even though none of the compounds showed significant activity against *Mtb,* with all values being in the millimolar range.

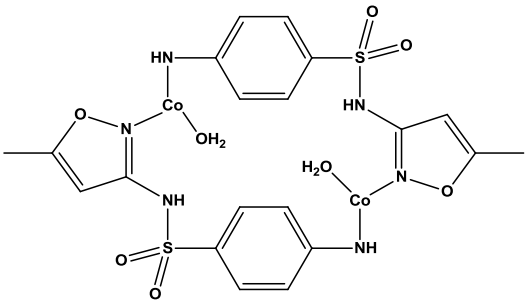

Figure 1.13 – Structure of the Co-Sulfamethoxazole complex made by Mondelli et al.[84]

Marques et al.[85] discovered gold and silver complexes of sulfamethoxazole (Figure 1.14) which functioned synergistically with trimethoprim as antibacterial agents in a 5 to 1 ratio.

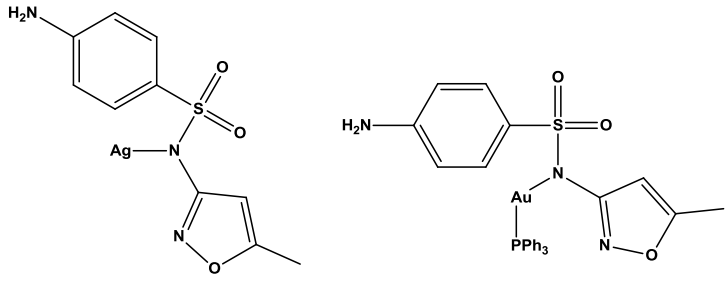

Figure 1.14 – Gold and silver sulfamethoxazole complexes discovered by Marques et al.[85]

Agertt et al.[86] subsequently decided to test these new compounds along with trimethoprim against mycobacterial strains to investigate if the same effect was seen and if they would be active, given the urgent need for new therapies against *Mtb*. They also incorporated cadmium, mercury and copper complexes into their investigations. They found only one complex, [Au(sulfathiazolato)(PPh_3)] (Figure 1.15), that showed synergistic effects against *Mycobacterium smegmatis*. They confirmed this synergistic effect with trimethoprim against *Mtb* and found activity levels (0.24 µg/mL) close to that of isoniazid which warranted further investigation.

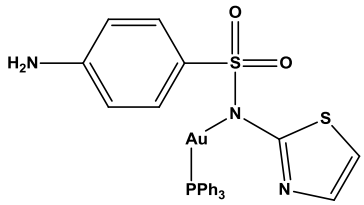

Figure 1.15 - Sulfathiazole complex found to be very active by Agertt et al.[86] in synergism with trimethoprim.

They went on to test these same complexes along with gold complexes of sulfadiazine, against rapidly growing mycobacteria to see if they achieved better activity and synergism.[87] Rapidly growing mycobacteria are a class of non-tubercular mycobacteria that function as opportunistic pathogens. They found that in most of the cases there was a symbiotic interaction and the drugs acted synergistically against all three strains of rapidly growing mycobacteria tested. The gold sulfamethoxazolate, silver methoxazole and dimeric gold sulfadiazine complexes had bactericidal

activity, as demonstrated by time kill curves, whereas all other complexes exhibited bacteriostatic activity. All the complexes were weakly active with MIC values in the low millimolar range. Upon administration with trimethoprim these values decreased to the mid micromolar range.[87]

Quintana et al.[88] investigated the effect of electron donating and electron withdrawing organometallic fragments on the activity and properties of sulfonamide complexes. They used a ferrocenyl amine as the electron donating metal and a cyrhetrenyl amine as the electron withdrawing metal. The general structure of the complexes are shown in Figure 1.16.

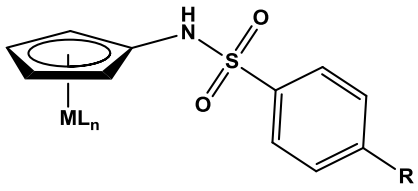

ML_n = $Re(CO)_3$ R = $-NO_2$; $-CH_3$; $-NHCOCH_3$

ML_n = $Fe(\eta^5\text{-}Cp)_3$ R = $-NO_2$; $-CH_3$; $-NHCOCH_3$

Figure 1.16 - General structure of the complexes synthesized by Quintana et al.[88]

The complexes were then tested against *Mtb* and the minimum concentration when 99% of all cell growth is inhibited (MIC_{99}) was determined. The activity was only moderate compared to isoniazid and lay in the range of 186 µM to 281 µM with the cyrhetrenyl complexes exhibiting the highest activity. The authors used DFT calculations to explain the nature of each of the organometallic fragments and postulated that the difference in activity was due to the electron withdrawing nature of the cyrhetrenyl group which influences the nucleophilicity of the sulfonamide group, generally believed to be responsible for the activity of sulfonamides.

There has been some research on purely organic sulfonamides, as well as platinum group metal complexes, targeting *Mtb* and malaria parasites, which both showed promising results.[52,89–92] Given the sparse nature of studies specifically targeting these infectious diseases, it was sought to combine these two concepts and investigate a series of platinum group sulfonamide metal complexes and their activities against malaria and *Mtb*.

1.8 Aims and Objectives

The first aim of the project was to synthesize a series of imino derivatised sulfadoxine iridium conjugates. These complexes are shown in Scheme 1.1 and had been prepared before by Chellan et al.[50], although they had not succeeded in investigating the difference in biological activity of the ligands as compared to the metals. It was subsequently decided it would be of value to obtain data on the activity difference, thus the purification and testing of the ligands were set as a secondary objective.

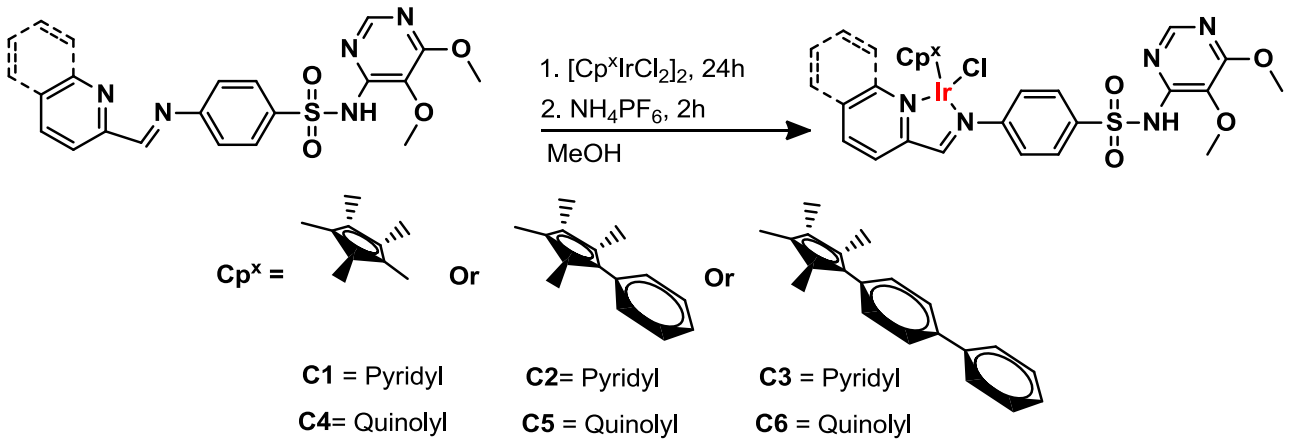

Scheme 1.1 - Imino sulfadoxine derivatised iridium conjugates to be prepared in this study.

The second aim of the project was to synthesize a small library of amido derivatised sulfadoxine iridium complexes. Both the complexes and ligands in this library had not been prepared before and their structures are shown in Scheme 1.2. The ligands were prepared by converting the appropriate carboxylic acid to its acid chloride and then quenching with sulfadoxine to afford the amide.

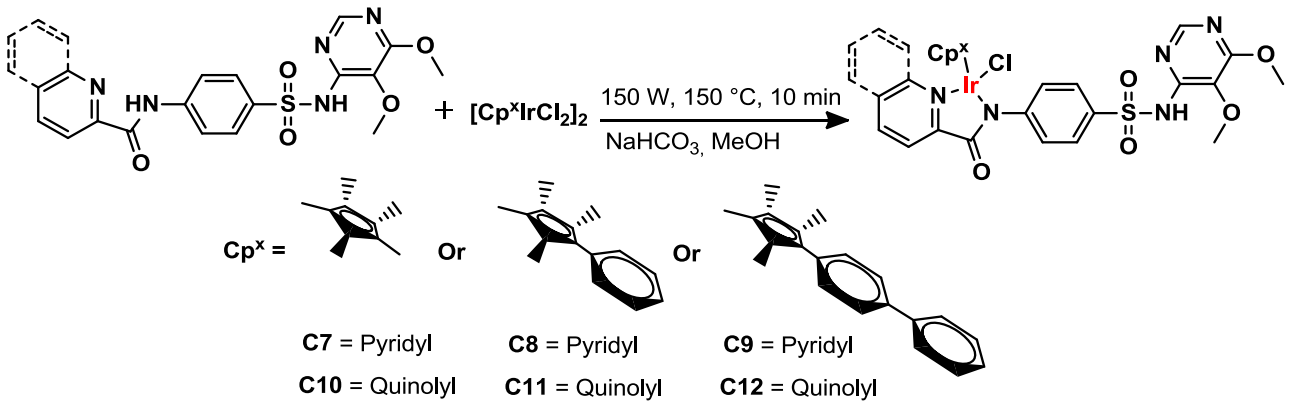

Scheme 1.2 - Amido derivatised sulfadoxine iridium complexes prepared in this study.

Thirdly, it was planned to investigate selected physico-chemical properties of these potential drug candidates to determine their suitability as pharmaceuticals and their drug-like character. In particular, the solubility of the complexes was to be investigated by means of a turbidimetric assay which analyses the dynamic light scattering of serial dilutions of the compounds to be tested and from which a graph of solubility can be drawn. It was also decided to investigate the nature of the active species and whether this is the chlorido or aqua analogue. This was done by comparing *in situ* synthesized aqua analogues with their incubated chlorido parent complexes with ^{1}H NMR and an internal standard under the same conditions. This allowed for different species to be identified and the determination of whether the aquation of the metal centre was a facile process. A complex,

C2 (Scheme 1.1), was also selected for a detailed study of the aquation process and was followed via ^{1}H NMR overnight.

Finally, the complexes were all to be tested against strains Dd2, 3D7 and HB3 of *P. falciparum* and the H37Rv strain of *Mtb* via dose response assays to determine their activity against these infectious diseases, respectively. Their cytotoxicity against HEK cells was also to be investigated. From the results, structure activity relationships were to be determined and the best candidates selected for further study and derivatisation.

1.9 References

(1) Blass, B. E. *Drug Discovery and Development*; Academic Press: Amsterdam, 2015.

(2) Antimicrobial resistance http://www.who.int/en/news-room/fact-sheets/detail/antimicrobial-resistance (accessed Jun 30, 2018).

(3) Who. WHO Global Strategy for Containment of Antimicrobial Strategy for Containment of Antimicrobial Resistance. *World Health* **2001**, *WHO/CDS/CS*, 105.

(4) Butler, J. C.; Hofmann, J.; Cetron, M. S.; Elliott, J. A.; Facklam, R. R.; Breiman, R. F. The Continued Emergence of Drug-Resistant Streptococcus Pneumoniae in the United States: An Update from the Centers for Disease Control and Prevention's Pneumococcal Sentinel Surveillance System. *J. Infect. Dis.* **1996**, *174* (5), 986–993.

(5) Koch, R. Die Aetiologie Der Tuberkulose. *Berliner Klin. Wochenschrift* **1882**, *15*, 221–230.

(6) Cambau, E.; Drancourt, M. Steps towards the Discovery of Mycobacterium Tuberculosis From Ancient Times to the Discovery of the Tubercle Bacillus. *Clin Microbiol Infect* **2014**, *20*, 196–201.

(7) World Health Organization. *Global Tuberculosis Report 2018*; 2018.

(8) World Health Organization. WHO Malaria Fact sheet https://www.who.int/news-room/fact-sheets/detail/malaria (accessed Jan 23, 2019).

(9) WHO. *World Malaria Report*; 2018.

(10) Cowman, A. F.; Berry, D.; Baum, J. The Cellular and Molecular Basis for Malaria Parasite Invasion of the Human Red Blood Cell. *J. Cell Biol.* **2012**, *198* (6), 961–971.

(11) Bonilla-Ramirez, L.; Rios, A.; Quiliano, M.; Ramirez-Calderon, G.; Beltrán-Hortelano, I.; Franetich, J. F.; Corcuera, L.; Bordessoulles, M.; Vettorazzi, A.; López de Cerain, A.; et al. Novel Antimalarial Chloroquine- and Primaquine-Quinoxaline 1,4-Di-N-Oxide Hybrids: Design, Synthesis, Plasmodium Life Cycle Stage Profile, and Preliminary Toxicity Studies. *Eur. J. Med. Chem.* **2018**, *158*, 68–81.

(12) Egan, T. J.; Combrinck, J. M.; Egan, J.; Hearne, G. R.; Marques, H. M.; Ntenteni, S.; Sewell, B. T.; Smith, P. J.; Taylor, D.; Van Schalkwyk, D. A.; et al. Fate of Haem Iron in the Malaria Parasite Plasmodium Falciparum. *Biochem. J.* **2002**, *365* (2), 342–347.

(13) De Villiers, K. A.; Egan, T. J. Recent Advances in the Discovery of Haem-Targeting Drugs for Malaria and Schistosomiasis. *Molecules* **2009**, *14* (8), 2868–2887.

(14) Chou, A. C.; Fitch, C. D. Hemolysis of Mouse Erythrocytes by Ferriprotoporphyrin IX and Chloroquine. Chemotherapeutic Implications. *J. Clin. Invest.* **1980**, *66* (4), 856–858.

(15) Brown, W. H. Malarial Pigment (so-Called Melanin): Its Nature and Mode of Production. *J. Exp. Med.* **1911**, *13* (2), 290 - 299.

(16) Farooq, U.; Mahajan, R. C. Drug Resistance in Malaria. *J. Vector Borne Dis.* **2004**, *41*, 45–53.

(17) Price, R. N.; Uhlemann, A. C.; Brockman, A.; McGready, R.; Ashley, E.; Phaipun, L.; Patel, R.; Laing, K.; Looareesuwan, S.; White, N. J.; et al. Mefloquine Resistance in Plasmodium Falciparum and Increased Pfmdr1 Gene Copy Number. *Lancet* **2004**, *364* (9432), 438–447.

(18) Li, Q.; O'Neil, M.; Xie, L.; Caridha, D.; Zeng, Q.; Zhang, J.; Pybus, B.; Hickman, M.; Melendez, V. Assessment of the Prophylactic Activity and Pharmacokinetic Profile of Oral Tafenoquine Compared to Primaquine for Inhibition of Liver Stage Malaria Infections. *Malar. J.* **2014**, *13*, 141 - 154.

(19) Na-Bangchang, K.; Karbwang, J. Current Status of Malaria Chemotherapy and the Role of Pharmacology in Antimalarial Drug Research and Development. *Fundam. Clin. Pharmacol.* **2009**, *23* (4), 387–409.

(20) L'abbate, F. P.; Müller, R.; Openshaw, R.; Combrinck, J. M.; de Villiers, K. A.; Hunter, R.; Egan, T. J. Hemozoin Inhibiting 2-Phenylbenzimidazoles Active against Malaria Parasites. *Eur. J. Med. Chem.* **2018**, *159*, 243–254.

(21) Rizzotto, M. Metal Complexes as Antimicrobial Agents. In *A Search for Antibacterial Agents*; Bobbarala, V., Ed.; INTECH, 2012; pp 73–88.

(22) Henry, R. J. The Mode of Action of Sulfonamides *. *Bacteriol. Rev.* **1943**, *7* (4), 175–262.

(23) Kołaczek, A.; Fusiarz, I.; Lawecka, J.; Branowska, D. Biological Activity and Synthesis of Sulfonamide Derivatives: A Brief Review. *Chemik* **2014**, *68* (7), 620–628.

(24) Veisi, H.; Ghorbani-Vaghei, R.; Hemmati, S.; Mahmoodi, J. Convenient One-Pot Synthesis of Sulfonamides and Sulfonyl Azides from Thiols Using N -Chlorosuccinimide. *Synlett* **2011**, *16*, 2315 - 2320.

(25) Rad, M. N. S.; Khalafi-Nezhad, A.; Asrari, Z.; Behrouz, S.; Amini, Z.; Behrouz, M. One-Pot Synthesis of Sulfonamides from Primary and Secondary Amine Derived Sulfonate Salts Using Cyanuric Chloride. *Synthesis (Stuttg).* **2009**, *23*, 3983 - 3988.

(26) Revankar, G. R.; Hanna, N. B.; Ramasamy, K.; Larson, S. B.; Smee, D. F.; Finch, R. A.; Avery, T. L.; Robins, R. K. Synthesis and In Vivo Antitumor and Antiviral Activities of 2′-deoxyribofuranosyl and Arabinofuranosyl Nucleosides of Certain Purine-6-sulfenamides, Sulfinamides and Sulfonamides. *J. Heterocycl. Chem.* **1990**, *27*, 909 - 918.

(27) Rosen, B. R.; Ruble, J. C.; Beauchamp, T. J.; Navarro, A. Mild Pd-Catalyzed N -Arylation of Methanesulfonamide and Related Nucleophiles: Avoiding Potentially Genotoxic Reagents and Byproducts. *Org. Lett.* **2011**, *13*, 2564 - 2567.

(28) Watson, A. J. A.; Maxwell, A. C.; Williams, J. M. J. Borrowing Hydrogen Methodology for Amine Synthesis under Solvent-Free Microwave Conditions. *J. Org. Chem.* **2011**, *76*, 2328 - 2331.

(29) Deng, W.; Liu, L.; Zhang, C.; Liu, M.; Guo, Q. X. Copper-Catalyzed Cross-Coupling of Sulfonamides with Aryl Iodides and Bromides Facilitated by Amino Acid Ligands. *Tetrahedron Lett.* **2005**, *46*, 7295 - 7298.

(30) Tang, X.; Huang, L.; Qi, C.; Wu, X.; Wu, W.; Jiang, H. Copper-Catalyzed Sulfonamides Formation from Sodium Sulfinates and Amines. *Chem. Commun.* **2013**, *49*, 6102 - 6104.

(31) Connor, E. Sulfonamide Antibiotics. *Prim. Care Updat. Ob Gyns* **1998**, *5* (1), 32–35.

(32) Maren, T. H. Relations Between Structure and Biological Activity of Sulfonamides. *Annu. Rev. Pharmacol. Toxicol.* **1976**, *16*, 309 - 327.

(33) Owa, T.; Nagasu, T. Novel Sulphonamide Derivatives for the Treatment of Cancer. *Expert Opin. Ther. Pat.* **2000**, *10*, 1725 - 1740.

(34) Kleemann, A.; Engel, J.; Kutscher, B.; Reichert, D. *Pharmaceutical Substances: Syntheses, Patents, Applications*, 1st ed.; Thieme: Stuttgart, 1999.

(35) Roush, W. R.; Gwaltney, S. L.; Cheng, J.; Scheidt, K. A.; McKerrow, J. H.; Hansell, E. Vinyl Sulfonate Esters and Vinyl Sulfonamides: Potent, Irreversible Inhibitors of Cysteine Proteases. *J. Am. Chem. Soc.* **1998**, *120*, 10994–10995.

(36) Roush, W. R.; Cheng, J.; Knapp-Reed, B.; Alvarez-Hernandez, A.; McKerrow, J. H.; Hansell, E.; Engel, J. C. Potent Second Generation Vinyl Sulfonamide Inhibitors of the Trypanosomal Cysteine Protease Cruzain. *Bioorganic Med. Chem. Lett.* **2001**, *11*, 2759–2762.

(37) Burger, A.; Wolff, M. *Burger's Medicinal Chemistry and Drug Discovery*, 1st ed.; Wiley: New York, 1995.

(38) Forgacs, P.; Wengenack, N. L.; Hall, L.; Zimmerman, S. K.; Silverman, M. L.; Roberts, G. D. Tuberculosis and Trimethoprim-Sulfamethoxazole. *Antimicrob. Agents Chemother.* **2009**, *53* (11), 4789–4793.

(39) Kolloff, H. G.; Hunter, J. H. Sulfanilamide Compounds. II. Arylidine Derivatives of N1-Substituted Sulfanilamides. *J. Am. Chem. Soc.* **1940**, *62* (6), 140–144.

(40) Mondal, S.; Mandal, S. M.; Mondal, T. K.; Sinha, C. Spectroscopic Characterization, Antimicrobial Activity, DFT Computation and Docking Studies of Sulfonamide Schiff Bases. *J. Mol. Struct.* **2017**, *1127*, 557–567.

(41) Thompson, K. H.; Orvig, C. Metal Complexes in Medicinal Chemistry: New Vistas and Challenges in Drug Design. *Dalt. Trans.* **2006**, No. 6, 761–764.

(42) Heynick, F. *Jews and Medicine: An Epic Saga*; KTAV Publishing House, Inc.: Hoboken, 2002.

(43) Rosenberg, B.; VanCamp, L.; Trosko, J. E.; Mansour, V. H. Platinum Compounds: A New Class of Potent Antitumour Agents. *Nature* **1969**, *222*, 385–386.

(44) Li, H.; Sun, H. Recent Advances in Bioinorganic Chemistry of Bismuth. *Curr. Opin. Chem. Biol.* **2012**, *16* (1–2), 74–83.

(45) Bruijnincx, P. C.; Sadler, P. J. New Trends for Metal Complexes with Anticancer Activity. *Curr. Opin. Chem. Biol.* **2008**, *12* (2), 197–206.

(46) Obaleye, J. A.; Tella, A. C.; Bamigboye, M. O. Metal Complexes as Prospective Antibacterial Agents. In *A Search for Antibacterial Agents*; Bobbarala, V., Ed.; INTECH, 2012; pp 197–218.

(47) Neirinckx, R. D.; Canning, L. R.; Piper, I. M.; Nowotnik, D. P.; Pickett, R. D.; Holmes, R.; Volkert, W.; Forster, M.; Weisner, P. S.; Marriott, J. Technetium-99m d,l-HM-PAO: A New Radiopharmaceutical for SPECT Imaging of Regional Cerebral Blood Perfusion. *J. Nucl. Med.* **1987**, *28* (2), 191–202.

(48) Sorenson, J. R. J. Copper Complexes – A Unique Class of Anti-Arthritic Drugs. *Prog. Med. Chem.* **1978**, *15*, 211–260.

(49) Sorenson, J. R. J.; Kishore, V.; Pezeshk, A.; Oberley, L. W.; Leuthauser, S. W. C.; Oberley, T. D. Copper Complexes: A Physiological Approach to the Treatment of “Inflammatory Diseases.” *Inorganica Chim. Acta* **1984**, *91* (4), 285–294.

(50) Chellan, P.; Avery, V. M.; Duffy, S.; Triccas, J. A.; Nagalingam, G.; Tam, C.; Cheng, L. W.; Liu, J.; Land, K. M.; Clarkson, G. J.; et al. Organometallic Conjugates of the Drug Sulfadoxine for Combatting Antimicrobial Resistance. *Chem. - A Eur. J.* **2018**, *24* (40), 10078–10090.

(51) Xing, B.; Yu, C. W.; Ho, P. L.; Chow, K. H.; Cheung, T.; Gu, H.; Cai, Z.; Xu, B. Multivalent Antibiotics via Metal Complexes: Potent Divalent Vancomycins against Vancomycin-Resistant Enterococci. *J. Med. Chem.* **2003**, *46* (23), 4904–4909.

(52) Eiter, L. C.; Hall, N. W.; Day, C. S.; Saluta, G.; Kucera, G. L.; Bierbach, U. Gold(I) Analogues of a Platinum-Acridine Antitumor Agent Are Only Moderately Cytotoxic but Show Potent Activity against Mycobacterium Tuberculosis. *J. Med. Chem.* **2009**, *52* (21), 6519–6522.

(53) Sousa, E. H. S.; Basso, L. A.; Santos, D. S.; Diógenes, I. C. N.; Longhinotti, E.; De França Lopes, L. G.; De Sousa Moreira, Í. Isoniazid Metal Complex Reactivity and Insights for a Novel Anti-Tuberculosis Drug Design. *J. Biol. Inorg. Chem.* **2012**, *17* (2), 275–283.

(54) Kremer, E.; Facchin, G.; Estévez, E.; Alborés, P.; Baran, E. J.; Ellena, J.; Torre, M. H. Copper Complexes with Heterocyclic Sulfonamides: Synthesis, Spectroscopic Characterization, Microbiological and SOD-like Activities: Crystal Structure of $[Cu(Sulfisoxazole)_2(H_2O)_4] \cdot 2H_2O$. *J. Inorg. Biochem.* **2006**, *100* (7), 1167–1175.

(55) Sharaby, C. M.; Amine, M. F.; Hamed, A. A. Synthesis , Structure Characterization and Biological Activity of Selected Metal Complexes of Sulfonamide Schiff Base as a Primary Ligand and Some Mixed Ligand Complexes with Glycine as a Secondary Ligand. *J. Mol. Struct.* **2017**, *1134*, 208–216.

(56) Ming, L. J. Structure and Function of “Metalloantibiotics.” *Med. Res. Rev.* **2003**, *23* (6), 697–762.

(57) Liu, Y. T.; Lian, G. D.; Yin, D. W.; Su, B. J. Synthesis, Characterization and Biological Activity of Ferrocene-Based Schiff Base Ligands and Their Metal (II) Complexes. *Spectrochim. Acta - Part A Mol. Biomol. Spectrosc.* **2013**, *100*, 131–137.

(58) Keypour, H.; Shayesteh, M.; Rezaeivala, M.; Chalabian, F.; Elerman, Y.; Buyukgungor, O. Synthesis, Spectral Characterization, Structural Investigation and Antimicrobial Studies of Mononuclear Cu(II), Ni(II), Co(II), Zn(II) and Cd(II) Complexes of a New Potentially Hexadentate N_2O_4 Schiff Base Ligand Derived from Salicylaldehyde. *J. Mol. Struct.* **2013**, *1032*, 62–68.

(59) Mondelli, M.; Bruné, V.; Borthagaray, G.; Ellena, J.; Nascimento, O. R.; Leite, C. Q.; Batista, A. A.; Torre, M. H. New Ni(II)-Sulfonamide Complexes: Synthesis, Structural Characterization and Antibacterial Properties. X-Ray Diffraction of $[Ni(Sulfisoxazole)_2(H_2O)_4] \cdot 2H_2O$ and $[Ni(Sulfapyridine)_2]$. *J. Inorg. Biochem.* **2008**, *102* (2), 285–292.

(60) Coombs, R. R.; Ringer, M. K.; Blacquiere, J. M.; Smith, J. C.; Neilsen, J. S.; Uh, Y. S.; Gilbert, J. B.; Leger, L. J.; Zhang, H.; Irving, A. M.; et al. Palladium(II) Schiff Base Complexes Derived from Sulfanilamides and Aminobenzothiazoles. *Transit. Met. Chem.* **2005**, *30* (4), 411–418.

(61) Zaki, M.; Arjmand, F.; Tabassum, S. Current and Future Potential of Metallo Drugs: Revisiting DNA-Binding of Metal Containing Molecules and Their Diverse Mechanism of Action. *Inorganica Chim. Acta* **2016**, *444*, 1–22.

(62) Chohan, Z. H.; Shad, H. A. Metal-Based New Sulfonamides: Design, Synthesis, Antibacterial, Antifungal, and Cytotoxic Properties. *J. Enzyme Inhib. Med. Chem.* **2012**, *27* (3), 403–412.

(63) Chohan, Z. H.; Shad, H. A.; Youssoufi, M. H.; Ben Hadda, T. Some New Biologically Active Metal-Based Sulfonamide. *Eur. J. Med. Chem.* **2010**, *45* (7), 2893–2901.

(64) Chohan, Z. H.; Mahmood-Ul-Hassan; Khan, K. M.; Supuran, C. T. In-Vitro Antibacterial, Antifungal and Cytotoxic Properties of Sulfonamide - Derived Schiff's Bases and Their Metal Complexes. *J. Enzyme Inhib. Med. Chem.* **2005**, *20* (2), 183–188.

(65) Khan, N. U. H.; Zaib, S.; Sultana, K.; Khan, I.; Mougang-Soume, B.; Nadeem, H.; Hassan, M.; Iqbal, J. Metal Complexes of Tosyl Sulfonamides: Design, X-Ray Structure, Biological Activities and Molecular Docking Studies. *RSC Adv.* **2015**, *5* (38), 30125–30132.

(66) Nocentini, A.; Ferraroni, M.; Carta, F.; Ceruso, M.; Gratteri, P.; Lanzi, C.; Masini, E.; Supuran, C. T. Benzenesulfonamides Incorporating Flexible Triazole Moieties Are Highly Effective Carbonic Anhydrase Inhibitors: Synthesis and Kinetic, Crystallographic, Computational, and Intraocular Pressure Lowering Investigations. *J. Med. Chem.* **2016**, *59* (23), 10692–10704.

(67) Yenikaya, C.; Ilkimen, H.; Demirel, M. M.; Ceyhan, B.; Bülbül, M.; Tunca, E. Preparation of Two Maleic Acid Sulfonamide Salts and Their Copper(II) Complexes and Antiglaucoma Activity Studies. *J. Braz. Chem. Soc.* **2016**, *27* (10), 1706–1714.

(68) Bruno, E.; Buemi, M. R.; Di Fiore, A.; De Luca, L.; Ferro, S.; Angeli, A.; Cirilli, R.; Sadutto, D.; Alterio, V.; Monti, S. M.; et al. Probing Molecular Interactions between Human Carbonic Anhydrases (HCAs) and a Novel Class of Benzenesulfonamides. *J. Med. Chem.* **2017**, *60* (10), 4316–4326.

(69) Mansour, A. M.; Abdel Ghani, N. T. Hydrogen-Bond Effect, Spectroscopic and Molecular Structure Investigation of Sulfamethazine Schiff-Base: Experimental and Quantum Chemical Calculations. *J. Mol. Struct.* **2013**, *1040*, 226–237.

(70) Mansour, A. M. Selective Coordination Ability of Sulfamethazine Schiff-Base Ligand towards Copper(II): Molecular Structures, Spectral and SAR Study. *Spectrochim. Acta - Part A Mol. Biomol. Spectrosc.* **2014**, *123*, 257–266.

(71) Nakahata, D. H.; Lustri, W. R.; Cuin, A.; Corbi, P. P. Crystal Structure, Spectroscopic Characterization and Antibacterial Activities of a Silver Complex with Sulfameter. *J. Mol. Struct.* **2016**, *1125*, 609–615.

(72) J.Gallagher, J.; K.Branski, L.; Williams-Bouyer, N.; Villarreal, C.; N.Herndon, D. Treatment of Infection in Burns. In *Total Burn Care*; Herndon, D. N., Ed.; Saunders Elsevier, 2012; pp 137–156.

(73) Ashraf, A.; Siddiqui, W. A.; Akbar, J.; Mustafa, G.; Krautscheid, H.; Ullah, N.; Mirza, B.; Sher, F.; Hanif, M.; Hartinger, C. G. Metal Complexes of Benzimidazole Derived Sulfonamide: Synthesis, Molecular Structures and Antimicrobial Activity. *Inorganica Chim. Acta* **2016**, *443*, 179–185.

(74) Alaghaz, A. N. M. A.; Bayoumi, H. A.; Ammar, Y. A.; Aldhlmani, S. A. Synthesis, Characterization, and Antipathogenic Studies of Some Transition Metal Complexes with N,O-Chelating Schiff's Base Ligand Incorporating Azo and Sulfonamide Moieties. *J. Mol. Struct.* **2013**, *1035*, 383–399.

(75) Ebrahimi, H. P.; Hadi, J. S.; Almayah, A. A.; Bolandnazar, Z.; Swadi, A. G.; Ebrahimi, A. Metal-Based Biologically Active Azoles and β-Lactams Derived from Sulfa Drugs. *Bioorganic Med. Chem.* **2016**, *24* (5), 1121–1131.

(76) Supuran, C. T. Carbonic Anhydrases: Novel Therapeutic Applications for Inhibitors and Activators. *Nat. Rev. Drug Discov.* **2008**, *7* (2), 168–181.

(77) Chohan, Z. H.; Supuran, C. T. Structure and Biological Properties of First Row D-Transition Metal Complexes with N-Substituted Sulfonamides. *J. Enzyme Inhib. Med. Chem.* **2008**, *23* (2), 240–251.

(78) Chohan, Z. H.; Shad, H. A.; Supuran, C. T. Synthesis, Characterization and Biological Studies of Sulfonamide Schiff's Bases and Some of Their Metal Derivatives. *J. Enzyme Inhib. Med. Chem.* **2012**, *27* (1), 58–68.

(79) Chohan, Z. H.; Supuran, C. T.; Ben Hadda, T.; Nasim, F. U. H.; Khan, K. M. Metal Based Isatin-Derived Sulfonamides: Their Synthesis, Characterization, Coordination Behavior and Biological Activity. *J. Enzyme Inhib. Med. Chem.* **2009**, *24* (3), 859–870.

(80) Mastrolorenzo, A.; Scozzafava, A.; Supuran, C. T. Antifungal Activity of Ag(I) and Zn(II) Complexes of Aminobenzolamide (5-Sulfanilylamido-1,3,4-Thiadiazole-2-Sulfonamide) Derivatives. *J. Enzyme Inhib.* **2000**, *15* (6), 517–531.

(81) Mastrolorenzo, A.; Scozzafava, A.; Supuran, C. T. Antifungal Activity of Silver and Zinc Complexes of Sulfadrug Derivatives Incorporating Arylsulfonylureido Moieties. *Eur. J. Pharm. Sci.* **2000**, *11* (2), 99–107.

(82) Chohan, Z. H.; Arif, M.; Akhtar, M. A.; Supuran, C. T. Metal-Based Antibacterial and Antifungal Agents: Synthesis, Characterization, and in Vitro Biological Evaluation of Co(II), Cu(II), Ni(II), and Zn(II) Complexes with Amino Acid-Derived Compounds. *Bioinorg. Chem. Appl.* **2006**, *2006*, 1–13.

(83) Chohan, Z. Metal-Based Sulfonamides: Their Preparation, Characterization and in-Vitro Antibacterial, Antifungal & Cytotoxic Properties. X-Ray Structure of 4-[(2-Hydroxybenzylidene) Amino] Benzenesulfonamide. *J. Enzyme Inhib. Med. Chem.* **2008**, *23* (1), 120–130.

(84) Mondelli, M.; Pavan, F.; De Souza, P. C.; Leite, C. Q.; Ellena, J.; Nascimento, O. R.; Facchin, G.; Torre, M. H. Study of a Series of Cobalt(II) Sulfonamide Complexes: Synthesis, Spectroscopic Characterization, and Microbiological Evaluation against M. Tuberculosis. Crystal Structure of $[Co(Sulfamethoxazole)_2(H_2O)_2]\cdot H_2O$. *J. Mol. Struct.* **2013**, *1036*, 180–187.

(85) Marques, L. L.; Manzoni de Oliveira, G.; Schulz Lang, E.; Anraku de Campos, M. M.; Soccol Gris, L. R. New Gold(I) and Silver(I) Complexes of Sulfamethoxazole: Synthesis, X-Ray Structural Characterization and Microbiological Activities of Triphenylphosphine(Sulfamethoxazolato-N_2)Gold(I) and (Sulfamethoxazolato)Silver(I). *Inorg. Chem. Commun.* **2007**, *10* (9), 1083–1087.

(86) Agertt, V. A.; Marques, L. L.; Bonez, P. C.; Dalmolin, T. V.; Manzoni De Oliveira, G. N.; De Campos, M. M. A. Evaluation of Antimycobacterial Activity of a Sulphonamide Derivative. *Tuberculosis* **2013**, *93* (3), 318–321.

(87) Agertt, V. A.; Bonez, P. C.; Rossi, G. G.; Flores, V. da C.; Siqueira, F. dos S.; Mizdal, C. R.; Marques, L. L.; de Oliveira, G. N. M.; de Campos, M. M. A. Identification of Antimicrobial Activity among New Sulfonamide Metal Complexes for Combating Rapidly Growing Mycobacteria. *BioMetals* **2016**, *29* (5), 807–816.

(88) Quintana, C.; Silva, G.; Klahn, A. H.; Artigas, V.; Fuentealba, M.; Biot, C.; Halloum, I.; Kremer, L.; Novoa, N.; Arancibia, R. New Cyrhetrenyl and Ferrocenyl Sulfonamides: Synthesis, Characterization, X-Ray Crystallography, Theoretical Study and Anti-Mycobacterium Tuberculosis Activity. *Polyhedron* **2017**, *134*, 166–172.

(89) Krátký, M.; Dzurková, M.; Janoušek, J.; Konečná, K.; Trejtnar, F.; Stolaříková, J.; VinŠová, J. Sulfadiazine Salicylaldehyde-Based Schiff Bases: Synthesis, Antimicrobial Activity and Cytotoxicity. *Molecules* **2017**, *22* (9), 1–15.

(90) Noreljaleel, A. E. M.; Wilhelm, A.; Bonnet, S. L.; Van Der Westhuizen, J. H. Synthesis and Bioactivity of Reduced Chalcones Containing Sulfonamide Side Chains. *J. Nat. Prod.* **2018**, *81* (1), 41–48.

(91) Gama, N. H.; Elkhadir, A. Y. F.; Gordhan, B. G.; Kana, B. D.; Darkwa, J.; Meyer, D. Activity of Phosphino Palladium(II) and Platinum(II) Complexes against HIV-1 and Mycobacterium Tuberculosis. *BioMetals* **2016**, *29* (4), 637–650.

(92) Chan, H.; Pearson, C. S.; Green, C. M.; Li, Z.; Zhang, J.; Belfort, G.; Shekhtman, A.; Li, H.; Belfort, M. Exploring Intein Inhibition by Platinum Compounds as an Antimicrobial Strategy. *J. Biol. Chem.* **2016**, *291* (43), 22661–22670.

Chapter 2
Synthesis and characterisation of imino pyridyl- and quinolyl iridium half-sandwich complexes

2.1 Introduction

Schiff bases and especially their metal complexes have been widely used for a vast multitude of applications and are vital in a number of fields not least of which include catalysis,[1] metal extraction,[2] electrochemistry[3] and several medical applications.[4–7] Schiff bases also play very important roles in biological systems, both of human and microbial origin and are widely found in nature.[8,9] This, coupled with the large scope of sulfonamides in medicine, as detailed in Chapter 1 and exemplified by sulfadiazine, sulfadoxine and sulfasalazine, make the combination of these two pharmacophores into one molecule the ideal drug candidate.[10] Such systems have widely been pursued in recent years with a further interest in the incorporation of metals which can greatly increase activity and provide an alternative targeting mechanism, thus decreasing chances of the development of drug resistance against such drug candidates.

Chellan et al.[11] previously found that such a system showed promising activity against malaria and surprisingly, a moderate activity against *Mycobacterium tuberculosis*. They had not, however, successfully purified some of their ligands as this was not the aim of their study nor was it vital to the final complexes that they were making. This however, meant that the ligands were not able to be tested alongside that of their complexes.[11] It could thus, not be definitively confirmed that the incorporation of the metal increased the activity for their system, though there was significant evidence for this, especially given the complete inactivity of their parent sulfonamide, sulfadoxine.[11]

It was therefore decided to investigate the purification of this ligand and if this proved unsuccessful, search for an alternative method of synthesis to obtain a pure sample. A variety of methods are available to synthesize Schiff bases with the most common method of preparation being the simple condensation of an aldehyde and an amine. It is this approach which was chosen to focus on. The ligands to be investigated are shown in Scheme 2.1.

2.2 Results and Discussion

2.2.1 Synthesis and characterisation of the Schiff base ligands, **L1 – L3**

An imino pyridyl sulfadoxine derivative, **L1** (Scheme 2.1), was synthesized through the Schiff base reaction of sulfadoxine and 2-pyridinecarboxaldehyde. The Schiff base condensation does not go to completion and purification is required, however, the polarity of sulfadoxine and the resulting ligand (**L1**) are very similar and their solubilities are near identical making the separation of these two compounds and the purification of the desired ligand challenging.

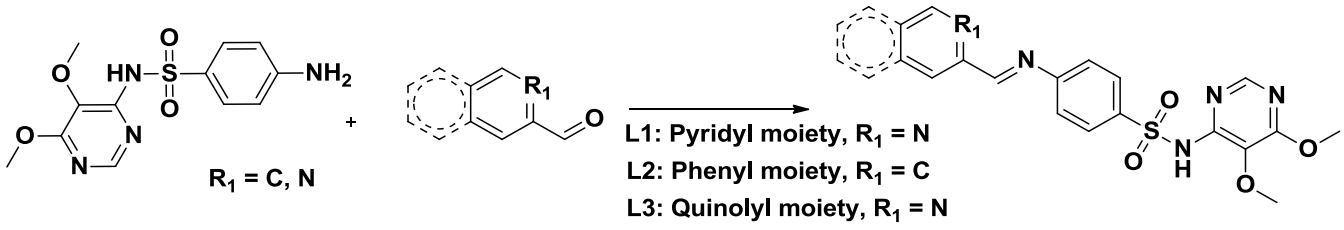

Scheme 2.1 – General reaction scheme for the synthesis of the sulfadoxine Schiff bases (**L1, L2** and **L3**).

Purification of **L1** is further complicated by its hydrolysis on silica, as numerous attempts with different solvent combinations failed to achieve any separation of sulfadoxine and **L1.** This is most likely due to the acidic nature of silica which can cause hydrolysis of these products.[12,13] Slight separation was achieved using neutral alumina TLC plates, however, subsequent attempts at using column chromatography with alumina only lead to co-elution of sulfadoxine and **L1** due to the similarity of their Rf values and the tailing of the compounds as they interact with the alumina. Recrystallisation using ethanol, methanol, toluene, acetone and dichloromethane was attempted, however, it was found that both sulfadoxine and **L1** would crystallise out together, requiring a large excess of **L1** to be in solution if this method was to result in a pure sample.

All infrared frequencies for the ligands and complexes were assigned while consulting a variety of references and more detailed information is available in the Experimental section.[14–17] The stretching frequencies observed for the imine bond and several other signals are generally lower than that seen in the references consulted, likely due to the greater electron-withdrawing nature of the systems under investigation.

L1 exhibits characteristic shifts in the IR spectrum (Figure 2.1) as the C=N stretches present in the pyrimidine ring of sulfadoxine shift from two strong absorption bands at 1597 cm^{-1} and 1580 cm^{-1} to a broad band at 1578 cm^{-1}. The C=N stretch of the imine is believed to contribute to the broad peak at 1578 cm^{-1} along with the C=N stretches of the pyrimidine and pyridine rings and as such, is masked. Additionally, the disappearance of the primary amine stretches at 3461 cm^{-1} and 3373 cm^{-1} and the N-H bend at 1650 cm^{-1} provide further support for its successful synthesis. The symmetric and asymmetric stretch of the S=O bond is seen at 1165 cm^{-1} and 1323 cm^{-1}, respectively. They have slightly shifted from their earlier positions in sulfadoxine at 1158 cm^{-1} and 1319 cm^{-1}. The C-O stretches of the methoxy groups are also clear, appearing at 1083 cm^{-1}, previously at 1090 cm^{-1}.

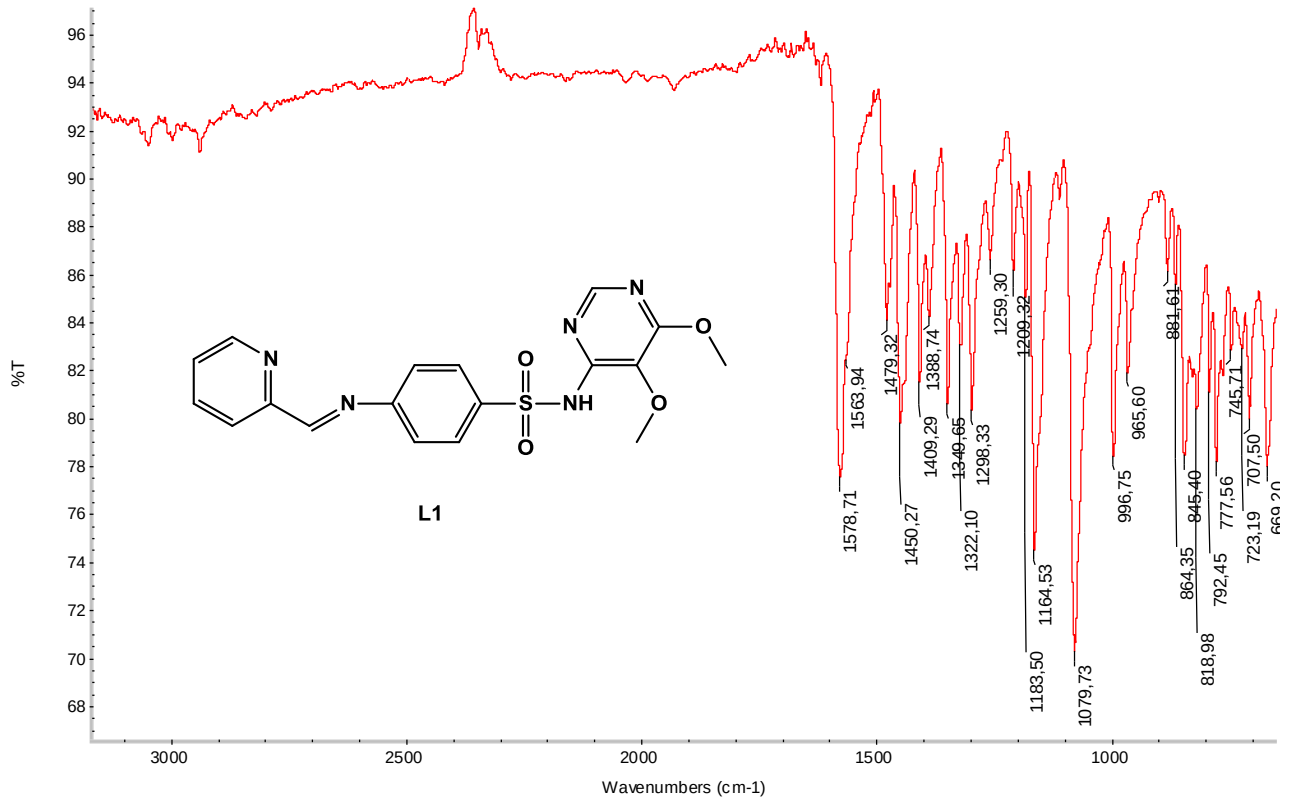

Figure 2.1 - IR spectrum of **L1** (ATR).

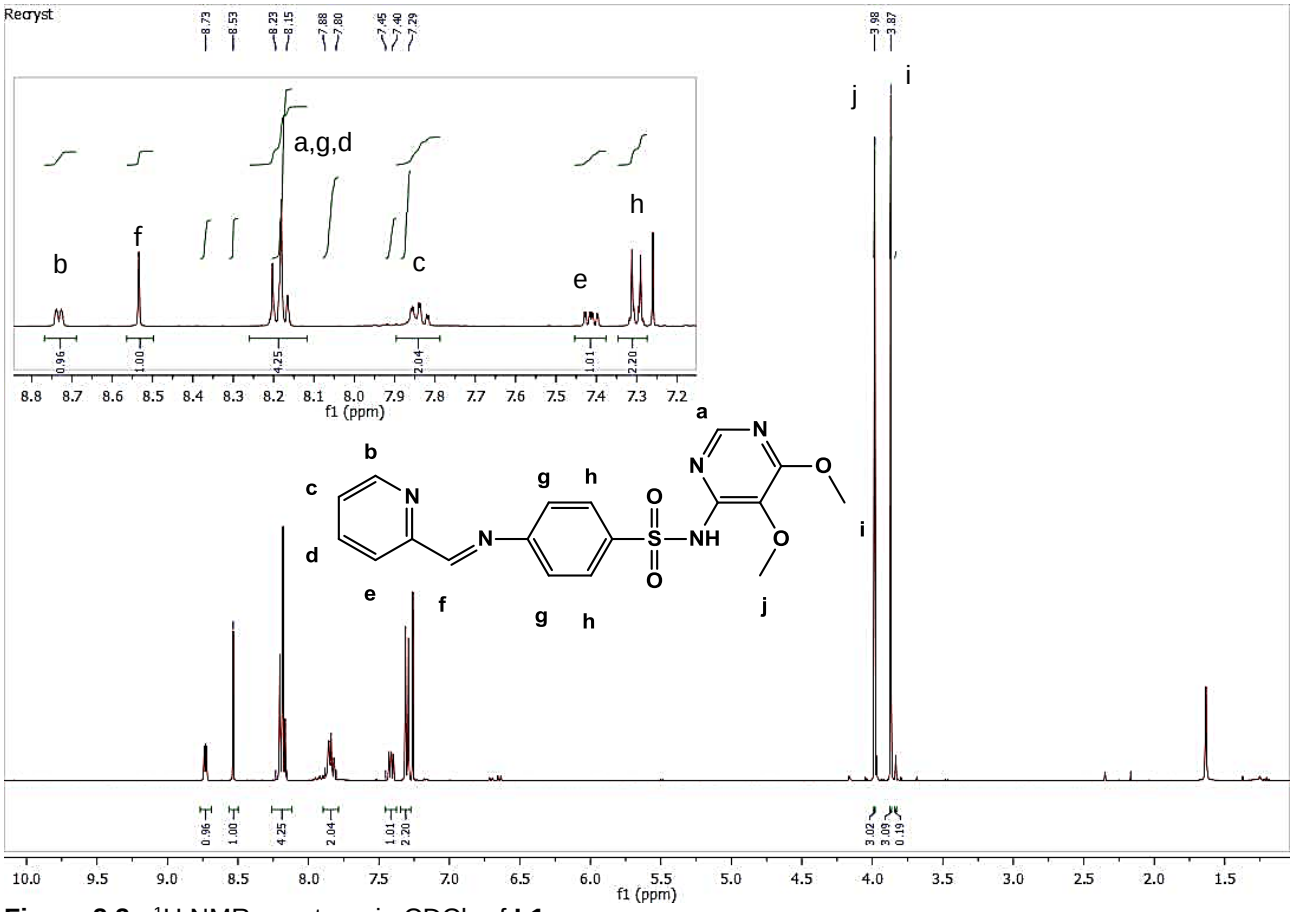

Figure 2.2 - ^{1}H NMR spectrum in $CDCl_3$ of **L1**.

The ^{1}H NMR spectrum in chloroform (Figure 2.2) shows the imine signal at 8.53 ppm and the proton *ortho* to the nitrogen of the pyridyl ring downfield at 8.73 ppm. The formation of **L1** is further confirmed by the shifting of the doublets of the benzene ring of sulfadoxine, usually seen around 6.7 ppm and 7.9 ppm, to 7.3 ppm and 8.2 ppm, respectively. The downfield shift is caused by withdrawal of electron density from the benzene ring which results in less effective shielding of the nuclei from the magnetic field. The two methoxy singlets are visible at 3.98 ppm and 3.87 ppm while the presence of trace amounts of sulfadoxine can be seen by the duplicate peaks slightly upfield at 3.97 ppm and 3.84 ppm.

The percentage product present can be calculated through the signals identified as those of sulfadoxine, **L1** and the aldehyde by means of quantitative NMR. There are two methods of quantitative NMR that can be used, namely, the relative method and the absolute method. The absolute method requires immense precision and all parameters to be kept constant. Additionally, it has certain prerequisites and conditions that need to be met regarding the experimental settings and experiment design.[18,19] The advantage of the absolute method is that it gives detailed information on the exact concentrations of the species in solution.[18,19]

The relative method is significantly less complicated and easy to use. It is based on the calculation of the mole fraction and the assumption that the signal intensity is directly related to the number of nuclei responsible for the signal.[18,19] This allows for the percentage fraction of a substance to be calculated if a representative signal of each species in solution can be identified. There is a general error of 1.5% associated with the values obtained through these methods which can be reduced through rigorous calibration.[18,19] If representative signals of all the species in solution are identified it is a simple matter to then calculate the percentage of each present. The ratio of sulfadoxine to ligand can easily be determined through the singlets of the methoxy protons in the case of the sulfonamide ligands worked with in this study (Figure 2.3).

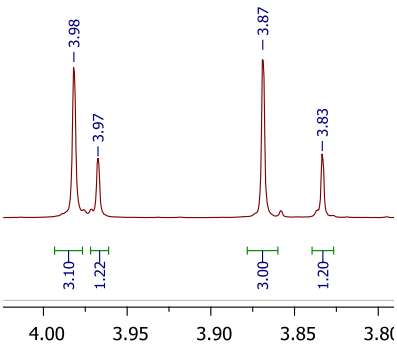

Figure 2.3 - Methoxy singlets of **L1** (3.98 ppm and 3.87 ppm) and sulfadoxine (3.97 ppm and 3.83 ppm) demonstrating the different ratios from which the yield can be calculated.

To determine the percentage yield of the product, the proton attached to the carbonyl of the aldehyde is also taken in to account. Equation 1 is then used, of which a full description can be found in literature.[19]

(Equation 1) $$\frac{\left(\frac{I_X}{N_X}\right)}{\left(\frac{\sum_{i=1}^{m} I_i}{N_i}\right)} \times 100\% = Percentage\ fraction\ X\ present\ in\ solution\ with\ m\ components$$

Where **I**, is the integral area and **N**, is the number of nuclei responsible for the signal. In summary, the mole fraction of the desired compound in solution is calculated and converted to mole percent. This method was used throughout this work to assist in optimising reactions to obtain a larger conversion of reagents to product and determine the yields obtained during synthesis.

Considering that full conversion was not obtained for the synthesis of **L1** and purification having proved unsuccessful, the search for a better method that would give a higher conversion of the Schiff base was continued with a preliminary investigation on a model system (**L2**, Scheme 2.1) using benzaldehyde as the aldehyde due to its greater affordability. Initially a microwave method similar to that employed in literature[11] with times ranging between 3 – 5 minutes and temperatures between 110 °C and 140 °C in ethanol was used. The percentage yield as determined by relative integration of the mixture of reagents and the product showed that 44% product had been obtained with no significant variation in yield obtained within these temperature and time variations. The crude was left to recrystallize from ethanol and after two weeks a precipitate formed which showed 74% product present leading to a hypothesis that a lengthy reaction time may be required, as the amine of sulfadoxine is not strongly nucleophilic due to the electron-withdrawing nature of the attached benzene ring. This was believed to be the case as previous recrystallisations had not led to any significant purification of the product due to the great similarity in solubility and polarity between the starting materials and the product as mentioned before.

In the pursuit of finding different synthetic methods for this reaction, the reagents were heated under reflux for 18 hours in ethanol. This led to a similar conversion as found for the microwave procedures thus far. The conversion to product was consistently close to the 50% mark, re-emphasising the equilibrium nature of this reaction. Attempts to push the equilibrium to form more product with catalytic amounts of acid, decreased its formation instead and a lower conversion was obtained, likely due to the increased rate of hydrolysis of the formed imine.

Crude **L2** was characterised by IR and ^{1}H NMR and very little variation was seen compared to the spectra of **L1**, as such its spectra have not been included. The characteristic broad signals of the ligand in the IR were seen at 1579 cm^{-1}, which was due to the overlapping of the various C=N stretches from the imine, pyridine and pyrimidine rings. The C-O stretches from the methoxy groups were at 1079 cm^{-1}. The imine is observed at 8.58 ppm and the two doublets of the sulfadoxine benzene ring at 7.43 ppm and 8.20 ppm.

Having determined that shorter microwave reaction times were not favourable and that lengthy reaction times in protic solvents did not significantly increase the yield obtained, it was decided to continue with the target molecule, **L1**. Wanting to compare the relative rates of the reactions, the reagents were heated under reflux in ethanol for 2.5 hours which led to a conversion of 69 %, significantly greater than that observed for **L2**. This is likely due to the presence of the nitrogen in the ring which is both more electron-withdrawing than carbon and can facilitate additional interactions between the amine. This occurs in the form of weak hydrogen bonding which helps orientate the molecule correctly for nucleophilic attack. The activation barrier is likely subsequently lowered, allowing the reaction to proceed much easier and faster than would be the case with benzaldehyde.

Toluene was used as a solvent following this, as water can have an adverse effect on the reaction. The reagents were heated under reflux in toluene for 48 hours giving a similar yield to the shorter reaction time in ethanol. It was decided to adapt the method with toluene for use in the microwave, which led to a reaction time of 1.5 hours at 175 °C, by estimating that half the reaction time is required for every 10 °C increase in reaction temperature. The new method gave a similar conversion to that of the non-microwave method in toluene, thus the reaction was increased to 2 hours which led to an increased yield of 78 %. This was significantly greater than had been achieved before. The improved conversion allowed for further purification via recrystallisation and trituration with ether, which had thus far proved inefficient, resulting in a sample that was 94% pure according to NMR, with only trace amounts of sulfadoxine still present.

Having obtained these promising results from the modification of the method, it was decided to apply this same method to the synthesis of the other ligand made by Chellan et al.[11] 2-Quinolinecarboxaldehyde and sulfadoxine were added together to a microwave vial and heated at 175 °C for 2 hours to obtain the crude ligand, **L3** (Scheme 2.1). The method was significantly less effective for this system and only 31% yield was obtained. Column chromatography was investigated and found that these Schiff bases were separable using silica TLC plates, however upon attempting a flash chromatography separation, several by-products formed with a large amount of tailing of the compounds on the silica, resulting in coelution. Various column conditions were probed, and a variety of percentages triethylamine were investigated to prevent the compounds from tailing. These were largely unsuccessful and other methods of separation were subsequently investigated instead, such as trituration and recrystallisation. These did not however afford product that was significantly purer than the initial crude. The reaction time was subsequently increased to 5 hours; however, the yield did not change significantly. The use of both a catalytic amount of acid and molecular sieves also failed to provide any breakthrough in the shifting of the equilibrium. It was then decided to increase the temperature to 200 °C and run the reaction for 3 hours. This method, followed by stirring in ether overnight, finally provided a purer crude sample, with **L3** constituting 50% of the sample. It exhibited characteristic signals at 1623 cm^{-1}, 1593 cm^{-1} and 1580 cm^{-1} for the C=N stretches, while the C-O stretches were observed at 1080 cm^{-1}. The symmetric and asymmetric S=O stretches were at

1161 cm^{-1} and 1317 cm^{-1}, respectively. Comparing the IR data of the three systems thus far discussed, the signals appear virtually the same with only slight differences. This would seem to indicate that the changes in the structure did not affect the bond strengths significantly enough to be observed by IR. The method obtained for **L3** was significantly less effective than that of **L1**, and the ligand signals of **L3** are just barely identifiable (Figure 2.4). The imine is not the signal furthest downfield for **L1**, however, in **L3** this is the case as the imine signal is at 8.72 ppm, while three of the four doublets of the quinoline ring are part of the multiplet between 8.28 ppm and 8.32 ppm, with the final doublet observed at 7.89 ppm. The phenylene protons are identified as doublets at 7.37 ppm and 8.22 ppm due to their characteristic look. The proton on the pyrimidine ring is at 8.19 ppm with the remaining aromatic signals appearing as multiplets shown on the spectrum in Figure 4 along with the other signals.

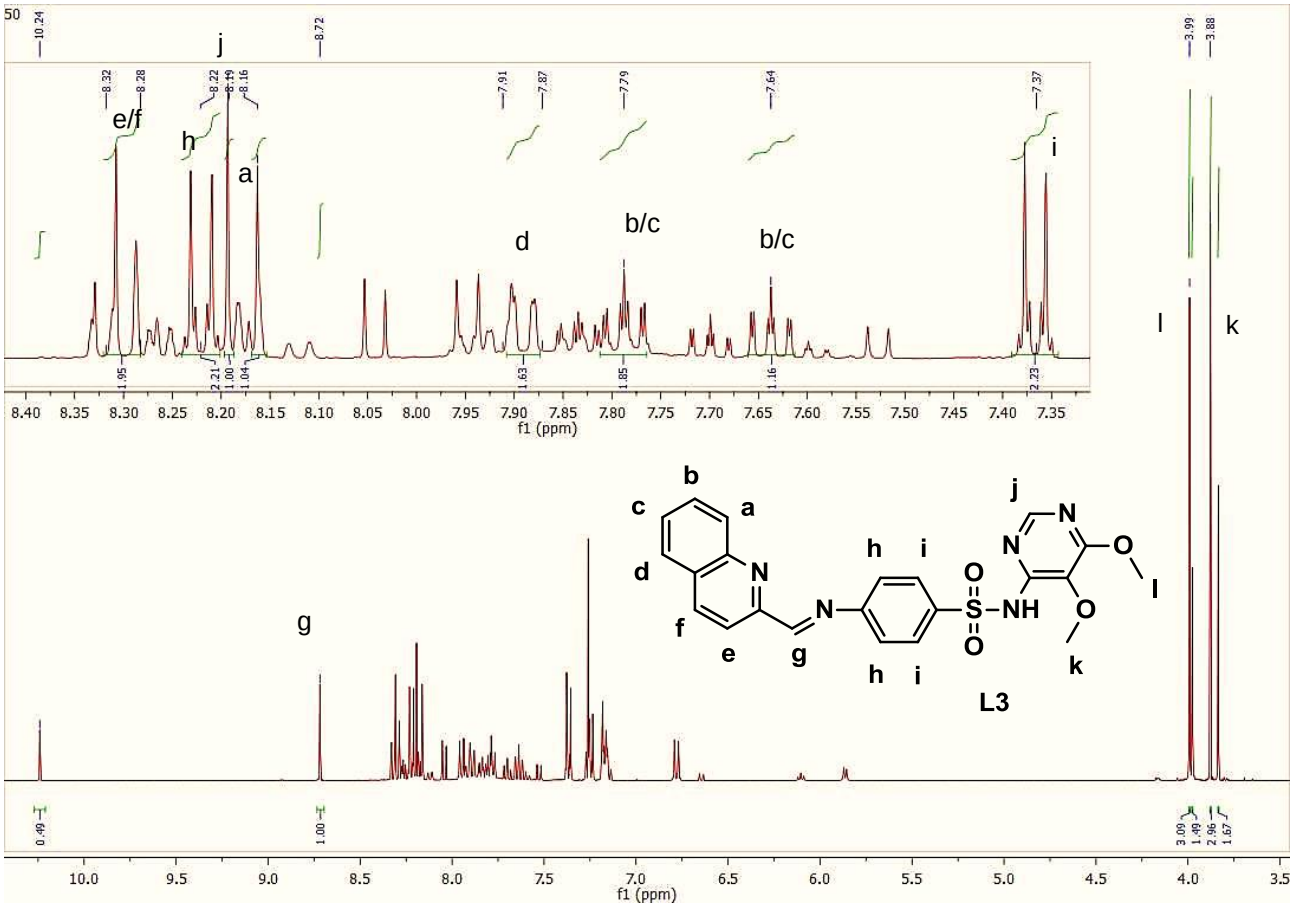

Figure 2.4 - ^{1}H NMR in $CDCl_3$ of crude **L3** identifying the signals of the ligand from that of the starting materials.

The crude ligand did not pose a major problem for the synthesis of the pure complexes as demonstrated by Chellan et al.[11], though it did complicate the purification in the case of the quinolyl complexes as expounded on later.

2.2.2 Synthesis of the iridium chlorido dimers

The iridium chlorido dimers were synthesized according to a literature method[24] which entailed heating hydrated iridium trichloride and an excess of the appropriate ligand in methanol at 140 °C for 5 min in a microwave reactor. The purification was simple and involved removing remaining excess ligand by washing with pentane several times.

Di-μ-chlorido(bis(chlorido(pentamethyl-η^5-cyclopentadienyl))iridium(III)) (iridium chlorido Cp^* dimer) was made by using pentamethylcyclopentadienyl as the ligand.

To prepare di-μ-chlorido(bis(chlorido(tetramethyl-η^5-cyclopentadienylbenzene))iridium(III)) (iridium chlorido Cp^{xPh} dimer) it was first necessary to synthesize its ligand. The ligand, (2,3,4,5-tetramethylcyclopenta-1,3-dien-1-yl)benzene (Cp^{xPh}), was prepared according to a procedure found in literature[25]. Phenyl magnesium bromide was added dropwise to a solution of 3,4,5-tetramethyl-2-cyclopentenone in freshly distilled THF and then heated under reflux for 3 hours after which it was quenched with HCl at 0 °C to give the required ligand in 67% yield. A detailed procedure can be found in the experimental section. Björgvinsson et al. noted that there are three positional isomers that can form.[26] These isomers are distinguished by the splitting pattern of the proton on the 5-membered ring (indicated in Figure 2.5 by an asterisk).

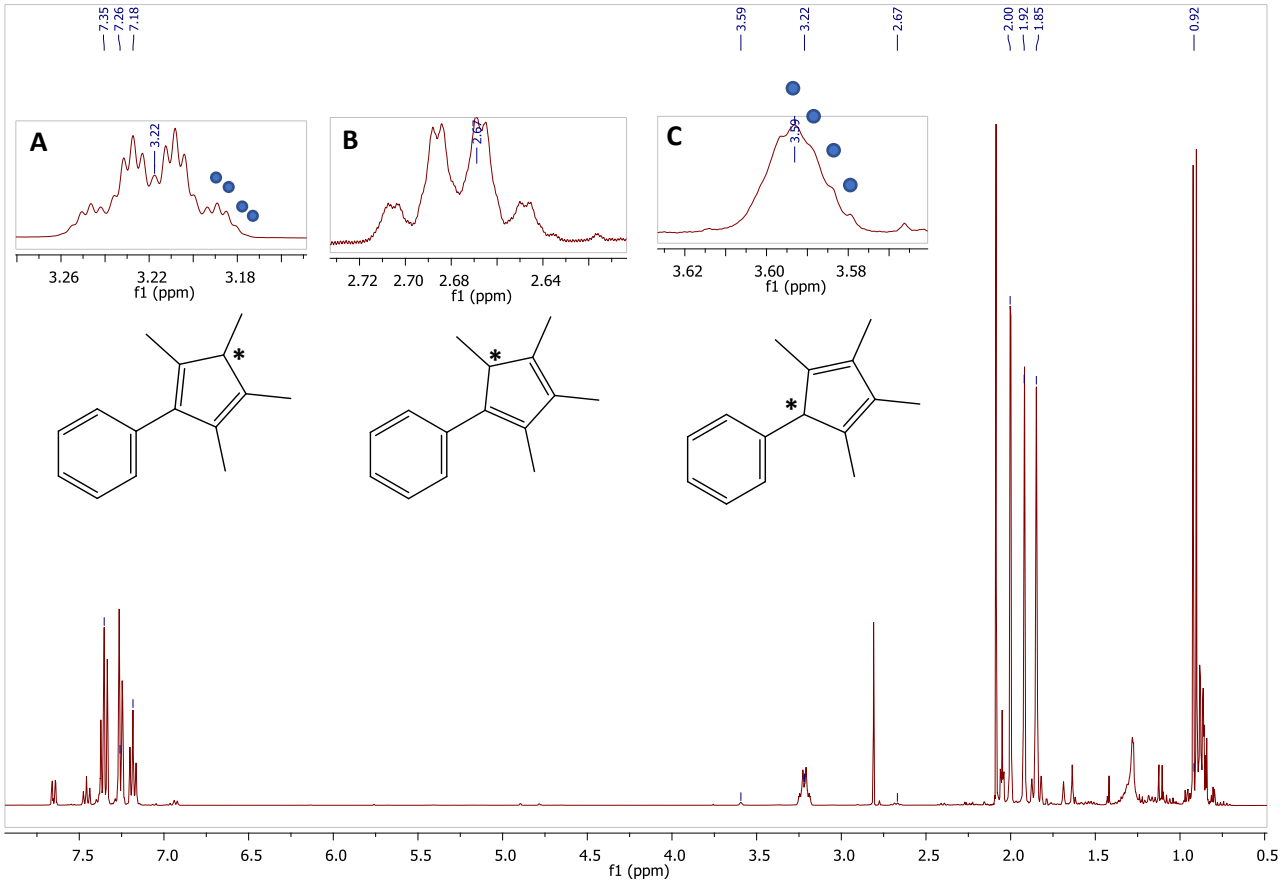

Figure 2.5 - ^{1}H NMR spectrum illustrating the major isomer (top left insert A) and two minor isomers (middle and top right inserts B and C) of the Cp^{xPh} ligand.

Insert A in Figure 2.5 is that of the major isomer and shows a quartet of septets. The other two isomers each have a quartet of quartets (insert B) and an ill resolved septet (insert C), respectively. One side of the peaks of the septets have been indicated with blue circles as they are difficult to spot due to the secondary splitting being the result of ^{4}J W-coupling. The major isomer composes about 90% of the product whereas the remaining two account for the other 10% of the product as seen from the relative integration of the protons in Figure 2.5. The *ortho* protons on the phenyl ring couple via w-coupling to the *para* proton indicated by their splitting and the same coupling constant of 1.3 Hz, which is typical for this type of coupling interaction. Furthermore, the coupling between the *meta* and *para* protons is also shown through the shared constant of 7.4 Hz. Due to unrestricted rotation, the *ortho* and *meta* protons are each only seen as one signal. The difference in the methyl shifts are because of the arrangements of the double bonds. This is illustrated by the rather upfield shift at 0.92 ppm which is the only methyl not attached to an alkene. This is further supported by considering the coupling constants of the methyl doublet and the CH quartet which both coincide, with a value of 7.6 Hz.

A comparison of the IR spectrum of Cp^{xPh} and its metal dimer shows a distinct shift in the ring substitution patterns of the phenyl ring, indicating that it has coordinated to the metal to form the bridged chlorido complex. Electron density is delocalized across the Cp ring as the ligand coordinates to the metal centre. Some of this delocalised charge feeds into the orbitals of the phenyl ring, thereby strengthening the bonds slightly as indicated by the shift to higher frequency of the ring substitution patterns between 1600 cm^{-1} and 2000 cm^{-1} as well as the C-H stretches around 3000 cm^{-1}. The Ir-Cl shift is unfortunately not visible as this usually appears below 500 wavenumbers. The presence of the three isomers do not make a difference to the final product obtained during the dimerization with the Iridium salt. This is due to the deprotonation of the hydrogen in the Cp ring which occurs as the metal coordinates to the two alkene bonds allowing the proton to be removed by one of the chlorides, resulting in one final product due to the delocalisation of the system and HCl as a by-product.

Samples of the third dimer, di-μ-chlorido(bis(chlorido(4-(tetramethyl-η^5-cyclopentadienyl)-1,1'-biphenyl))iridium(III)), were provided by a laboratory colleague, Lydia Jordaan.

2.2.3 Synthesis of the iridium (III) Schiff base complexes (**C1 – C6**)

Having successfully synthesized the iridium chlorido dimers, **L1** and **L3**, the complexes were subsequently synthesized by stirring the respective dimer in dry methanol at room temperature, followed by the addition of the required ligand. Ammonium hexafluorophosphate was added 24 hours later and the products were isolated as a microcrystalline red to orange powders 2 hours after its addition. Scheme 2.2 illustrates the complexes and their structures.

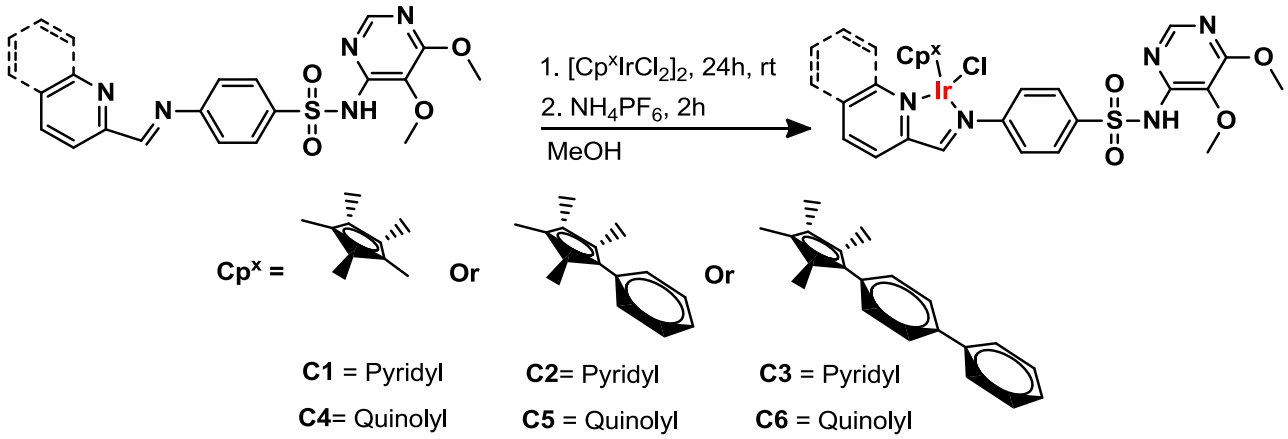

Scheme 2.2 - General synthetic approach to complexes **C1** through **C6** and their respective structures.

Complexes of **L1** (**C1** – **C3**) were easily synthesized and purified even though the crude ligand was used, however, the complexes of **L3** (**C4** – **C6**) were not as easily purified and several different purification methods and various recrystallizations were used to finally obtain pure complexes. This is most likely due to the significantly lower percentage of **L3** present in the ligand samples used, as was for **L1**. The FTIR for all complexes generally had little variation with the C=N stretches between 1579 cm^{-1} and 1582 cm^{-1} as a broad peak. The asymmetric sulfonamide stretches are found between 1334 cm^{-1} and 1338 cm^{-1}, while the symmetric stretches are between 1164 cm^{-1} and 1168 cm^{-1}. The C-O stretch from the methoxy groups appears between 1077 cm^{-1} and 1083 cm^{-1}. Finally, the counterion, PF_6, exhibits stretching frequencies between 832 cm^{-1} and 844 cm^{-1} with its bending vibration seen between 557 cm^{-1} and 558 cm^{-1}. There was a significant shift of the ligand signals upon complexation, indicating the large change in the distribution of electron density that takes place. A representative spectrum is shown in Figure 2.6.

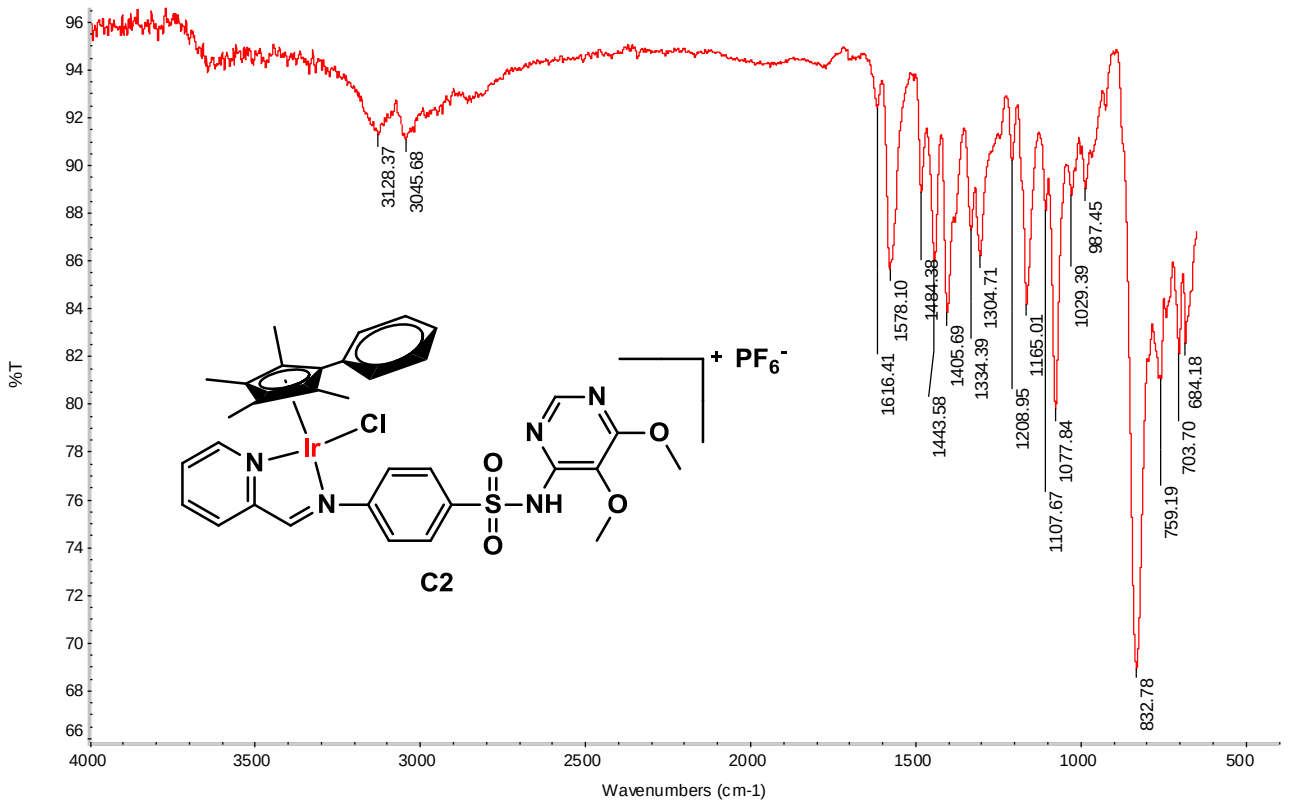

Figure 2.6 - IR spectrum of **C2**.

The reaction of **L1** with the iridium chlorido Cp^{xPh} dimer resulted in an orange microcryalline powder (**C2**) in a good yield of 72%. The FTIR spectrum (Figure 2.6) showed the strong stretch of the PF_6 counter ion at 832 cm^{-1}. A slight shift was also seen in the C=N stretch of the ligand from 1583 cm^{-1} in **L1** to 1578 cm^{-1}, showing a weakening of the bond as electron density is withdrawn from the pi cloud. Similar small shifts were seen for the symmetric and asymmetric S=O stretches of the sulfonamide group which appear in the complex at 1165 cm^{-1} and 1334 cm^{-1}, respectively, while no significant shift is observed for the C-O stretches.

The ^1H NMR spectra for the complexes in general show that the imine proton is observed between 9.26 ppm and 9.86 ppm with a downfield shift occurring as the Cp^x moiety is extended or moving from a pyridyl to quinolyl system. This is to be expected as the addition of groups with increasingly electron-withdrawing nature would result in the nuclei being less shielded from the external magnetic field. The same phenomenon was observed for the methyl signals on the Cp^x moiety which had signals appearing between 1.32 ppm and 1.82 ppm. The Cp* complexes (**C1** and **C4**) exhibited only one signal for the methyls due to the rapid rotation around the centroidal bond to the metal, while separate signals were seen for all the other complexes (**C2**, **C3**, **C5** and **C6**). Both the methyl groups of the methoxys and the aromatic signals of the substituted Cp^x ring did not show any significant shift. The methoxy methyls appeared around 3.82 – 3.83 ppm and 3.98 – 3.99 ppm and the aromatic region of the Cp^x moiety between 7.40 ppm and 7.82 ppm. Interesting to note are the protons of the phenylene ring attached to the sulfonamide which shift upfield with the increase in electron-withdrawing nature of the group added and are identified as two doublets between 8.31 ppm –

8.37 ppm and 7.92 ppm – 8.21 ppm, respectively. The same occurrence is observed for the proton directly attached to the pyrimidine ring which appears between 8.08 ppm and 8.13 ppm. This upfield shift with the extension of the Cp^x moiety could be due to an interaction between the respective aromatic rings which results in a greater shielding effect for these specific nuclei. Alternatively, the increased electron-withdrawing effect could be shifting the ring currents slightly which result in a more effective shielding of the protons.

The synthesis of **C2** is discussed below as a representative for the six complexes. The ^{1}H NMR spectrum (Figure 2.7) of **C2** in acetone showed the imine shift from 8.58 ppm in **L1** to 9.55 ppm indicating coordination to the metal centre. The downfield shift occurred due to the withdrawal of electron density by the metal centre which caused de-shielding of the imine proton by shifting the pi electron cloud of the double bond. This also further confirmed earlier observations from the FTIR spectrum.

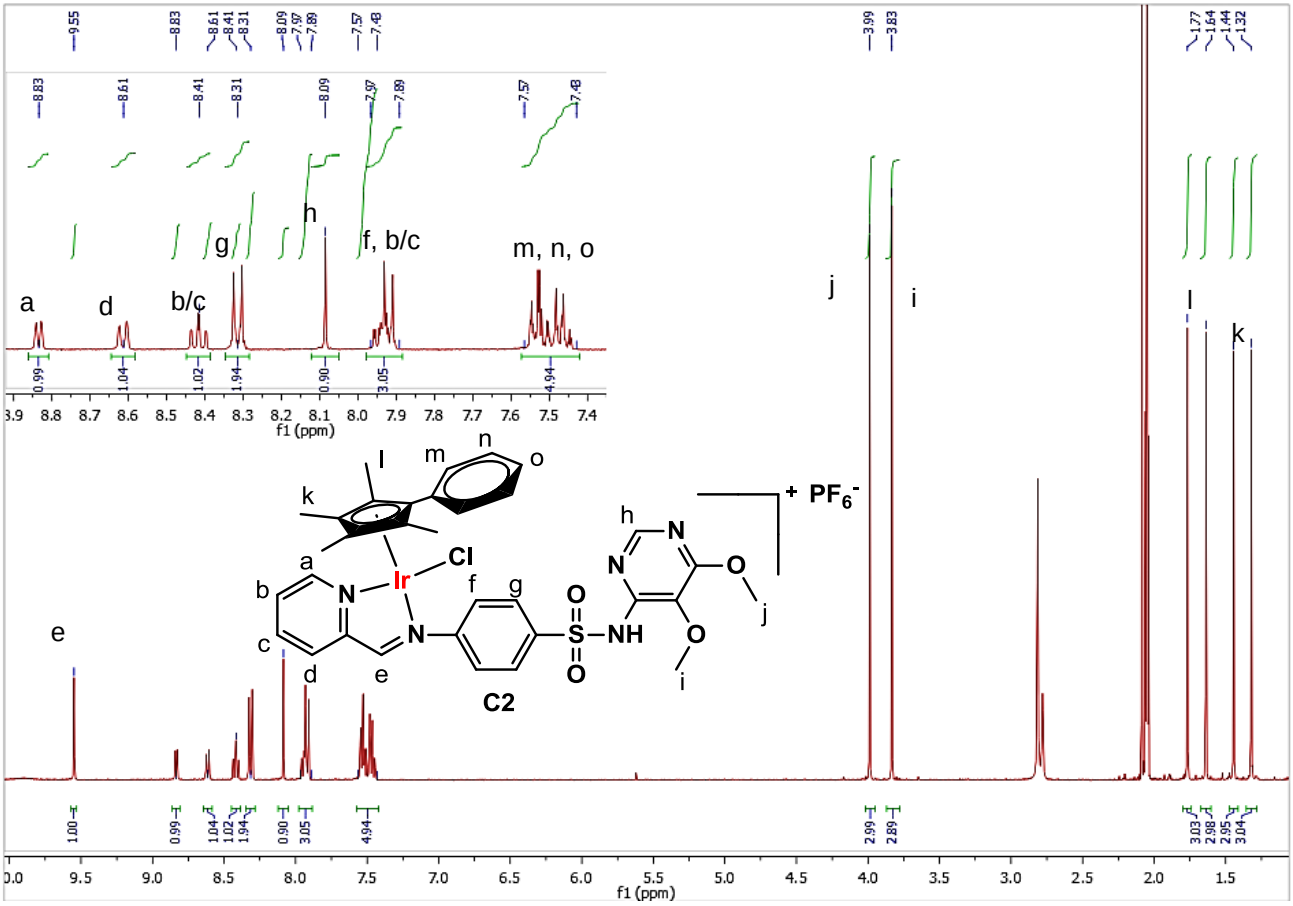

Figure 2.7- ^{1}H NMR spectrum in acetone-d_6 of the complex, **C2**.

The proton *ortho* to the nitrogen of the pyridyl ring shifts from 8.73 ppm to 8.83 ppm, showing the same pattern. Due to the chirality of the metal complex and addition of the phenyl group to the Cp* group, the methyls all have different shifts and are seen at 1.77 ppm, 1.64 ppm, 1.44 ppm and 1.32 ppm. One of the phenylene doublets shifts from 7.29 ppm to the multiplet at 7.93 ppm in **C2**, while the other appears in **L1** as a multiplet at 8.20 ppm which resolves upon complexation, appearing at

8.31 ppm in **C2**. Given that the doublet at 7.93 ppm experienced the largest downfield shift, it would likely indicate that this doublet is closest to the imine, while the doublet at 8.31 ppm is next to the sulfonamide group. Only one of the methoxy singlets shift from 3.87 ppm in **L1** to 3.83 ppm in **C2**, while the other stays at 3.99 ppm. Because of the large distance between these nuclei and the coordinated metal centre, no change would be expected, it is thus interesting to note that the electron density is affected on one of these groups. The methoxy group at 3.99 ppm is in a *meta* position of the ring which is likely why no change was observed for these nuclei as this position is not sensitive to changes in electron density, whereas the *ortho* substituted methoxy group is affected to a much greater extent due to its closer proximity as well as the additional hydrogen bonding interaction that is possible between the NH of the sulfonamide and the oxygen on this group. This is also why it is significantly more shielded than the nuclei of the *meta* methoxy, as the additional electrons from the hydrogen bonding interaction shield it slightly from the external magnetic field. From the spectrum it is noted that there are no longer any signs of duplicate methoxy peaks, indicating that the sulfadoxine impurity was successfully removed during purification of the complex. HPLC purity for all the complexes except **C5** was determined to be between 96.9% and 98.4%. The purity of **C5** was > 87%.

2.3 Conclusion

A successful method was developed for the synthesis of **L1** which achieved good conversion of 78%, despite the equilibrium nature of the reaction. The use of a model system was fundamental to the successful development of the new synthetic method. Furthermore, this method was applied to **L3** as well, but found to be lacking. This resulted in the determination of a new method for the synthesis of **L3** giving a final crude composition of 50% which was an improvement on that obtained previously, before other aspects of the project had to be focussed on.

The synthesis of the iridium chlorido bridge dimers was generally a facile process except for the biphenyl chlorido dimer which was provided by Lydia Jordaan.

Although the ligands had not been purified completely, this did not prevent the isolation of pure metal complexes in the case of **C1** – **C3**, however, in the case of the complexes with **L3** (**C4** – **C6**) their purification proved more challenging. This was because of the crude ligand, **L3**, which was significantly less pure than **L1** was.

2.4 Experimental

Chemicals and reagents. Sulfadoxine (95 %), 2-pyridinecarboxaldehyde, 2-quinolinecarboxaldehyde, 1,2,3,4,5-pentamethylcyclopentadiene, 2,3,4,5-tetramethyl-2-cyclopentenone, 4-bromobiphenyl, ammonium hexafluorophosphate, phenyl magnesium bromide solution in THF (1 M), $IrCl_3 \bullet nH_2O$, n-butyllithium solution, benzaldehyde, glacial acetic acid, p-toluenesulfonic acid monohydrate, all reagent solvents and deuterated solvents (methanol-d_4, acetone-d_6, dimethylsulfoxide-d_6, chloroform-d_1, deuterium oxide) were obtained from Sigma Aldrich (Merck). Di-μ-chlorido(bis(chlorido(pentamethyl-η^5-cyclopentadienyl))iridium(III)), di-μ-chlorido-(bis(chlorido(tetramethyl-η^5-cyclopentadienylbenzene))iridium(III)) and di-μ-chlorido(bis(chlorido(4-(tetramethyl-η^5-cyclopentadienyl)-1,1'-biphenyl))iridium(III)) were synthesized according to a literature method.[23] **L1**, **L3**, and **C1** – **C6** have been previously synthesized.[10]

Instrumentation. IR spectroscopy was performed using a Thermo Nicolet Nexus 470 by means of Attenuated Total Reflectance (ATR) mode and transmission esp. for compounds **L1**, **L2**, Cp^{xPh}, all Iridium chlorido dimers, **C1** and **C2**, while potassium bromide pellets and transmission esp. was used for all remaining samples. NMR data (^1H, ^{13}C) were recorded on either a 300 MHz Varian VNMRS or a 400 MHz Varian Unity Inova spectrometer. ^1H NMR chemical shifts are reported in ppm and coupling constants in Hertz and were internally referenced to methanol-d_4 (3.31 ppm), acetone-d_6 (2.05 ppm), dimethylsulfoxide-d_6 (2.50 ppm), chloroform-d_1 (7.26 ppm), or deuterium oxide (4.79 ppm). Data was processed using MestReNova 11.0.4-18998.

Microwave syntheses were carried out in a CEM Discover SP microwave reactor. Solvents were removed *in vacuo*, using a rotary evaporator, followed by removal of trace amounts of the remaining solvent using a high vacuum pump at *ca*. 0.08 mm Hg.

2.4.1 Synthesis of N-(5,6-dimethoxypyrimidin-4-yl)-4-((pyridin-2-ylmethylene) amino)benzenesulfonamide (**L1**)

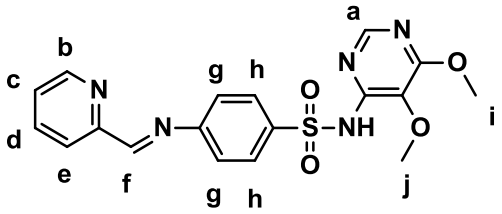

Sulfadoxine (1.00 x 10^2 mg, 0.322 mmol) was suspended in toluene (3 mL) in a 10 mL microwave vial. 2-pyridinecarboxaldehyde (41.4 mg, 36.8 µl, 0.386 mmol) was added to this suspension and the vial was placed in the microwave reactor (175 °C, 200 W, 2 h). The resulting yellow solution was allowed to cool and the solvent removed which resulted in a cream coloured solid which was then triturated with ether 5 times, then dried under high vacuum for 7 hours. The crude powder was recrystalized from hot toluene resulting in a crude yield of 95.4 mg. ^{1}H NMR (400 MHz, $CDCl_3$) δ 8.73 (d, 1H, H_b, $^3J_{(Hb-Hc)}$ 5.1 Hz), 8.53 (s, 1H, H_f), 8.23 - 8.15 (m, 4H, H_h, H_a and H_d), 7.88 - 7.80 (m, 1H, H_c), 7.45 - 7.39 (m, 1H, H_e), 7.30 (d, 2H, H_g, $^3J_{(Hg-Hh)}$ 8.2 Hz), 3.98 (s, 3H, H_i), 3.86 (s, 3H, H_j). FT-IR: 1583 cm^{-1} ($C=N_{imine}$, $C=N_{pyr}$, $C=N_{pyrim}$).

2.4.2 Synthesis of 4-(benzylideneamino)-N-(5,6-dimethoxypyrimidin-4-yl) benzenesulfonamide (**L2**)

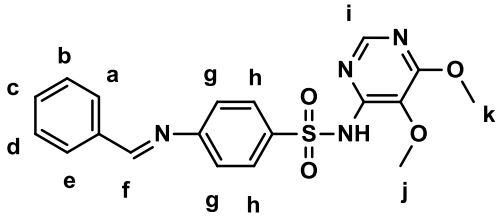

A suspension of sulfadoxine (507 mg, 1.63 mmol) in ethanol (10 mL) was added to a microwave vial (35.0 ml) followed by benzaldehyde (208 mg, 2.00 x 10^2 µl, 1.2 eq, 1.96 mmol) and the vial was sealed and placed in the microwave reactor (1.10 x 10^2 °C, 150 W, 3 min). The vial was then cooled, and the yellowish-brown solution filtered through Celite™. $MgSO_4$ was then used to dry the solution and was filtered off and the solvent removed from the filtrate. Recrystallisation was then attempted in ethanol layered with hexane, after nearly two weeks a brown tinged powder formed. The product was then dried under high vacuum for 4 hours and a crude yield of 496 mg was isolated. ^{1}H NMR (300 MHz, acetone) δ 8.73 (d, 1H, H_a, $^3J_{(Ha-Hb)}$ 4.8 Hz), 8.58 (s, 1H, H_f), 8.26 - 8.16 (m, 4H, H_b, H_d, and H_h), 8.11 (s, 1H, H_i), 7.99 - 7.93 (m, H, H_c), 7.56 - 7.50 (m, H, H_e), 7.43 (d, H_g, 2H, $^3J_{(Hg-Hh)}$ 8.8 Hz), 3.97 (s, H_k, 3H), 3.81 (s, H_j, 3H). FT-IR: 1581 cm^{-1} ($C=N_{imine}$, $C=N_{pyr}$, $C=N_{pyrim}$).

2.4.3 Synthesis of N-(5,6-dimethoxypyrimidin-4-yl)-4-((isoquinolin-3-yl methylene)amino)benzenesulfonamide (**L3**)

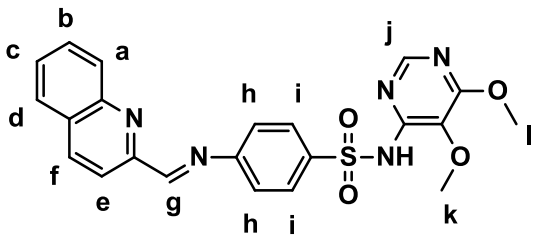

Sulfadoxine (50.0 mg, 0.161 mmol) was suspended in toluene (3.00 mL) in a microwave vial (10.0 mL) and 2-quinolinecarboxaldehyde (30.4 mg, 0.193 mmol) was added. The vial was then placed in the microwave reactor (200 °C, 250 W, 3 h). The solution was cooled, and the solvent removed. It was then stirred in ether overnight to remove any excess aldehyde, thereafter it was dried under high vacuum for 4 hours and a crude yield of 31.1 mg was obtained. ^{1}H NMR (400 MHz, $CDCl_3$) δ 8.72 (s, $H_{\mathbf{g}}$, 1H), 8.32 - 8.28 (m, $H_{\mathbf{f}}$ and $H_{\mathbf{e}}$, 2H), 8.22 (d, $H_{\mathbf{h}}$, 2H, $^{3}J_{(Hh\text{-}Hi)}$ 8.6 Hz), 8.19 (s, $H_{\mathbf{j}}$, 1H), 8.16 (m, $H_{\mathbf{a}}$, 1H), 7.91 - 7.87 (m, $H_{\mathbf{d}}$, 1H), 7.79 (t, $H_{\mathbf{c}}$, 1H, $^{3}J_{(Hc\text{-}Hb,d)}$ 7.5 Hz), 7.64 (t, $H_{\mathbf{b}}$, 1H, $^{3}J_{(Hb\text{-}Hc,a)}$ 7.5 Hz), 7.37 (d, $H_{\mathbf{i}}$, 2H, $^{3}J_{(Hi\text{-}Hh)}$ 8.6 Hz), 3.99 (s, $H_{\mathbf{l}}$, 3H), 3.88 (s, $H_{\mathbf{k}}$, 3H). FT-IR: ($C{=}N_{imine}$, $C{=}N_{pyr}$, $C{=}N_{pyrim}$) 1580 cm^{-1}.

2.4.4 Synthesis of (2,3,4,5-tetramethylcyclopenta-1,3-dien-1-yl) benzene (HCp^{xPh})[24]

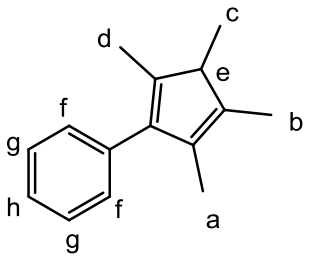

2,3,4,5-tetramethyl-2-cyclopentenone (2.73 mL, 18.1 mmol) was added to freshly distilled THF (25.0 mL). Phenyl magnesium bromide (23.5 mL ,1 M in THF, 23.5 mmol.) was added to this solution dropwise over 10 min and the reaction was heated under reflux (67.0 °C, 3 h) thereafter, while under positive pressure of argon. The reaction was cooled to 0 °C and quenched with HCl (25.0 mL, 1 M), stirring for a further 1 hour while allowing it to warm to room temperature. The mixture was diluted with ether (40.0 mL) and washed with distilled water (3 x 30.0 mL) and dried over $MgSO_4$. It was then filtered, and the solvent removed to yield 3.50 g of a light pale-yellow liquid. This was dry loaded onto a column (220 - 440, approx. 24.0 g, hexane) and a pale-yellow liquid was obtained in 67% yield. ^{1}H NMR (400 MHz, Acetone-d_6) δ 7.35 (t, $H_{\mathbf{g}}$, 2H, $^{3}J_{(Hg\text{-}Hf,h)}$ 7.4 Hz), 7.26 (dd, $H_{\mathbf{f}}$, 2H, $^{3}J_{(Hf\text{-}Hg)}$ 8.3 Hz, $^{4}J_{(Hf\text{-}Hh)}$ 1.3 Hz), 7.18 (tt, $H_{\mathbf{h}}$, 1H, $^{3}J_{(Hh\text{-}Hg)}$ 7.4 Hz, $^{4}J_{(Hh\text{-}Hf)}$ 1.3 Hz), 3.22 (quartet of septets, $H_{\mathbf{e}}$, 1H, $^{3}J_{(He\text{-}Hc)}$ 7.6 Hz, $^{4}J_{(He\text{-}Hb,d)}$ 1.7 Hz), 2.00 (s, $H_{\mathbf{d}}$, 3H), 1.92 (s, $H_{\mathbf{a}}$, 3H), 1.85 (s, $H_{\mathbf{b}}$, 3H), 0.92 (d, $H_{\mathbf{c}}$, 3H, $^{3}J_{(Hc\text{-}He)}$ 7.6 Hz).

2.4.5 General synthesis of the Schiff base complexes

The respective Iridium chlorido dimer was stirred in MeOH for 2 minutes after which the crude ligand (**L1** or **L3**) was added and the solution stirred at room temperature for 24 hours. Thereafter, NH_4PF_6 was added and the solution stirred for a further 2 hours. The solvent was then removed and the crude residue redissolved in acetone and then filtered through a plug of Celite™ to remove the ammonium chloride that precipitated out. The crude residue was recrystallised from an appropriate solvent system and in the cases of **C4** and **C5**, column chromatography was employed thereafter.

2.4.6 Synthesis of $[IrCl(C_{18}H_{17}N_5O_4S)(C_{10}H_{15})PF_6]$ (**C1**)

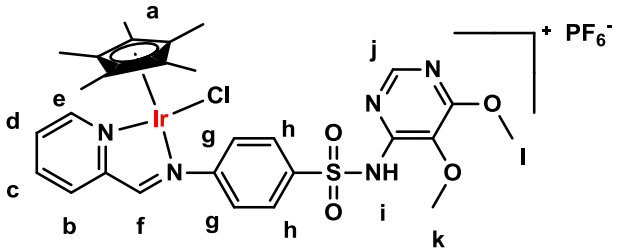

Di-μ-chlorido(bis(chlorido(pentamethyl-η^5-cyclopentadienyl))iridium(III)) (200 mg, 0.250 mmol), crude **L1** (200 mg, 0.500 mmol) and NH_4PF_6 (81.6 mg, 0.500 mmol) was reacted in MeOH (35.0 mL) and recrystallised from MeOH/ether to give an orange microcrystalline powder in 82% yield (372 mg). ^{1}H NMR (400 MHz, Acetone-d_6) δ 9.88 (broad singlet, NH (H_i)), 9.49 (s, H_f, 1H), 9.22 (d, H_e, 1H, $^3J_{(He-Hd)}$ 5.4 Hz) 8.56 (d, H_b, 1H, $^3J_{(Hb-Hc)}$ 7.4 Hz), 8.43(t, H_d, 1H, $^3J_{(Hd-Hc,e)}$ 7.3 Hz), 8.37 (d, H_h, 2H, $^3J_{(Hh-Hg)}$ 8.8 Hz), 8.11 (s, H_j, 1H), 8.05 (t, H_c, 1H, $^3J_{(Hc-Hd,b)}$ 7.3 Hz) , 7.97 (d, H_g, 2H, $^3J_{(Hg-Hh)}$ 8.8 Hz), 3.98 (s, H_l, 3H), 3.83 (s, H_k, 3H), 1.52 (s, H_a, 15H). FT-IR: 1579 cm^{-1} ($C=N_{imine}$, $C=N_{quin}$, $C=N_{pyrim}$), 1338 cm^{-1} $(SO_2)_{As}$, 1168 cm^{-1} $(SO_2)_{Sym}$, 1079 cm^{-1} (C-O), 840 cm^{-1} (PF_6). HPLC purity: 97.0%; t_r = 12.97 min.

2.4.7 Synthesis of $[IrCl(C_{18}H_{17}N_5O_4S)(C_{15}H_{17})PF_6]$ (**C2**)

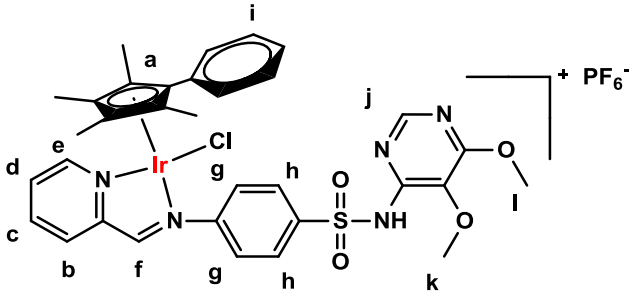

Di-μ-chlorido(bis(chlorido(tetramethyl-η^5-cyclopentadienylbenzene))iridium(III)) (50.0 mg, 0.0626 mmol), crude **L1** (50.0 mg, 0.125 mmol) and NH_4PF_6 (20.4 mg, 0.125 mmol) was reacted in MeOH (5.00 mL) and recrystallised from acetone/hexane to give a microcrystalline red powder isolated in 72% yield (80.1 mg). ^{1}H NMR (300 MHz, Acetone-d_6) δ 9.89 (broad peak, **NH**), 9.54 (s, H_f, 1H), 8.83 (d, H_e, 1H, $^3J_{(He-Hd)}$ 5.6 Hz), 8.61 (d, H_b, 1H, $^3J_{(Hb-Hc)}$ 7.6 Hz), 8.41 (t, H_c, 1H, $^3J_{(Hc-Hb,d)}$ 7.6 Hz) , 8.32 (d, H_h, 2H, $^3J_{(Hh-Hg)}$ 8.1 Hz), 8.09 (s, H_j, 1H), 7.88-7.97 (m, H_d and H_g, 3H), 7.42-7.57 (m, H_i, 5H), 3.99 (s, H_l, 3H), 3.83 (s, H_k, 3H), 1.76 (s, H_a, 3H), 1.63 (s, H_a, 3H), 1.44 (s, H_a, 3H), 1.32 (s, H_a, 3H). FT-

IR: 1578 cm^{-1} ($C=N_{imine}$, $C=N_{quin}$, $C=N_{pyrim}$), 1334 cm^{-1} $(SO_2)_{As}$, 1165 cm^{-1} $(SO_2)_{Sym}$, 1077 cm^{-1} (C-O), 832 cm^{-1} (PF_6). HPLC purity: 98.4%; t_r = 16.51 min.

2.4.8 Synthesis of $[IrCl(C_{18}H_{17}N_5O_4S)(C_{21}H_{21})PF_6]$ (**C3**)

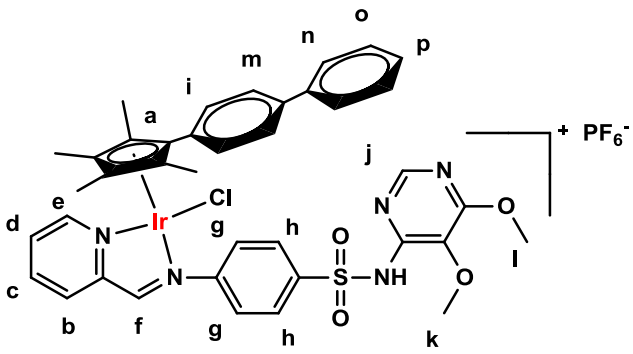

Di-μ-chlorido(bis(chlorido(4-(tetramethyl-η^5-cyclopentadienyl)-1,1'-biphenyl))iridium(III)) (47.3 mg, 0.0440 mmol), crude **L1** (88.0 mg (40% pure), 0.0880 mmol) and NH_4PF_6 (14.4 mg, 0.0880 mmol) was reacted in MeOH (5.00 mL) and recrystallized from acetone/ether to give a red crystalline solid in 72% yield (66.0 mg). ^{1}H NMR (400 MHz, Acetone-d_6) δ 9.90 (broad peak, **NH**), 9.56 (s, H_f, 1H), 8.88 (d, H_e, 1H, $^3J_{(He-Hd)}$ 5.6 Hz), 8.62 (d, H_b, 1H, $^3J_{(Hb-Hc)}$ 7.8 Hz), 8.42 (t, H_c, 1H, $^3J_{(Hc-Hb,d)}$ 7.8 Hz) , 8.33 (d, H_h, 2H, $^3J_{(Hh-Hg)}$ 8.8 Hz), 8.08 (s, H_j, 1H), 7.98-7.91 (m, H_d and H_g, 3H), 7.82-7.71 (m, H_i and H_n, 4H), 7.65 (d, H_m, 2H, $^3J_{(Hm-Hi)}$ 8.5 Hz), 7.56 - 7.40 (m, H_o and H_p, 3H), 3.99 (s, H_l, 3H), 3.82 (s, H_k, 3H), 1.82 (s, H_a, 3H), 1.65 (s, H_a, 3H), 1.50 (s, H_a, 3H), 1.32 (s, H_a, 3H). FT-IR: 1581 cm^{-1}, 1617 cm^{-1} ($C=N_{imine}$, $C=N_{quin}$, $C=N_{pyrim}$), 1336 cm^{-1} $(SO_2)_{As}$, 1166 cm^{-1} $(SO_2)_{Sym}$, 1082 cm^{-1} (C-O), 842 cm^{-1} (PF_6), 557 cm^{-1} (PF_6). HPLC purity: 98.4%; t_r = 20.73 min.

2.4.9 Synthesis of $[IrCl(C_{22}H_{21}N_5O_4S)(C_{10}H_{15})PF_6]$ (**C4**)

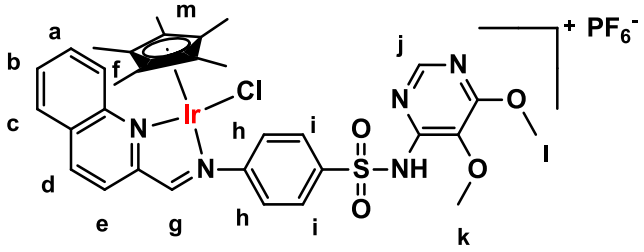

Di-μ-chlorido(bis(chlorido(pentamethyl-η^5-cyclopentadienyl))iridium(III)) (18.4 mg, 0.0230 mmol), crude **L3 (**52.0 mg (40% pure), 0.0460 mmol) and NH_4PF_6 (7.50 mg, 0.046 mmol) was reacted in MeOH (5.00 mL) and recrystallised from DCM/Hexane. A dark oily residue was isolated which was recrystallised two more times before it was purified using column chromatography (220 - 440, approx. 35 g, 2% MeOH/DCM) to give a dark brown powder in 40% yield (17.6 mg). ^{1}H NMR (400 MHz, $CDCl_3$) δ 9.26 (s, H_g, 1H), 8.56 (d, H_d, 1H, $^3J_{(Hd-He)}$ 8.3 Hz), 8.50 (d, H_f, 1H, $^3J_{(Hf-Ha)}$ 8.8 Hz), 8.42 (d, H_d, 1H, $^3J_{(Hd-He)}$ 8.3 Hz), 8.35 (d, H_i, 2H, $^3J_{(Hi-Hh)}$ 8.8 Hz), 8.21 (d, H_h, 2H, $^3J_{(Hh-Hi)}$ 8.8 Hz), 8.13 (s, H_j, 1H), 8.08 (d, H_c, 1H, $^3J_{(Hc-Hb)}$ 8.0 Hz), 7.95 (t, H_a, 1H, $^3J_{(Ha-Hf)}$ 7.6 Hz), 7.88 (t, H_b, 1H, $^3J_{(Hb-Hc)}$ 8.0 Hz), 3.99 (s, H_l, 3H), 3.92 (s, H_k, 3H), 1.38 (s, H_m, 15H). FT-IR: 1582 cm^{-1} ($C=N_{imine}$, $C=N_{quin}$,

C=N_{pyrim}), 1338 cm^{-1} $(SO_2)_{As}$, 1167 cm^{-1} $(SO_2)_{Sym}$, 1083 cm^{-1} (C-O), 844 cm^{-1} (PF_6), 558 cm^{-1} (PF_6). HPLC purity: 98.1%; $t_{r'}$ = 15.53 min.

2.4.10 Synthesis of $[IrCl(C_{22}H_{21}N_5O_4S)(C_{15}H_{17})PF_6]$ (**C5**)

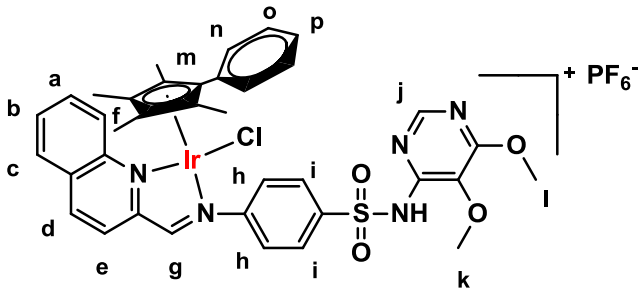

Di-μ-chlorido(bis(chlorido(tetramethyl-η^5-cyclopentadienylbenzene))iridium(III)) (50.0 mg, 0.0543 mmol), crude **L3** (97.6 mg (50% pure), 0.109 mmol) and NH_4PF_6 (17.7 mg, 0.109 mmol) was reacted in MeOH (5.00 mL) and then recrystallized from Acetone/Hexane. The crude brown solid was then columned (220 - 440, approx. 35 g, 2% MeOH/DCM) to give a crude dark brown powder, which was stirred with NH_4PF_6 (17.7 mg, 0.109 mmol) in MeOH (5.00 mL) and recrystallised from DCM/Hexane resulting in 60.0 mg of a crude brown solid. ^{1}H NMR (400 MHz, $CDCl_3$) δ 10.29 (s, H_g, 1H), 8.96 (d, H_d, 1H, $^3J_{(Hd-He)}$ 8.5 Hz), 8.47 (d, H_f, 1H, $^3J_{(Hf-Ha)}$ 8.1 Hz), 8.43 - 8.37 (m, H_i, 2H), 8.30 (d, H_e, 1H, $^3J_{(He-Hd)}$ 8.5 Hz), 8.28 - 8.23 (m, H_h, 2H), 8.11 (s, H_j, 1H), 7.95 (d, H_c, 1H, $^3J_{(Hc-Hb)}$ 8.1 Hz), 7.66 (m, $H_{a/b}$, 1H), 7.57 - 7.38 (m, $H_{n,o,p}$, 5H), 7.27 - 7.22 (m, $H_{a/b}$, 1H), 3.98 (s, H_l, 3H), 3.88 (s, H_k, 3H), 1.73 (s, H_m, 3H), 1.57 (s, H_m, 3H), 1.30 (s, H_m, 3H), 1.15 (s, H_m, 3H). FT-IR: 1581 cm^{-1} 1620 cm^{-1} ($C=N_{imine}$, $C=N_{quin}$, $C=N_{pyrim}$), 1337 cm^{-1} $(SO_2)_{As}$, 1164 cm^{-1} $(SO_2)_{Sym}$, 1082 cm^{-1} (C-O), 844 cm^{-1} (PF_6), 558 cm^{-1} (PF_6). HPLC purity: 87.7%; $t_{r'}$ = 18.63 min.

2.4.11 Synthesis of $[IrCl(C_{22}H_{21}N_5O_4S)(C_{21}H_{21})PF_6]$ (**C6**)

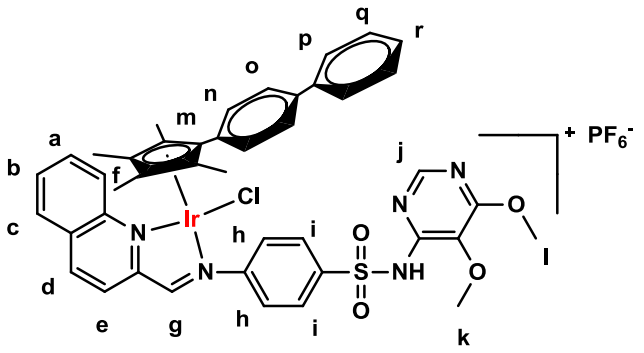

Di-μ-chlorido(bis(chlorido(4-(tetramethyl-η^5-cyclopentadienyl)-1,1'-biphenyl))iridium(III)) (50.0 mg, 0.0466 mmol), crude **L3** (83.8 mg (50% pure), 0.0932 mmol) and NH_4PF_6 (15.2 mg, 0.0932 mmol) was reacted in MeOH (5.00 mL) and then recrystallized from acetone/ether 5 times to obtain a dark brown powder in 10% yield (10.2 mg). ^{1}H NMR (300 MHz, Acetone-d_6) δ 9.86 (s, H_g, 1H), 8.98 (d, H_d, 1H, $^3J_{(Hd-He)}$ 8.3 Hz), 8.63 (d, H_e, 1H, $^3J_{(He-Hd)}$ 8.3 Hz), 8.49 (d, H_f, 1H, $^3J_{(Hf-Ha)}$ 8.8 Hz), 8.36 (m, H_h, 2H), 8.30 (d, H_c, 1H, $^3J_{(Hc-Hb)}$ 8.3 Hz), 8.15 (m, H_i, 2H), 8.10 (s, H_j, 1H), 7.94 - 7.88 (m, $H_{a/b}$, 1H), 7.78 - 7.72 (m, $H_{n,o,a/b}$, 5H), 7.65 - 7.60 (m, H_p, 2H), 7.55 - 7.43 (m, $H_{q,r}$, 3H), 3.98 (s, H_l, 3H), 3.83 (s, H_k,

3H), 1.77 (s, H_m, 3H), 1.58 (s, H_m, 3H), 1.38 (s, H_m, 3H), 1.33 (s, H_m, 3H). FT-IR: 1582 cm^{-1}, 1620 cm^{-1} ($C=N_{imine}$, $C=N_{quin}$, $C=N_{pyrim}$), 1338 cm^{-1} $(SO_2)_{As}$, 1166 cm^{-1} $(SO_2)_{Sym}$, 1082 cm^{-1} (C-O), 843 cm^{-1} (PF_6), 558 cm^{-1} (PF_6). HPLC purity: 96.9%; $t_{r'}$ = 22.39 min.

2.4.12 HPLC method and purity determination

Purity measurements by HPLC were carried out using the Agilent 1220 system with a DAD and 100 µL loop. The column used was a Kinetex® 5 µm C18 100 Å, 150 x 4.6 mm with a 5 µm pore size. The mobile phase was H_2O 0.1% TFA/MeCN 0.1% TFA at gradients of t=0 min 10% B, t=30 min 80% B, t=40 min 80% B, t=41 min 10% B, and t=55 min 10% B over a 55 min period. The flow rate was 1 mL min^{-1}, and the detection wavelength was set at 254 nm and 400 nm with the reference wavelength at 360 nm. Samples were dissolved in 10% MeCN/90% H_2O at ca. 100 µM. Sample injections were half the loop volume (50 µL) with needle washes of MeCN and H_2O between injections. It was assumed that all species in a sample have the same extinction coefficient at 254 nm and 400 nm. All peaks were manually integrated.

2.5 References

(1) Jacobsen, E. N.; Zhang, W.; Muci, A. R.; Ecker, J. R.; Deng, L. Highly Enantioselective Epoxidation Catalysts Derived from l,2-Diaminocyclohexane. *J. Am. Chem. Soc.* **1991**, *113* (18), 7063–7064.

(2) Hirayama, N.; Takeuchi, I.; Honjo, T.; Kubono, K.; Kokusen, H. Ion-Pair Extraction System for the Mutual Separation of Lanthanides Using Divalent Quadridentate Schiff Bases. *Anal. Chem.* **1997**, *69* (23), 4814–4818.

(3) Yurt, A.; Bereket, G.; Kivrak, A.; Balaban, A.; Erk, B. Effect of Schiff Bases Containing Pyridyl Group as Corrosion Inhibitors for Low Carbon Steel in 0.1 M HCl. *J. Appl. Electrochem.* **2005**, *35* (10), 1025–1032.

(4) Padhye, S.; Yang, H.; Jamadar, A.; Cui, Q. C.; Chavan, D.; Dominiak, K.; McKinney, J.; Banerjee, S.; Dou, Q. P.; Sarkar, F. H. New Difluoro Knoevenagel Condensates of Curcumin, Their Schiff Bases and Copper Complexes as Proteasome Inhibitors and Apoptosis Inducers in Cancer Cells. *Pharm. Res.* **2009**, *26* (8), 1874–1880.

(5) Da Silva, C. M.; Da Silva, D. L.; Modolo, L. V.; Alves, R. B.; De Resende, M. A.; Martins, C. V. B.; De Fátima, Â. Schiff Bases: A Short Review of Their Antimicrobial Activities. *J. Adv. Res.* **2011**, *2* (1), 1–8.

(6) Gaballa, A. S.; Asker, M. S.; Barakat, A. S.; Teleb, S. M. Synthesis, Characterization and Biological Activity of Some Platinum(II) Complexes with Schiff Bases Derived from Salicylaldehyde, 2-Furaldehyde and Phenylenediamine. *Spectrochim. Acta - Part A Mol. Biomol. Spectrosc.* **2007**, *67* (1), 114–121.

(7) Pandeya, S. N.; Sriram, D.; Nath, G.; de Clercq, E. Synthesis, Antibacterial, Antifungal and Anti-HIV Evaluation of Schiff and Mannich Bases of Isatin and Its Derivatives with Triazole. *Arzneimittelforschung.* **2000**, *50* (1), 55–59.

(8) Garrett, R. H.; Grisham, C. M. *Biochemistry, Fifth Edition, International Edition*; Brooks/Cole Cengage learning: London, 2013.

(9) Eliot, A. C.; Kirsch, J. F. Pyridoxal Phosphate Enzymes: Mechanistic, Structural, and Evolutionary Considerations. *Annu. Rev. Biochem.* **2004**, *73*, 383–415.

(10) World Health Organization. *WHO Model Formulary 2008*; Couper, M. R., Mehta, D. K., Eds.; World Health Organization, 2008.

(11) Chellan, P.; Avery, V. M.; Duffy, S.; Triccas, J. A.; Nagalingam, G.; Tam, C.; Cheng, L. W.; Liu, J.; Land, K. M.; Clarkson, G. J.; et al. Organometallic Conjugates of the Drug Sulfadoxine for Combatting Antimicrobial Resistance. *Chem. -Eur. J.* **2018**, *24* (40), 10078–10090.

(12) Sahai, N. Is Silica Really an Anomalous Oxide? Surface Acidity and Aqueous Hydrolysis Revisited. *Environ. Sci. Technol.* **2002**, *36*, 445–452.

(13) Clayden, J.; Greeves, N.; Warren, S. Nucleophilic Substitution at C=O with Loss of Carbonyl Oxygen. In *Organic Chemistry*; Oxford University Press: New, 2012.

(14) Mondal, S.; Mandal, S. M.; Mondal, T. K.; Sinha, C. Spectroscopic Characterization, Antimicrobial Activity, DFT Computation and Docking Studies of Sulfonamide Schiff Bases. *J. Mol. Struct.* **2017**, *1127*, 557–567.

(15) Mansour, A. M. Selective Coordination Ability of Sulfamethazine Schiff-Base Ligand towards Copper(II): Molecular Structures, Spectral and SAR Study. *Spectrochim. Acta - Part A Mol. Biomol. Spectrosc.* **2014**, *123*, 257–266.

(16) Mondelli, M.; Pavan, F.; De Souza, P. C.; Leite, C. Q.; Ellena, J.; Nascimento, O. R.; Facchin, G.; Torre, M. H. Study of a Series of Cobalt(II) Sulfonamide Complexes: Synthesis, Spectroscopic Characterization, and Microbiological Evaluation against M. Tuberculosis. Crystal Structure of $[Co(Sulfamethoxazole)_2(H_2O)_2]\cdot H_2O$. *J. Mol. Struct.* **2013**, *1036*, 180–187.

(17) Lampman, G.; Pavia, D.; Kriz, G.; Vyvyan, J. *Spectroscopy International Edition*, 4th ed.; Brooks/Cole Cengage learning: Belmont, 2010.

(18) Bharti, S. K.; Roy, R. Quantitative H NMR Spectroscopy. *Trends Anal. Chem.* **2012**, *35*, 5–26.

(19) Malz, F. Quantitative NMR in the Solution State. In *NMR Spectroscopy in Pharmaceutical Analysis*; Holzgrabe, U., Wawer, I., Diehl, B., Eds.; Elsevier B.V., 2008; pp 43–62.

(20) Hayes, B. L. *Microwave Synthesis Chemistry at the Speed of Light*, 1st ed.; CEM Publishing: Matthews, 2002.

(21) Gedye, R.; Smith, F.; Westaway, K.; Ali, H.; Baldisera, L.; Laberge, L.; Rousell, J. The Use of Microwave Ovens for Rapid Organic Synthesis. *Tetrahedron Lett.* **1986**, *27* (3), 279–282.

(22) Mingos, D. M. P.; Baghurst, D. R. Tilden Lecture. Applications of Microwave Dielectric Heating Effects to Synthetic Problems in Chemistry. *Chem. Soc. Rev.* **1991**, *20*, 1–47.

(23) Larhed, M.; Hallberg, A. Microwave-Assisted High-Speed Chemistry: A New Technique in Drug Discovery. *Drug Discov. Today* **2001**, *6* (8), 406–416.

(24) Tönnemann, J.; Risse, J.; Grote, Z.; Scopelliti, R.; Severin, K. Efficient and Rapid Synthesis of Chlorido-Bridged Half-Sandwich Complexes of Ruthenium, Rhodium, and Iridium by Microwave Heating. *Eur. J. Inorg. Chem.* **2013**, *2013* (26), 4558–4562.

(25) Morris, D. M.; McGeagh, M.; De Peña, D.; Merola, J. S. Extending the Range of Pentasubstituted Cyclopentadienyl Compounds: The Synthesis of a Series of Tetramethyl(Alkyl or Aryl)Cyclopentadienes (Cp^{*R}), Their Iridium Complexes and Their Catalytic Activity for Asymmetric Transfer Hydrogenation. *Polyhedron* **2014**, *84*, 120–135.

(26) Björgvinsson, M.; Halldorsson, S.; Arnason, I.; Magull, J.; Fenske, D. Preparation and Characterization of $(C_5Me_4Ph)TiCl_3$, the Oxochloride Complexes $[(C_5Me_4Ph)TiCl_2]_2(\mu\text{-}O)$ and $[(C_5Me_4Ph)TiCl(\mu\text{-}O)]_3$ and the Oxo-Complex $[(C_5Me_4Ph)Ti]_4(\mu\text{-}O)_6$. The X-Ray Crystal Structures of $[(C_5Me_4Ph)TiCl_2]_2(\mu\text{-}O)$ and $[(C_5Me_4Ph)Ti]_4(\mu\text{-}O)_6$. *J. Organomet. Chem.* **1997**, *544*, 207–215.

Chapter 3
Synthesis and characterisation of pyridyl and quinolyl amido iridium half-sandwich complexes

3.1 Introduction

The amide functional group is widely found in the natural environment and the human world and has found a great variety of applications in both areas. This is illustrated by its incredible importance in proteins as it is peptide linkages which are essentially the backbone of proteins and influence the secondary structure of these proteins through its hydrogen bonding interactions.[1,2] Proteins are fundamental to many physiological processes and we could not exist without them. Furthermore, upon polymerisation to form polyamides many useful products such as nylon can be obtained which consists of chains of carbon atoms linked together through amide bonds.[1,3,4] When the amide bonds link together benzene rings instead of aliphatic carbon chains then Kevlar is formed which has been extremely important in the production of body armour, bicycle tyres and sails to name but a few of its applications.[1] The functional group consists primarily of a nitrogen atom bonded to a carbonyl group in a planar fashion due to the resonance between the lone pair of the nitrogen and that of the carbonyl double bond.[1,3] Amides are primarily formed from their parent carboxylic acids and free amines by means of a condensation reaction after the acid has been activated, though there are a wide variety of other methods to obtain the functionality.[1,3–6] Amides also have a wide variety of medicinal applications and are found in many useful drugs such as paracetamol and penicillin. It is estimated that at least a single amide bond is present in more than 25% of all drugs.[1,2]

Given the relevance of the amido functionality as a potential potent pharmacophore against a variety of diseases it was decided to incorporate it as part of the sulfonamide derivatives that were being investigated. This was especially favoured in light of the equilibrium nature of the imine systems that had thus far been investigated and had posed significant hurdles in their synthesis and purification.

In addition, several amide metal complexes have exhibited promising antimicrobial[7,8] and antiproliferative[9,10] activity, further prompting the synthesis and testing of the metal complexes of our derivatives in the hope that the metal complexes may prove effective against other diseases as well.

3.2 Results and Discussion

3.2.1 Synthesis and characterisation of the amido-sulfadoxine ligands, **L4** and **L5**

There are many ways that amides can be synthesized and various coupling agents can be employed when attempting these reactions.[11] One of the most commonly used methods was chosen and involved the generation of an acid chloride followed by the subsequent substitution with the primary amine of sulfadoxine. The specific methodology used in this case was adapted from three different sources.[12–14] The acid chloride was generated *in situ* from the parent acid (2-picolinic acid or

quinaldic acid) using oxalyl chloride and a catalytic amount of DMF as this method was envisioned to produce the least number of by-products, namely only carbon monoxide and carbon dioxide. Several literature methods[15–22] used triethylamine to neutralise or limit the quantity of free HCl that is formed upon substitution with a free amine, however, it was a point of concern that this base, though weak, might be able to deprotonate the sulfonamide NH and thus potentially cause the reaction to fail or greatly impact the yield. A test reaction was thus carried out and sulfadoxine was stirred with two equivalents of triethylamine under the same conditions of the reaction procedure that would be followed. Thereafter, an extraction with water was done and both the organic and water layers analysed to see which layer sulfadoxine was in. Only the water layer contained sulfadoxine, which confirmed the earlier hypothesis that triethylamine would not only neutralise the HCl but could also affect the starting material.

The base was initially left out, however after seeing no significant change in the TLC after 24 hours it was decided to add a weaker base such as pyridine. Likely due to the late stage that the base was added there was still no reaction seen. The low solubility of sulfadoxine in DCM could also have contributed to the absence of a reaction. After workup only starting material was obtained, thus the reaction was reattempted with the weaker base from the beginning while simultaneously changing the solvent in the quenching step to acetonitrile in which sulfadoxine is significantly more soluble. The general method for the reaction is shown in Scheme 3.1.

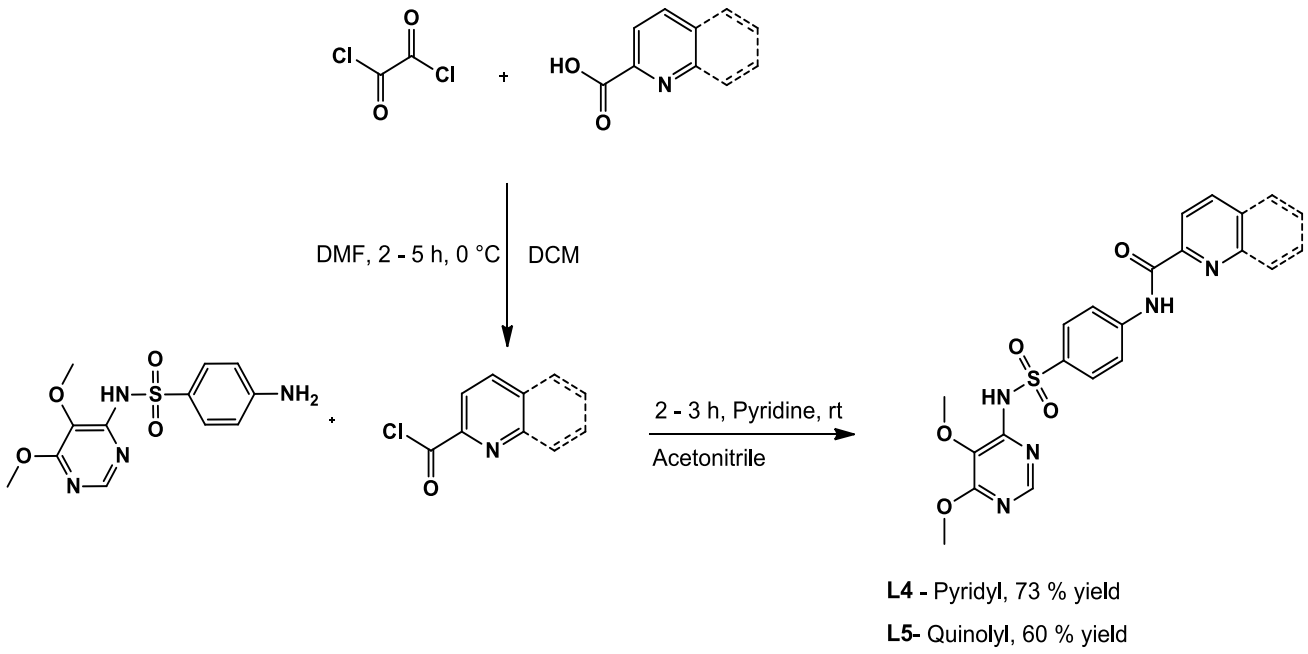

Scheme 3.1 - Generation of the required amido ligands, **L4** and **L5**, via an acid chloride in moderate yields.

Under these new conditions the reaction was successful as indicated by both its IR spectrum (Figure 3.1) and the ^{1}H NMR spectrum (Figure 3.2).

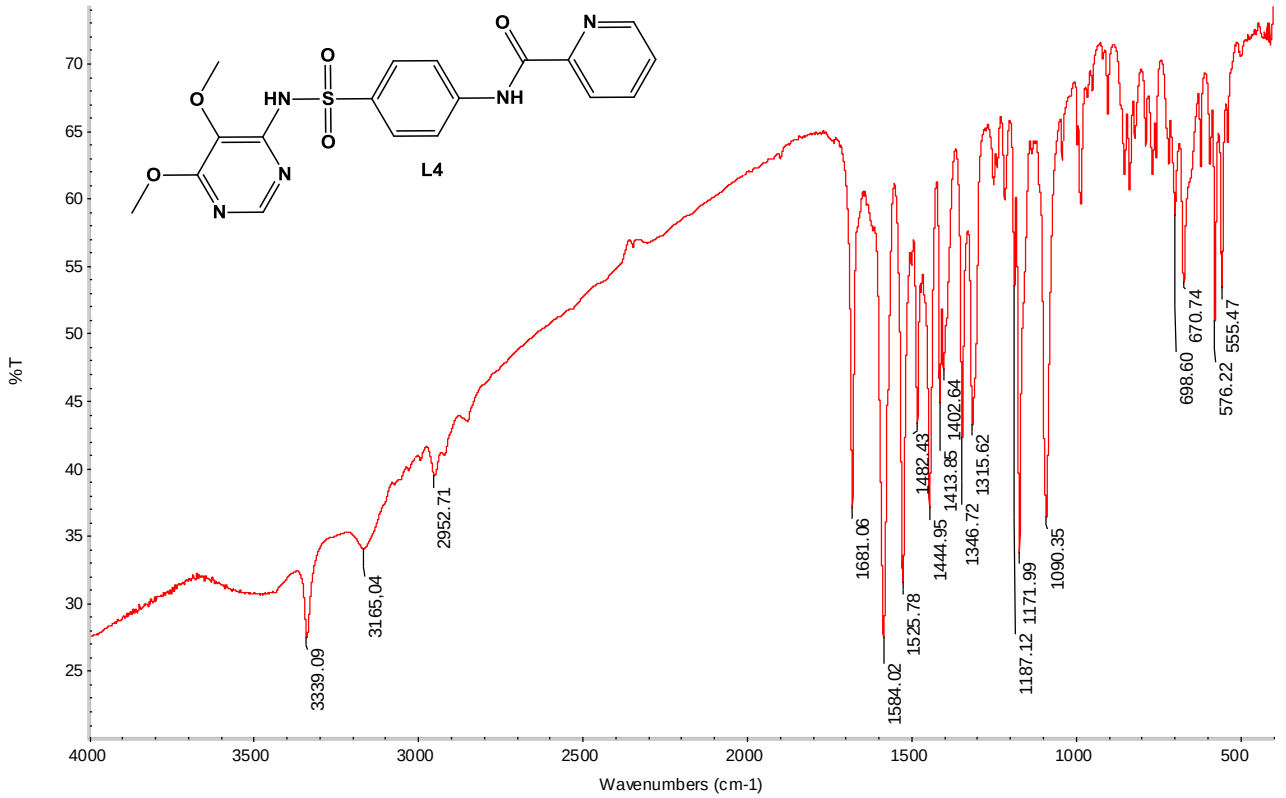

Figure 3.1 - IR spectrum (KBr) of **L4** illustrating the N-H stretches clearly.

The IR spectrum of **L4** (Figure 3.1) shows the amide N-H stretch at 3339 cm^{-1} with the sulfonamide N-H stretch appearing at 3165 cm^{-1}, with a slightly lower frequency as compared to sulfadoxine, indicating a slight weakening of the N-H bond induced by the increased electron withdrawing character of the aromatic moiety introduced. The carbonyl stretch appears at 1681 cm^{-1} previously seen in the acid as a very broad signal at 1720 cm^{-1}.

The ^{1}H NMR (Figure 3.2) shows the two NH protons at 10.27 ppm (amide) and 7.82 ppm (sulfonamide) with the proton *ortho* to the nitrogen of the pyridyl ring appearing at 8.62 ppm. This ligand, nor its quinolyl analogue, had been synthesized before, thus their ^{13}C NMR and MS spectra were also obtained.

The ^{13}C NMR is shown in Figure 3.3 and all seven of the quaternary carbons for **L4** are seen, with the amide carbon identified as the most deshielded at 162.35 ppm. The methoxy CH_3 carbons are also readily identified at 60.57 ppm and 54.15 ppm, respectively. The phenylene CH carbons overlap due to symmetry resulting in two signals instead of four. Overall, only six signals are observed instead of the expected seven for the CH carbon signals.

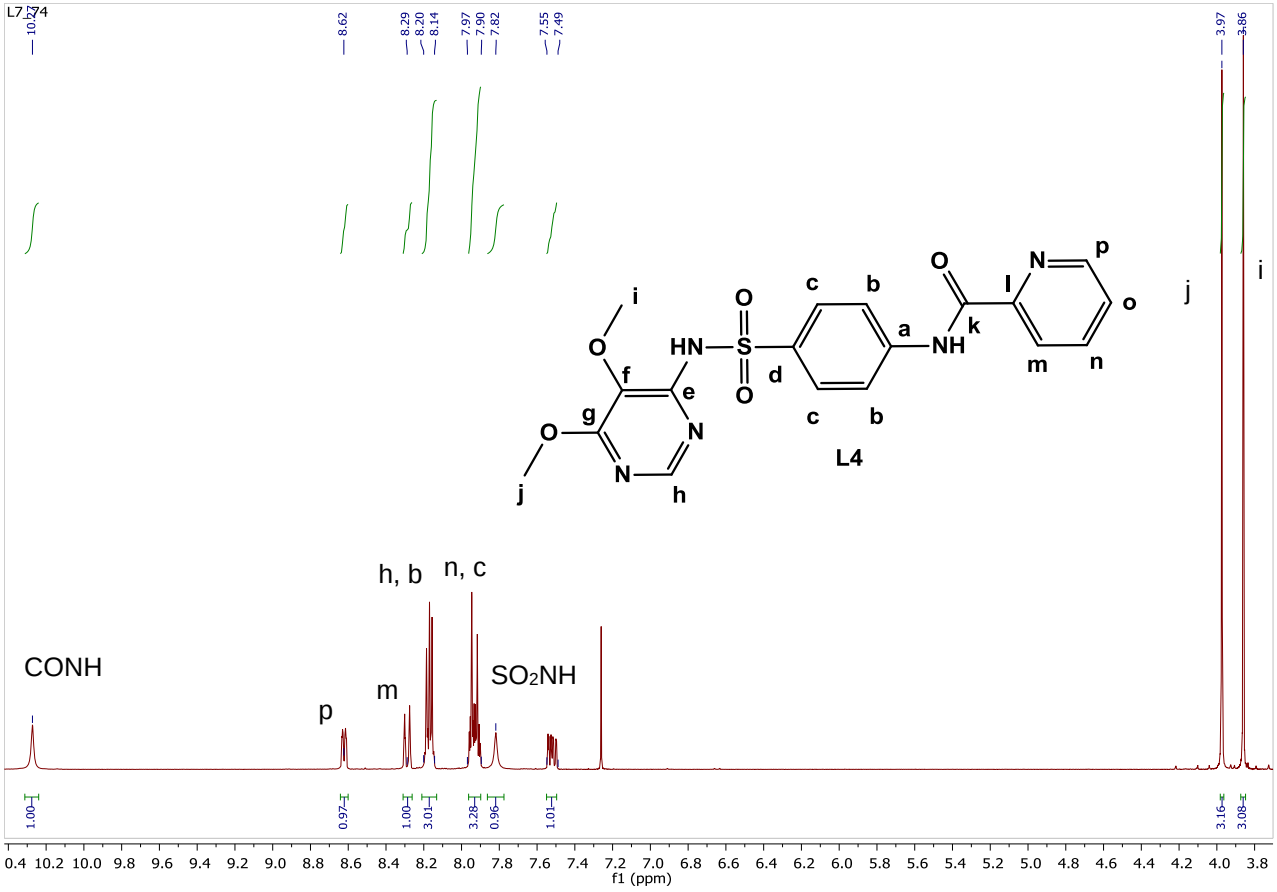

Figure 3.2 - ^{1}H NMR of **L4** in $CDCl_3$.

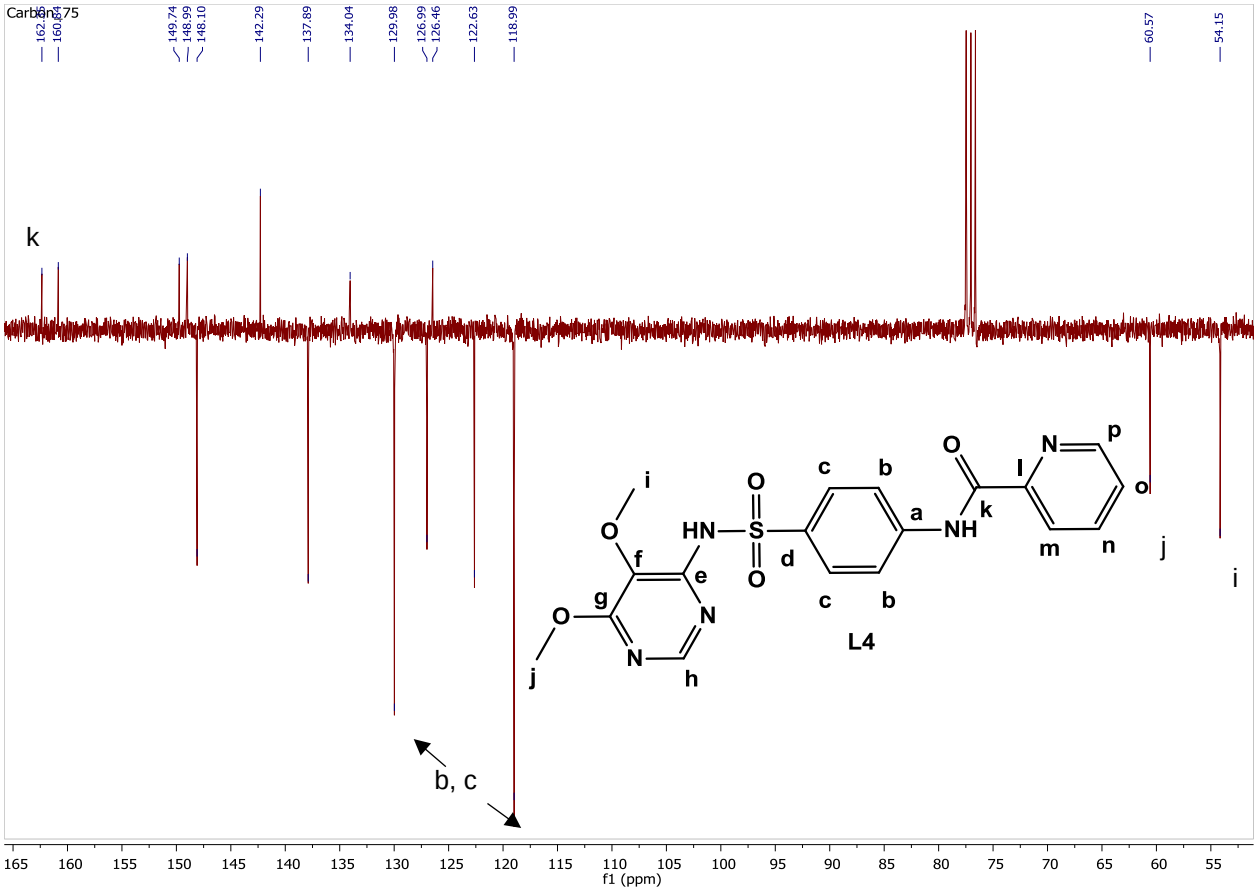

Figure 3.3 - ^{13}C NMR of **L4** in $CDCl_3$.

This means, given that all other characterisation data shows that the structure of the compound is correct, that two other CH signals overlap due to the similarity of their environment. Alternatively, a third CH signal could overlap with one of the phenylene groups, which could explain the difference in intensity between the two signals which are hypothesized to appear at 129.98 ppm and 118.99 ppm due to their higher intensity. Signal magnitude is related to the number of carbons contributing to a signal, though not as clearly as in proton NMR unless rigorous measures are taken so that quantitative carbon analysis is possible. Both the $[M + H]^+$ ion and the $[M + Na]^+$ ion are seen at 416.1023 m/z and 438.0841 m/z, respectively, where 416.1023 m/z is the base peak. This coincides well with the molecular weight of **L4**, which is 415.42 g/mol.

Crystals of **L4** were obtained by layering a DCM solution of **L4** with hexane and leaving to stand in a sealed vial for several days at room temperature. The crystal structure for **L4** is shown in Figure 3.4 below.

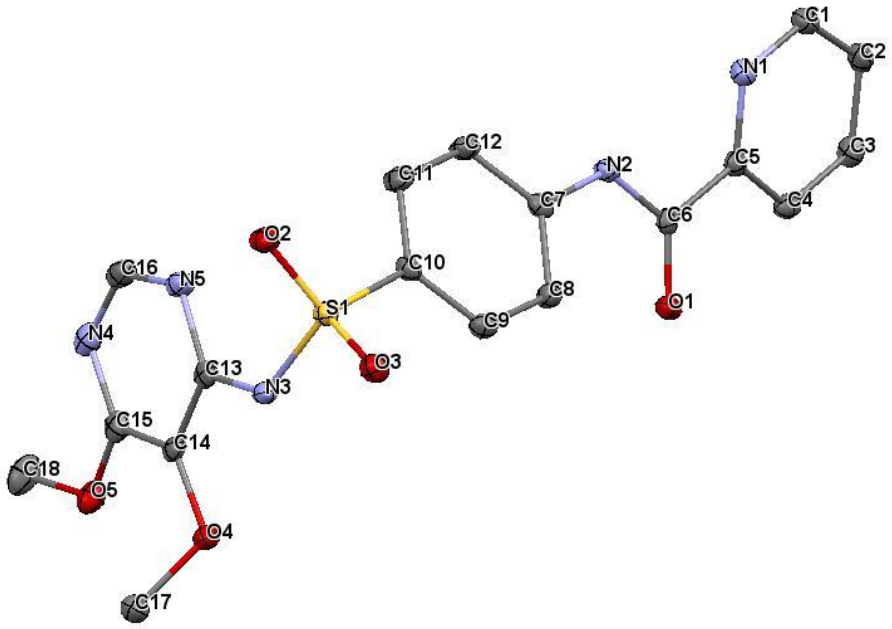

Figure 3.4 - Molecular structure of **L4** with atom labelling. ORTEP thermal ellipsoids are drawn at 50% probability level. Hydrogen atoms have been omitted for clarity.

The needle like crystals were transparent and crystallised in the triclinic space group, $P\bar{1}$. Selected bond lengths and angles are given in Table 3.1 and general crystal data are shown in Table 3.2. The

bond lengths and angles of the sulfonamide group are generally similar to those found in literature.[23,24] The majority of the sulfonamide angles conform to the traditional angles expected for tetrahedral geometry which lie in the region of 109.5 °. The N3-S1-C10 and N3-S1-O3 angles are slightly smaller at 103.45 ° and 105.71 °, respectively. This is due to both the double bond character of the S=O bonds and the two lone pairs on each oxygen atom which causes a greater repulsion between them increasing the O3-S1-O2 bond angle to 119.55 ° which in turn pushes the other atoms closer together. The sulfonamide nitrogens expected bond angles should be close to 120 ° due to the interaction with the pi orbitals of the adjacent pyrimidine ring which shift its character more towards sp^2 hybridisation; this is also seen in the relatively shorter bond length of 1.396 Å of the N3-C13 bond.[25] The tetrahedral geometry of the sulfur, however, influences these bond angles resulting in a H-N3-S1 angle closer to tetrahedral geometry at 110.2 °. This results in a much larger S1-N3-C13 angle of 125.5 °. The electron density of the N2 nitrogen of the amide group can conjugate with both the adjacent phenylene ring and the carbonyl group resulting in a near trigonal planar geometry with expected bond angles close to 120 °. The N2-C6 bond is 1.358 Å, even shorter than the previous example for the sulfonamide nitrogen. Due to the greater repulsion experienced between carbon - carbon atoms as compared to carbon – hydrogen atoms the C7-N2-C6 bond angle is larger at 126.9 ° than the two subsequent angles with the hydrogen atom.

Table 3.1 - Selected bond lengths and angles of L4

At1	At2	Length (Å)	At1	At2	At3	Angle (°)	At1	At2	At3	At4	Torsion (°)
N2	C6	1.358(2)	O3	S1	O2	119.55(9)	C4	C5	C6	N2	-166.8(2)
O1	C6	1.230(2)	O3	S1	N3	103.45(9)	C6	N2	C7	C8	21.6(3)
C7	N2	1.407(3)	O3	S1	C10	108.58(9)	S1	N3	C13	N5	-13.1(3)
C6	C5	1.501(3)	O2	S1	N3	109.32(9)	N3	S1	C10	C11	105.9(2)
C10	S1	1.761(2)	O2	S1	C10	109.29(9)					
S1	O3	1.434(1)	N3	S1	C10	105.71(9)					
S1	O2	1.429(1)	C7	N2	C6	126.9(2)					
S1	N3	1.649(2)	C7	N2	H5	117(2)					
N3	C13	1.396(2)	C6	N2	H5	116(2)					
O5	C15	1.339(3)	S1	N3	C13	125.5(1)					
C14	O4	1.372(2)	S1	N3	H6	110(2)					
H6	N3	0.84(2)	C13	N3	H6	118(2)					
H5	N2	0.84(3)									

Hydrogen bonding interactions through both the sulfonamide and amide moieties to each other stabilise the crystal packing and are shown in Figure 3.5 as dotted lines. Individual molecules act as both donors and acceptors from the oxygen and nitrogen of the functional groups mentioned and the hydrogen bonding interactions cause the molecules to pack along the *a* axis. The hydrogen bond between the sulfonamide oxygen and the amide nitrogen is 2.360 Å in length while that between the amide oxygen and sulfonamide nitrogen is slightly shorter, being 2.105 Å in length.

There are also parallel-displaced pi stacking interactions between the phenylene and pyridyl rings, as well as what appears to be T-shaped stacking interactions between the pyrimidine and pyridyl rings.[26,27] The aromatic rings involved in the parallel-displaced stacking interactions are at a slight angle so as to maximise the individual interactions possible for each molecule within the cluster, as illustrated in Figure 3.5.[27] This results in four molecules that are at slight angles to each other to facilitate these stabilising interactions within the cluster and is also likely why the phenylene and pyridyl rings are not parallel but slightly twisted. The angle between the planes of the two rings can be estimated by examining two sets of torsion angles between them, one representing the phenylene plane and the other representing the pyridyl plane, the sum of which give you the angle between the planes of the ring. This method must be applied as the planes are not directly adjacent to each other. Doing this for the torsion angles of C4-C5-C6-N2 and C6-N2-C7-C8, the angle of the twist between the plane of the phenylene and pyridyl rings is 34.8 °. The angle between the plane of the pyrimidine ring and the phenylene ring, using torsion angles S1-N3-C13-N5 and N3-S1-C10-C11, is found to be 92.8 °. A visual confirmation of the geometry shown in Figure 3.5, ascertains that the estimate is close.

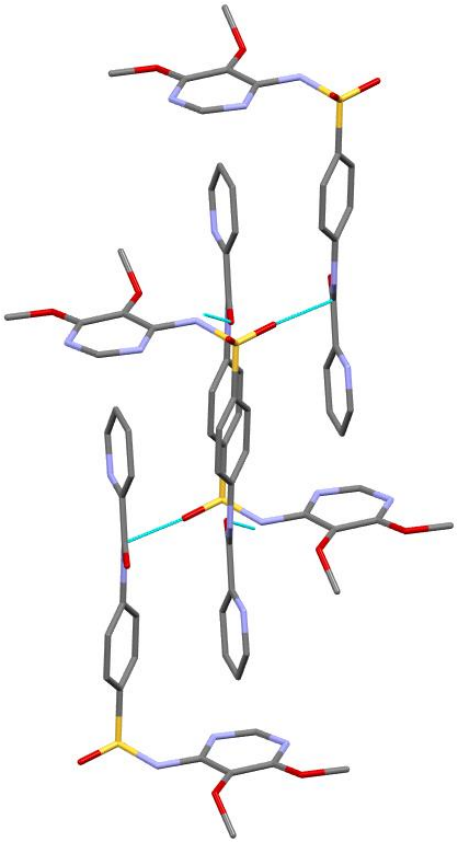

Figure 3.5 - Packing of **L4** demonstrating the favourable twisting of the aromatic rings to incorporate the maximum number of individual interactions within the cluster.

Table 3.2 - Crystal data and structure refinement for **L4**.

Identification code	**L4**	
Empirical formula	$C_{18}H_{17}N_5O_5S$	
Formula weight	415.42	
Temperature (K)	100(2)	
Wavelength (Å)	0.71073	
Crystal system	triclinic	
Space group	*P*-1	
Unit cell dimensions (Å, °)	*a* = 8.319(2)	α = 109.559(4)
	b = 10.194(3)	β = 100.736(4)
	c = 12.280(3)	γ = 103.451(4)
Volume (Å)	913.9(4)	
Z	2	
Calculated density (g cm^{-3})	1.510	
Absorption coefficient (mm^{-1})	0.221	
F_{000}	432	
Crystal size (mm^3)	0.118 × 0.073 × 0.048	
θ range for data collection (°)	1.838 to 27.572	
Miller index ranges	$-10 \le h \le 10$, $-13 \le k \le 13$, $-15 \le l \le 15$	
Reflections collected	24537	
Independent reflections	4207 [R_{int} = 0.0496]	
Completeness to θ_{max} (%)	0.998	
Max. and min. transmission	0.9354 and 1.000	
Refinement method	Full-matrix least-squares on F^2	
Data / restraints / parameters	4207 / 0 / 272	
Goodness-of-fit on F^2	1.045	
Final *R* indices [$I > 2\sigma(I)$]	*R*1 = 0.0402, *wR*2 = 0.0970	
R indices (all data)	*R*1 = 0.0512, *wR*2 = 0.1028	
Largest diff. peak and hole (e Å^{-3})	0.508 and -0.443	

The synthesis of **L5** was completed in a similar fashion to **L4**, however, during the optimisation of the reaction it was found that an increase in time for both the generation of the acid chloride and the subsequent quenching with sulfadoxine gave an improvement in the yield. Furthermore, the workup required adjusting as the compound was remaining on the magnesium sulfate, as such, washing with brine was employed in the drying of the organic layer instead. The synthetic procedure and characterisation data for **L5** was similar to **L4** in all other respects, thus only one set of data has

been discussed in detail above. Detailed characterisation information can be found in the experimental section.

3.2.2 Synthesis of the iridium (III) amido complexes (**C7** – **C12**)

Chelating the ligand to the metal centre via the nitrogens of the amide and pyridyl functionalities requires a base to remove the proton of the amide. Previously it had been hypothesized that the competing acidic NH of the sulfonamide was preventing the complexation from being a success when the *N, O* ligands were being investigated. In this case it was hoped that the softer donor atom and the longer reaction time would favour the formation of the complex. The complexation was thus attempted with **L4** using triethylamine as base while being stirred overnight at room temperature in the presence of di-μ-chlorido(bis(chlorido(pentamethyl-η^5-cyclopentadienyl))iridium(III)).

Characterisation data showed that **C7** (Scheme 3.2), the Cp* pyridyl amido complex had successfully been isolated, however, given the low yield of this reaction it is likely that the sulfonamide moiety was still largely competing for the base and complexation at the desired site was not as favourable as hoped. Having nonetheless established the success of this method it was decided to search for an alternative route as the current method suffered not only from low yield but also from long reaction times. A microwave protocol[28] was found in literature and proved significantly more successful, giving yields of up to 84% as compared to the previous 10% - 20% that had been achieved. The specific conditions are detailed below.

The ligand, **L4,** was combined with di-μ-chlorido(bis(chlorido(pentamethyl-η^5-cyclopentadienyl))iridium(III)) and sodium bicarbonate in methanol and subjected to microwave irradiation for 10 min at 150 °C, resulting in a canary yellow powder in good yield of 84% with characterisation data confirming that the same complex was made (**C7**). Having obtained a method which was both significantly faster and gave a higher yield, the remaining complexes were also made via this method using the relevant ligand and chlorido iridium dimer. The general synthetic procedure for the complexes is shown in Scheme 3.2.

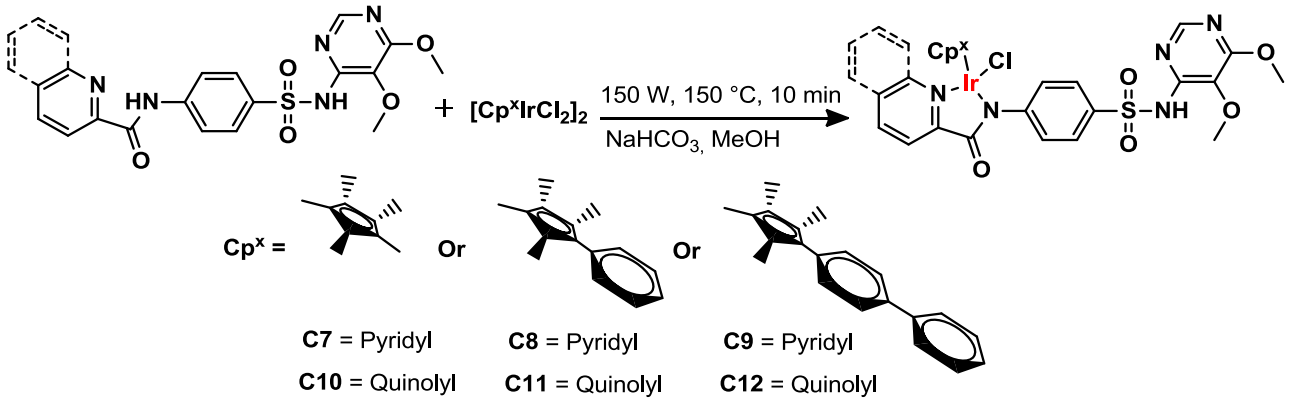

Scheme 3.2 - General synthetic procedure for the complexes **C7** - **C12**.

The infrared spectra for all the complexes in this series along with their NMR had few differences due to the changing electron density on the metal centre and as such a representative example has been discussed in detail below with any notable changes or differences specifically mentioned.

The IR spectrum of **C7** (Figure 3.6) shows a large shift in the carbonyl signal from 1681 cm^{-1} in the ligand (**L4**) to 1621 cm^{-1} with the signal for the NH stretch of the amide disappearing from 3339 cm^{-1}. Furthermore, the C=N stretch of the pyridine ring shifts from the region of 1584 cm^{-1} to 1603 cm^{-1}. These shifts are indicative of coordination through the nitrogens of the pyridyl ring and that of the amide resulting in the strengthening and weakening of the bonds, respectively.[28,29] This indicates that metalation has occurred at the desired site. The signal at 1525 cm^{-1} in the ligand, which is only present for the amido ligands also disappears and could be attributed to the amide N-H bend which would disappear upon complexation as was the case for the N-H stretch. As the electronegativity of the metal centre increases within the series there is a slight general shift to higher frequencies. In particular, the quinolyl C=N stretch combines with the C=O stretch to form a broad band from which they cannot be separately identified.

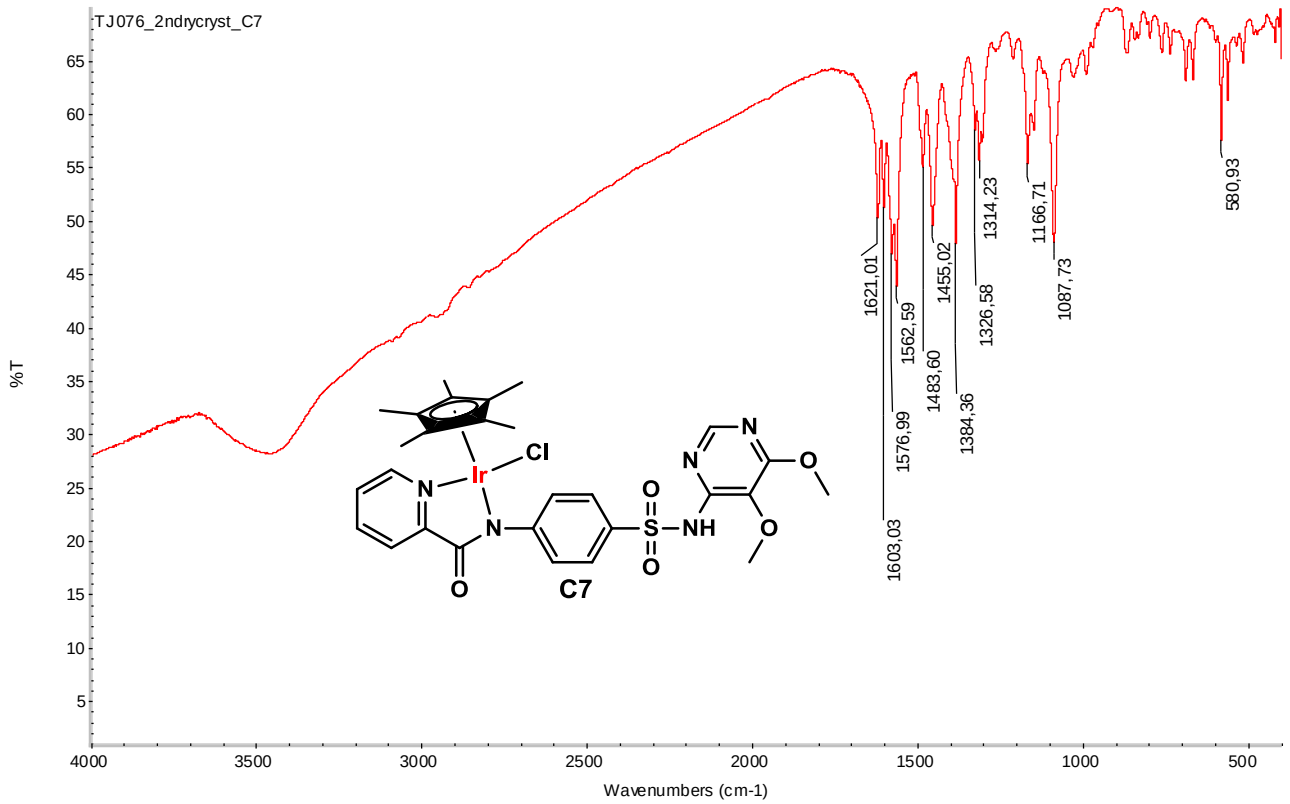

Figure 3.6 - FTIR spectrum of **C7**, the pyridyl amido Cp* complex.

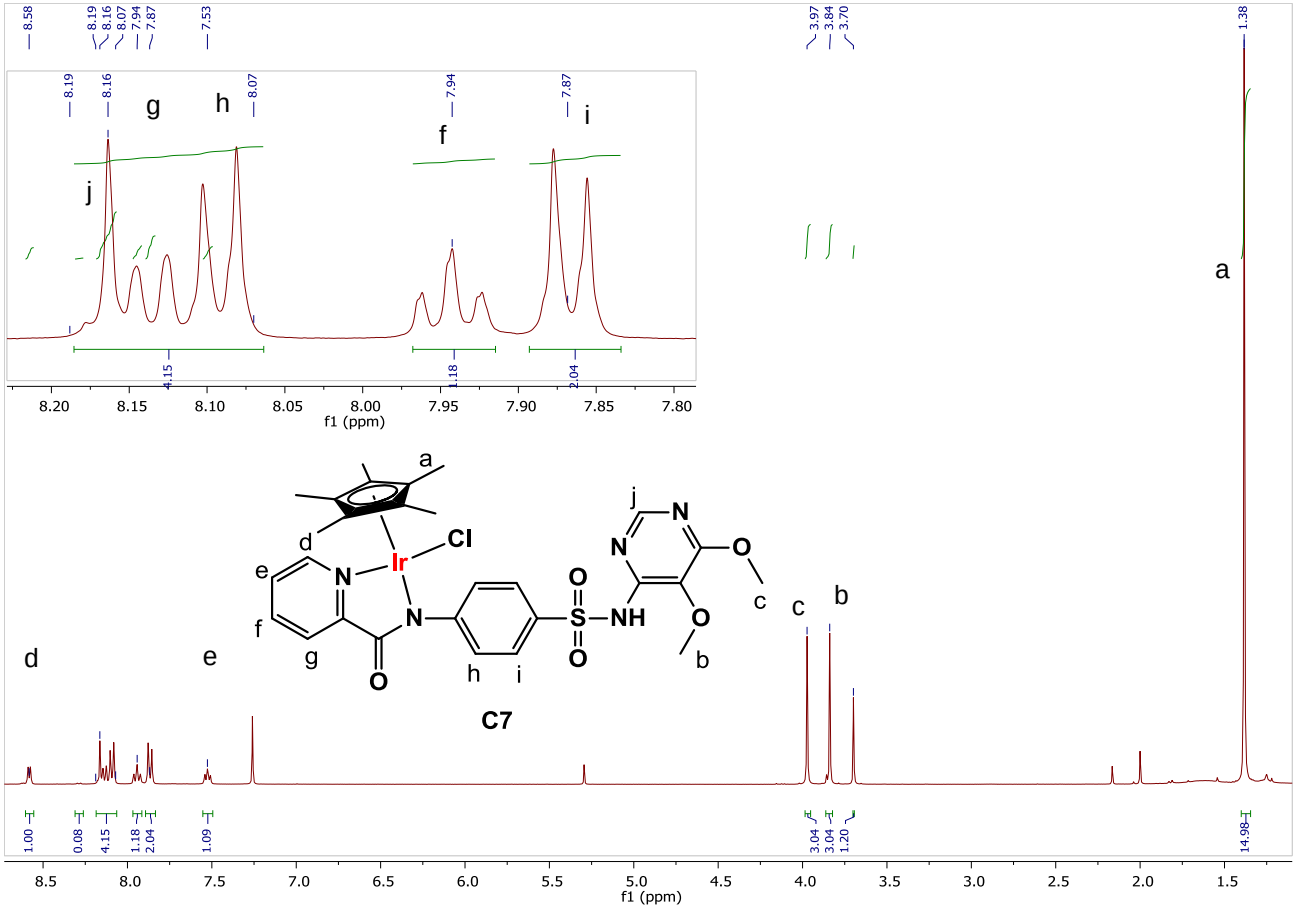

Figure 3.7 - ^{1}H NMR spectrum of **C7** in $CDCl_3$.

The successful formation of the complex is further confirmed through ^{1}H NMR by the disappearance of the amide NH. The spectrum is shown in Figure 3.7. The shifts in the spectrum upon complexation are not large, with the proton attached *ortho* to the nitrogen of the pyridyl ring seen to shift from 8.62 ppm to 8.58 ppm and similar sized shifts for protons e, f and g of the pyridyl ring (Figure 3.7). The protons for the methyls of the Cp* ring are seen at 1.38 ppm. Most of the protons are also seen to shift upfield, most likely due to the electron rich character of the metal centre which more effectively shields them. All complexes aside from those formed from the Cp* iridium dichloride dimer show separate methyl peaks for the coordinating Cp^{x} moiety. This is the result of the inequivalence introduced by the attached phenyl or biphenyl ring along with the chirality of the metal centre. As the Cp^{x} moiety is extended the addition of the new multiplets from the added phenyl rings appear between 7.3 ppm and 7.7 ppm.

As discussed in the ^{13}C NMR of **L4,** the phenylene carbons overlap in the complexes due to the symmetry involved.[30,31] There are also two other CH carbon signals that overlap to only give one observed signal as was mentioned for the ligand. The quaternary carbons of the Cp^{x} ring appear as one signal in **C7** and **C10** (the Cp* complexes) but, are seen separately for complexes **C8**, **C9**, **C11** and **C12** for the same reasons as discussed for the methyl protons of these complexes in the ^{1}H NMR spectrum. A representative spectrum for the series is shown in Figure 3.8.

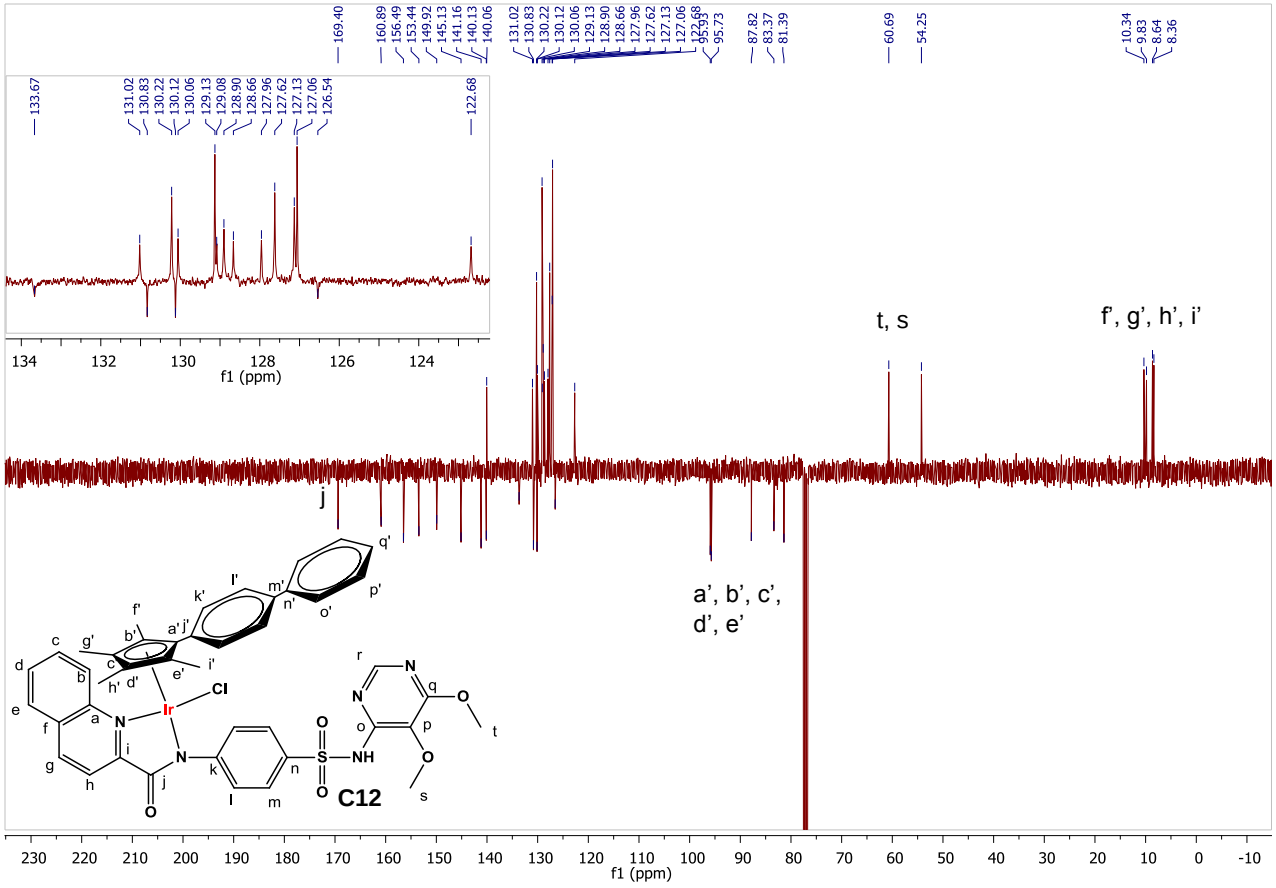

Figure 3.8 - ^{13}NMR in DMSO-d_6 of **C12**, with the insert magnifying the region between 122 ppm and 134 ppm.

The MS spectra for the complexes did not give the expected $[M+H]^+$ ions as the base peak, but rather, the base peak was the $[M - Cl]^+$ ion. The $[M+H]^+$ ion was still observable though, especially under softer ionisation conditions. Detailed results are given in the experimental section.

Instead of having *N*, *N* coordination it is possible that coordination occurs through the oxygen of the carbonyl to form a *N*, *O* system instead. The disappearance of the hydrogen on the amide does not provide any significant insight into the coordination mode as the subsequent ketoxime could have formed in which case the hydrogen would still be missing. Literature indicates that the current complexes should coordinate through both nitrogens.[28,32] To confirm exactly in which manner coordination takes place on these systems, however, it is necessary to look for metal to nitrogen or metal to oxygen bands in the far IR region with FTIR or RAMAN spectroscopy or through obtaining a crystal structure.[33,34] Unfortunately, despite many attempts only microcrystalline powders were obtained and thus single-crystal X-ray diffraction could not be used to confirm the coordination mode. The far IR region was thus investigated for both **L5** and **C10** as examples by pressing a pellet of caesium iodide which does not absorb in this region as potassium bromide is not adequate for analysis past 400 cm^{-1}. The region analysed was between 200 cm^{-1} – 600 cm^{-1} to provide sufficient overlap with the mid IR region and confirm reproducibility between beam splitters and detectors. Comparing both the far-IR spectra of **L5** and **C10** with their respective mid-IR spectra gave good overlap between 600 cm^{-1} and 400 cm^{-1} confirming the reproducibility of analysing the two different

regions. This was seen particularly for the signals at 583 cm^{-1} and 561 cm^{-1}. The spectra of the compounds showing the overlap are shown in Figures 3.9 and 3.10, with Figure 3.11 showing the far-IR spectrum of **L5** and **C10** in comparison with one another.

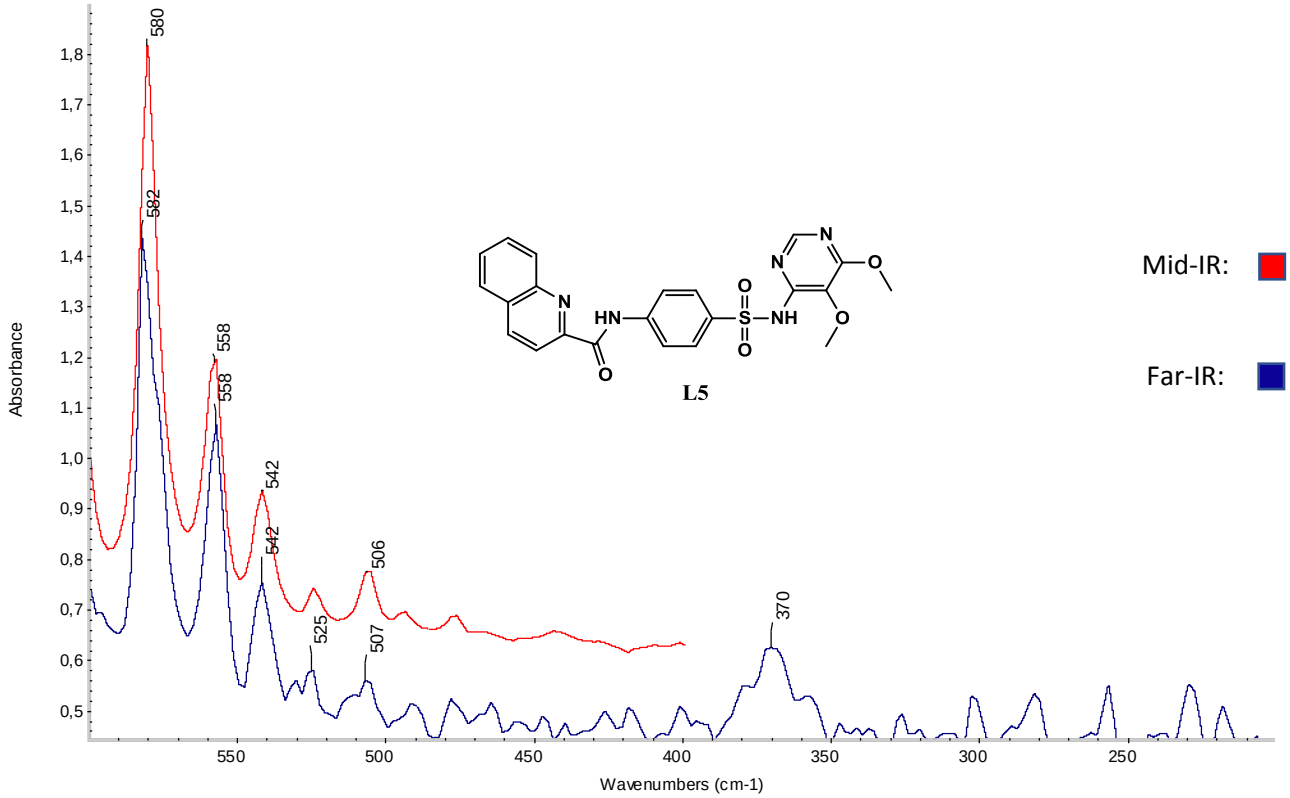

Figure 3.9 - A comparison of the mid-IR (top, red) region of **L5** with that of the far-IR (bottom, blue) region with spectra displayed as absorbance data.

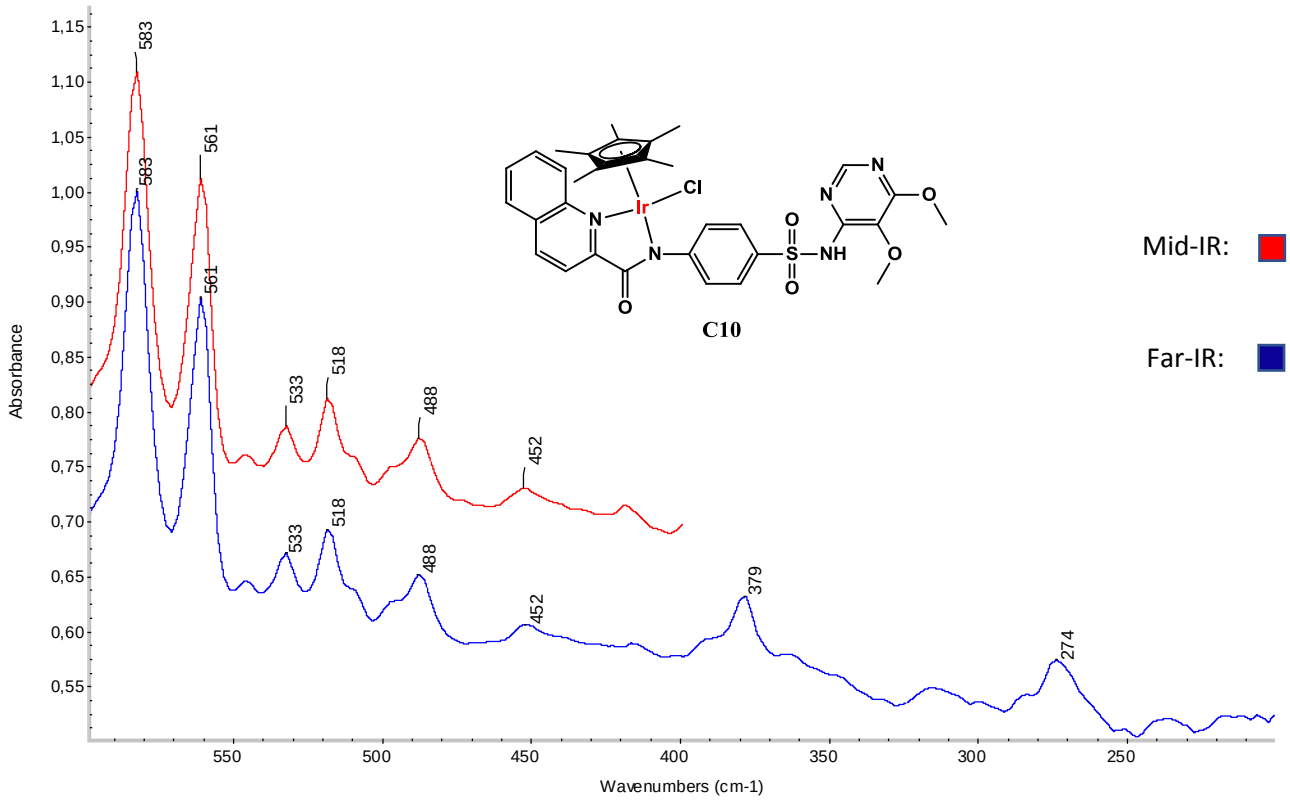

Figure 3.10 - A comparison of the mid-IR (top, red) region of **C10** with that of the far-IR (bottom, blue) region with spectra displayed as absorbance data.

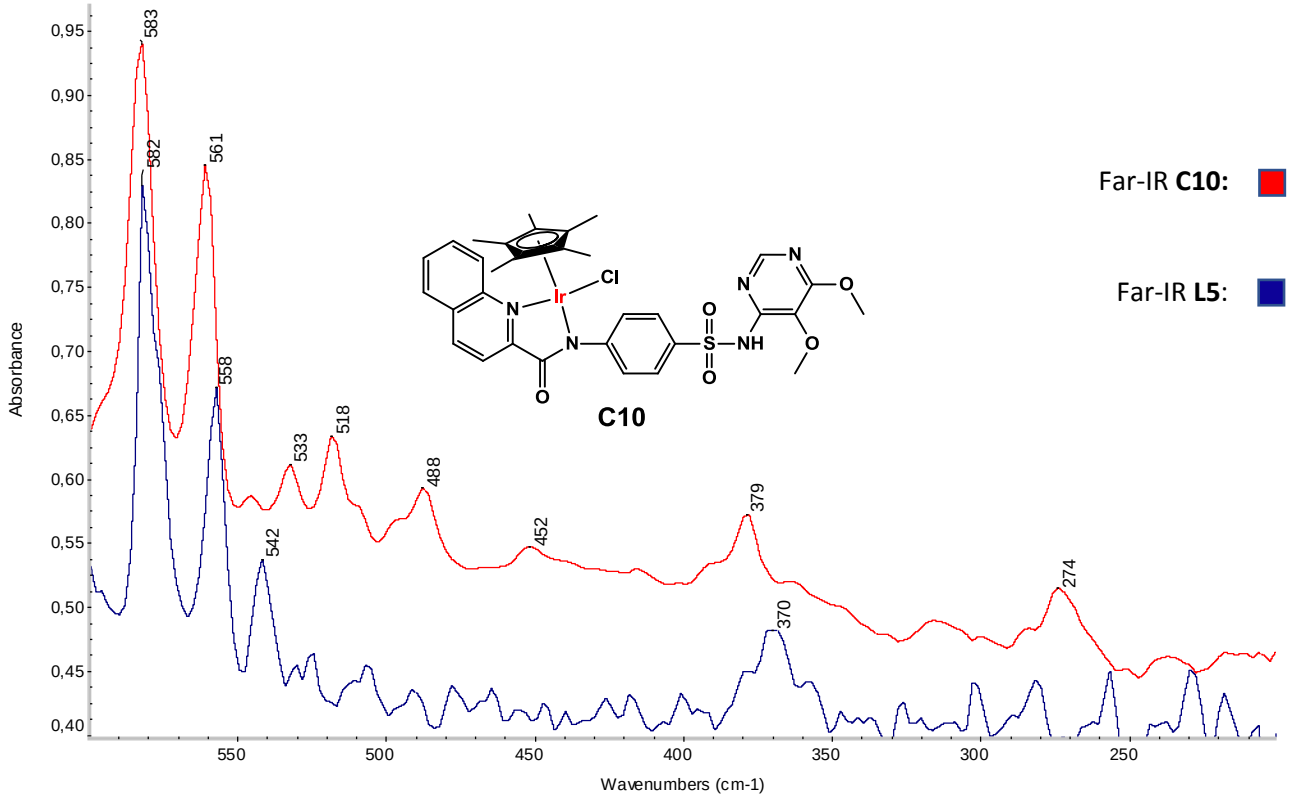

Figure 3.11 – A comparison of the Far-IR of **C10** (top, red) and the Far-IR of **L5** (bottom, blue) illustrating M - N bonds at 488 cm^{-1} and 452 cm^{-1}. The spectra are displayed as absorbance data.

The far-IR spectrum of **L5** (Figure 3.11, bottom) shows a new ligand band not previously seen at 370 cm^{-1} which shifts to higher frequency in **C10**. Additionally, in the far-IR of **C10** (Figure 3.11, top) the iridium-chloride band is now visible at 274 cm^{-1} and the two bands at 488 cm^{-1} and 452 cm^{-1} are proposed to be due to the iridium-nitrogen bonding through the amide and heterocyclic nitrogen of the quinolyl moiety, respectively. Their low intensity is a consequence of the small difference in dipole moment between the respective groups. Both their proximity to each other as well as their relatively low frequency would indicate that they are the metal-nitrogen bonding bands as metal-oxygen bands generally appear at slightly higher frequencies.[35,36] Coordination takes place in this fashion for all the complexes, given their similarity. Although metal to oxygen bonds are fairly prevalent in complexes of amides, the presence of an anchor group in the form of a heterocyclic nitrogen[37] and the borderline softer character of iridium along with the data is evidence enough to support the hypothesis of metal to nitrogen bonding in the current systems. The purity of all ligands and complexes was determined by HPLC to be between 94.6% and 98.9%

3.3 Conclusion

Two new ligands – amido pyridyl (**L4**) and quinolyl (**L5**) sulfadoxine derivatives, were successfully identified, synthesized and purified for the second library of complexes that was to be tested against *Mtb* and malaria. Both ligands gave moderate yields of 73% and 60%, respectively. A crystal structure was obtained for **L4** and crystallised in the triclinic space group.

Three complexes were subsequently synthesized from each of the ligands (**C7** – **C12)**, through a facile microwave reaction that was discovered in the literature after initial synthetic routes that gave low yields and employed long reaction times. The microwave method had short reaction times and gave moderate to excellent yields ranging between 56% and 84% yield. The successful synthesis of **C7** – **C12** was characterized by the disappearance of the amide NH signal in both the IR and ^{1}H NMR spectra. Additionally, the phenylene carbons symmetrical to one another overlapped in the NMR spectra with an additional tertiary carbon signal overlapping with either one of the phenylene signals or another tertiary signal as there was consistently one less carbon signal than expected (taking symmetry into account) for both the ligands and the complexes. The MS spectra for the complexes generally gave the $[M\text{-}Cl]^{+}$ ion, though the $[M+H]^{+}$ ion could also be observed in the spectrum. Finally, it was determined that coordination of the iridium metal centre takes place between the nitrogen of the amide and of the quinolyl moiety with far-IR, Identifying the iridium-nitrogen bands at 488 cm^{-1} and 452 cm^{-1}, respectively. It was proposed that this is the coordination for all the complexes presented in this chapter. All compounds discussed in this chapter had not been made before as far as we are aware.

3.4 Experimental

Chemicals and reagents. Sulfadoxine (95 %), 2-picolinic acid, quinaldic acid, salicylaldehyde, 2-hydroxynapthaldehyde, oxalyl chloride (2M in DCM), pyridine, magnesium sulfate, sodium bicarbonate, 1,2,3,4,5-pentamethylcyclopentadiene, 2,3,4,5-tetramethyl-2-cyclopentenone, phenyl magnesium bromide solution in THF (1 M), $IrCl_3 \bullet nH_2O$, all reagent solvents and deuterated solvents (dimethylsulfoxide-d_6 and chloroform-d_1) were obtained from Sigma Aldrich (Merck). Di-μ-chlorido(bis(chlorido(pentamethyl-η^5-cyclopentadienyl))iridium(III)), di-μ-chlorido(bis(chlorido(tetra methyl-η^5-cyclopentadienylbenzene))iridium(III)) and di-μ-chlorido(bis(chlorido(4-(tetramethyl-η^5-cyclopentadienyl)-1,1'-biphenyl))iridium(III)) were synthesized according to a literature method.[38]

Instrumentation. IR spectroscopy was performed using a Thermo Nicolet Nexus 470 by means of potassium bromide pellets and transmission esp for mid-IR spectra and using caesium iodide pellets and transmission esp for far-IR spectra except when comparisons had to be drawn between the mid and far IR regions in which case caesium iodide was used for both spectra. NMR data (^1H, ^{13}C) were recorded on either a 300 MHz Varian VNMRS or a 400 MHz Varian Unity Inova spectrometer. ^1H NMR chemical shifts are reported in ppm and coupling constants in Hertz and were internally referenced to dimethylsulfoxide-d_6 (2.50 ppm) or chloroform-d_1 (7.26 ppm). Data was processed using MestReNova 11.0.4-18998. Mass spectrometry was performed on a Waters Synapt G2 with an ESI probe in ESI Positive mode using a Cone Voltage of 15 V.

Microwave syntheses were carried out in a CEM Discover SP microwave reactor. Uv-Vis data were recorded with a Shimadzu Uv - vis spectrophotometer. Solvents were removed *in vacuo*, using a rotary evaporator, followed by removal of trace amounts of the remaining solvent using a high vacuum pump at *ca*. 0.08 mm Hg.

3.4.1 Synthesis of N-(4-(N-(5,6-dimethoxypyrimidin-4-yl)sulfamoyl) phenyl) picolinamide (**L4**)

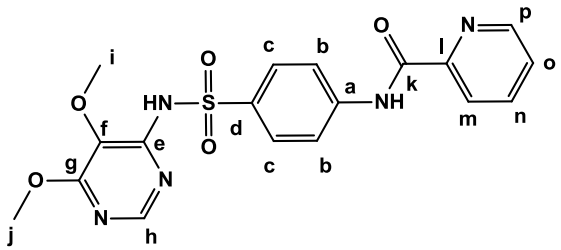

2-Picolinic acid (516 mg, 4.19 mmol) was stirred in dry DCM (100 mL) under nitrogen. Oxalyl chloride (2 M in DCM, 2.42 mL, 4.83 mmol) was added to this solution while it was kept on ice after which a catalytic amount of DMF (100 µL) was added. The solution was stirred for 2 hours at 0 °C before the solvent was removed and the crude residue re-dissolved in acetonitrile (50.0 mL). Sulfadoxine (1.00 g, 3.22 mmol) was then added dropwise (50.0 mL) over 5 min while the solution was kept on ice. Pyridine (389 µL, 4.83 mmol) was then added and the solution stirred at 0 °C for 30 min before stirring a further 1.5 hours at room temperature. The purple precipitate formed was filtered off, washed with acetonitrile and kept aside. The solvent was removed from the filtrate and the crude residue re-dissolved in DCM (80.0 mL). This was washed with a solution of saturated sodium bicarbonate (3 x 30.0 mL) and the organic portions dried over $MgSO_4$. The solvent was removed and the off-white powder was combined with the purple precipitate and recrystallised from DCM/Hex and then washed with acetonitrile to give a pure white powder in 73% yield (979 mg). ^{1}H NMR (300 MHz, $CDCl_3$) δ 10.27 (s, $H_{NH(C=O)}$, 1H), 8.62 (d, H_p, 1H, $^{3}J_{(Hp-Ho)}$ 4.7 Hz), 8.29 (d, H_m, 1H, $^{3}J_{(Hm-Hn)}$ 7.8 Hz), 8.20 - 8.14 (m, $H_{b,h}$, 3H), 7.97 - 7.90 (m, $H_{c,n}$, 3H), 7.82 (s, $H_{NH(SO2)}$, 1H), 7.55 - 7.49 (m, H_o, 1H), 3.97 (s, H_j, 3H), 3.86 (s, H_i, 3H). ^{13}C NMR (75 MHz, $CDCl_3$) δ 162.35 (C_k), 160.84 (C), 149.74 (C), 148.99 (C), 148.10 (CH), 142.29 (C), 137.89 (CH), 134.04 (C), 129.98 ($C_{b/c}$), 126.99 (CH), 126.46 (C), 122.63 (CH), 118.99 ($C_{c/b}$), 60.57 (C_j), 54.15 (C_i). FT-IR (KBr): 1681 cm^{-1} (C=O), 1584 cm^{-1}, 1525 cm^{-1} (C=N_{pyr}, C=N_{pyrim}), 3339 cm^{-1}, 3165 cm^{-1} (N-H). (+)-HR-ESI-MS: *m/z* (%) 416.1023 ([M + H]+, 100 %), 438.0841 ([M+Na]+, 5 %); HPLC purity: 97.4%; t_r = 15.08 min.

3.4.2 Synthesis of N-(4-(N-(5,6-dimethoxypyrimidin-4-yl)sulfamoyl)phenyl) quinoline-2-carboxamide (**L5**)

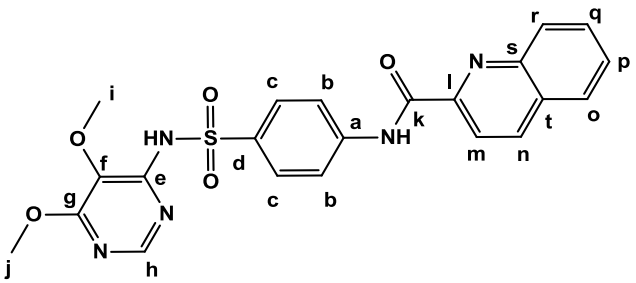

Quinaldic acid (109 mg, 0.628 mmol) was stirred in dry DCM (15.0 mL) under nitrogen. Oxalyl chloride (2 M in DCM, 363 µL, 0.725 mmol) was added to this solution while it was kept on ice after which a catalytic amount of DMF (50.0 µL) was added. The solution was stirred for 5 hours at 0 °C

before the solvent was removed and the crude residue re-dissolved in acetonitrile (10.0 mL). Sulfadoxine (150 mg, 0.483 mmol) was then added dropwise (10.0 mL) over 5 min while the solution was kept on ice. Pyridine (58.4 µL, 0.725 mmol) was then added and the solution stirred at 0 °C for 30 min before stirring a further 2.5 hours at room temperature. The solvent was removed from the reaction mixture and the crude residue re-dissolved in DCM (20.0 mL) and washed with saturated sodium bicarbonate (3 X 10.0 mL), distilled water (3 X 10.0 mL) and brine (2 X 10.0 mL). After the washing with brine the solvent was removed and left to dry overnight on the high vacuum pump where-after it was re-dissolved in DCM and filtered through Celite™ to remove any residual NaCl. The crude powder was recrystallised from DCM/hexane (1:2) to give a pure off-white microcrystalline solid in 60% yield (134 mg). ^{1}H NMR (400 MHz, $CDCl_3$) δ 10.49 (s, $H_{NHC=O}$, 1H), 8.42 - 8.36 (m, $H_{m,n}$, 2H), 8.24 - 8.16 (m, $H_{h,b,r}$, 4H), 8.05 - 7.99 (d, H_c, 2H, $^{3}J_{(Hc-Hb)}$ 8.8 Hz), 7.96 - 7.91 (d, H_o, 1H, $^{3}J_{(Ho-Hp)}$ 8.2 Hz), 7.87 - 7.81 (m, H_p, 1H), 7.81 - 7.77 (s, H_{NHSO2}, 1H), 7.72 - 7.65 (m, H_q, 1H), 3.98 (s, H_i, 3H), 3.87 (s, H_j, 3H). ^{13}C NMR (101 MHz, $CDCl_3$) δ 162.67 (C_k), 160.97 (C), 149.88 (C), 148.95 (C), 146.39 (C), 142.48 (C), 138.30 (CH), 134.19 (C), 130.75 (CH), 130.18 (CH), 129.79 (CH), 129.77 (C), 128.69 (CH), 128.03 (CH), 126.58 (C), 119.20 ($C_{c/b}$), 118.83 (CH), 60.72 (C_j), 54.30 (C_i). FT-IR (KBr): 1679 cm^{-1} (C=O), 1577 cm^{-1}, 1531 cm^{-1} (C=N_{quin}, C=N_{pyrim}), 3287 cm^{-1}, 3177 cm^{-1} (N-H). (+)-HR-ESI-MS: *m*/*z* (%) 466.1179 ([M + H]+, 100 %), 488.1001 ([M+Na]+, 2 %); HPLC purity: 98.1%; t_r = 20.51 min.

3.4.3 General method for complex synthesis

The appropriate ligand was added to a stirred suspension of the appropriate iridium metal dimer and $NaHCO_3$ in dry methanol in a microwave vial. The vial was then placed in the microwave reactor (150 °C, 10 min, 150 W) after which any effervescence was allowed to subside before the vial was opened and cooled to room temperature. The resulting solid was filtered off and washed with MeOH/Ether before it was recrystallised from DCM/Hex to afford the pure metal complex.

3.4.4 Synthesis of [IrCl($C_{18}H_{16}N_5O_5S$)($C_{10}H_{15}$)] (**C7**)

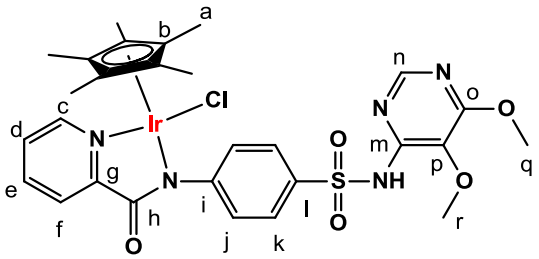

N-(4-(N-(6-hydroxy-5-methoxypyrimidin-4-yl)sulfamoyl)phenyl)picolinamide (**L4)** (52.1 mg, 0.126 mmol), di-μ-chlorido(bis(chlorido(pentamethyl-η^5-cyclopentadienyl))iridium(III)) (50.0 mg, 0.0628 mmol) and $NaHCO_3$ (10.5 mg, 0.126 mmol) was reacted in methanol (1.50 mL) in a 10 mL microwave vial to afford a canary yellow powder in 84% yield (82.8 mg). ^{1}H NMR (400 MHz, $CDCl_3$) δ 8.58 (d, H_c, 1H, $^{3}J_{(Hc-Hd)}$ 5.6 Hz), 8.19 - 8.07 (m, $H_{n,j,f}$, 4H), 7.94 (t, H_e, 1H, $^{3}J_{(He-Hf)}$ 7.7 Hz), 7.87 (d, H_k, 2H, $^{3}J_{(Hk-Hj)}$ 8.8 Hz), 7.53 (m, H_d, 1H), 3.97 (s, H_r, 3H), 3.84 (s, H_q, 3H), 1.38 (s, H_a, 15H). ^{13}C NMR (101 MHz, DMSO) δ 167.86 (C_h), 161.52 (C), 153.46 (C), 152.99 (C), 151.40 (CH), 150.62 (C), 139.42

(CH), 134.79 (C), 128.59 (CH), 127.48 ($C_{j/k}$), 127.12 (C), 126.81 ($C_{k/j}$), 125.43 (CH), 86.39 (C_b), 60.26 (C_q), 54.04 (C_r), 7.93 (C_a). FT-IR (KBr): 1619 cm^{-1} (C=O), 1599 cm^{-1}, 1577 cm^{-1}, 1561 cm^{-1} ($C=N_{pyr}$, $C=N_{pyrim}$). (+)-HR-ESI-MS: *m/z* (%) 742.1687 ([M - Cl]+, 100%), 778.1456 ([M+H]+, 2%); HPLC purity: 96.7%; $t_{r'}$ = 10.93 min.

3.4.5 Synthesis of $[IrCl(C_{18}H_{16}N_5O_5S)(C_{15}H_{17})]$ (**C8**)

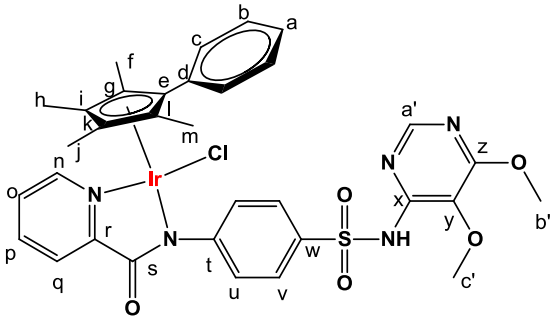

Di-μ-chlorido(bis(chlorido(tetramethyl-η^5-cyclopentadienylbenzene))iridium(III)) (50.0 mg, 0.054 mmol), **L4** (45.1 mg, 0.109 mmol) and $NaHCO_3$ (9.10 mg, 0.109 mmol) were reacted together in MeOH (1.50 mL) to afford a bright yellow powder in 75% yield (68.7 mg). ^{1}H NMR (300 MHz, $CDCl_3$) δ 8.28 (d, H_n, 1H, $^3J_{(Hn-Ho)}$ 5.4 Hz), 8.19 - 8.07 (m, $H_{q,u,a'}$, 4H), 7.94 – 7.86 (m, H_o, 1H), 7.82 (d, H_v, 2H, $^3J_{(Hv-Hu)}$ 8.6 Hz), 7.49 - 7.38 (m, $H_{c,b,a}$, 5H), 7.38 - 7.34 (m, H_p, 1H), 3.98 (s, $H_{c'}$, 3H), 3.85 (s, $H_{b'}$, 3H), 1.70 (s, H_f, 3H), 1.48 (s, H_m, 3H), 1.21 (s, H_h, 3H), 1.12 (s, H_j, 3H). ^{13}C NMR (101 MHz, $CDCl_3$) δ 168.69 (C_s), 160.77 (C), 154.54 (C), 153.19 (C), 149.88 (CH), 149.78 (C), 138.80 (CH), 134.12 (C), 130.16 (C), 130.06 ($C_{u/v/b/c}$), 129.16 ($C_{u/v/b/c}$), 128.80 (CH), 128.62 (CH), 127.77 (CH), 127.21 ($C_{u/v/b/c}$), 126.67 (CH), 126.42 (C), 99.00 ($C_{e/g/l/i/k}$), 92.58 ($C_{e/g/l/i/k}$), 86.04 ($C_{e/g/l/i/k}$), 82.64 ($C_{e/g/l/i/k}$), 81.65 ($C_{e/g/l/i/k}$), 60.55 ($C_{b'}$), 54.10 ($C_{c'}$), 9.71 ($C_{f/m}$), 9.38 ($C_{f/m}$), 8.52 ($C_{j/h}$), 8.09 ($C_{j/h}$). FT-IR (KBr): 1623 cm^{-1} (C=O), 1600 cm^{-1}, 1577 cm^{-1}, 1560 cm^{-1} ($C=N_{pyr}$, $C=N_{pyrim}$). (+)-HR-ESI-MS: *m/z* (%) 804.1844 ([M - Cl]+, 100 %), 840.1575 ([M+H]+, 2%); HPLC purity: 96.8%; $t_{r'}$ = 13.79 min.

3.4.6 Synthesis of $[IrCl(C_{18}H_{16}N_5O_5S)(C_{21}H_{21})]$ (**C9**)

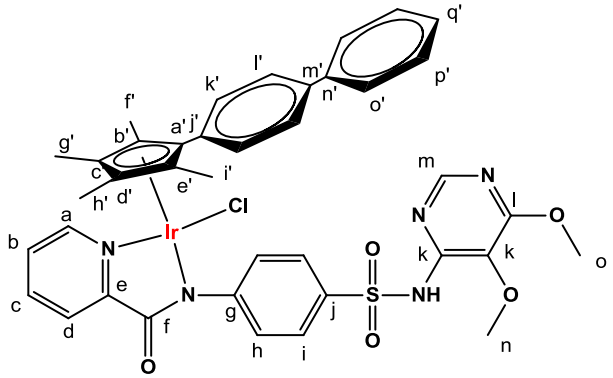

Di-μ-chlorido(bis(chlorido(4-(tetramethyl-η^5-cyclopentadienyl)-1,1'-biphenyl))iridium(III)) (50.0 mg, 0.0470 mmol), **L4** (38.7 mg, 0.0930 mmol) and $NaHCO_3$ (7.80 mg, 0.0930 mmol) were reacted together in MeOH (1.50 mL) to afford a light-yellow powder in 65% yield (55.9 mg). ^{1}H NMR (300 MHz, $CDCl_3$) δ 8.32 (d, H_a, 1H, $^3J_{(Ha-Hb)}$ 5.5 Hz), 8.19 - 8.09 (m, $H_{m,h,d}$, 4H), 7.94 – 7.87 (m, H_c, 1H),

7.84 (d, H_i, 2H, $^3J_{(Hi-Hh)}$ 8.9 Hz), 7.67 - 7.61 (m, $H_{k',l'}$ 4H), 7.58 - 7.32 (m, $H_{q',p',o',b}$, 6H), 3.98 (s, H_n, 3H), 3.85 (s, H_o, 3H), 1.74 (s, $H_{f'}$, 3H), 1.49 (s, $H_{i'}$, 3H), 1.27 (s, $H_{h'}$, 3H), 1.11 (s, $H_{g'}$, 3H). ^{13}C NMR (75 MHz, $CDCl_3$) δ 168.84 (C_f), 160.91 (C), 154.62 (C), 153.30 (C), 150.07 (CH), 149.94 (C), 141.41 (C), 140.03 (C), 138.97 (CH), 134.34 (C), 130.59 (CH), 129.22 (C), 129.10 (CH), 128.90 (CH), 127.98 (CH), 127.95 (CH), 127.84 (CH), 127.34 (CH), 127.04 (CH), 126.77 (CH), 126.59 (C), 99.22 ($C_{a'/b'/c'/d'/e'}$), 92.76 ($C_{a'/b'/c'/d'/e'}$), 86.10 ($C_{a'/b'/c'/d'/e'}$), 82.90 ($C_{a'/b'/c'/d'/e'}$), 81.39 ($C_{a'/b'/c'/d'/e'}$), 60.67 (C_o), 54.21 (C_n), 9.89 ($C_{f'/i'}$), 9.57 ($C_{f'/i'}$), 8.64 ($C_{g'/h'}$), 8.17 ($C_{g'/h'}$). FT-IR (KBr): 1618 cm^{-1} (C=O), 1598 cm^{-1}, 1580 cm^{-1}, 1661 cm^{-1} (C=N_{pyr}, C=N_{pyrim}). (+)-HR-ESI-MS: *m/z* (%) 880.2172 ([M - Cl]+, 100%), 916.1915 ([M+H]+, 2%) HPLC purity: 97.9%; $t_{r'}$ = 18.07 min.

3.4.7 Synthesis of [IrCl($C_{22}H_{19}N_5O_5S$)($C_{10}H_{15}$)] (**C10**)

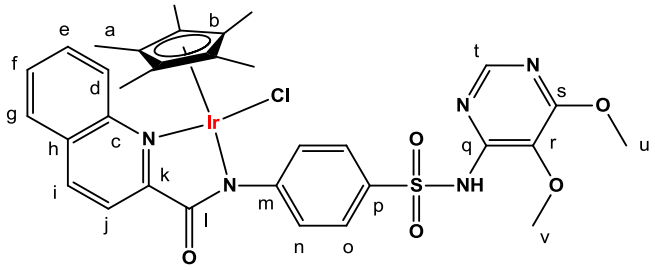

Di-μ-chlorido(bis(chlorido(pentamethyl-η^5-cyclopentadienyl))iridium(III)) (50.0 mg, 0.0630 mmol), N-(4-(N-(5,6-dimethoxypyrimidin-4-yl)sulfamoyl)phenyl)quinoline-2-carboxamide (**L5**) (58.4 mg, 0.126 mmol) and $NaHCO_3$ (10.6 mg, 0.126 mmol) were reacted in MeOH (1.50 mL) to afford an orange powder in 77% yield (80.5 mg). ^{1}H NMR (400 MHz, $CDCl_3$) δ 8.60 (d, H_i, 1H, $^3J_{(Hi-Hj)}$ 8.7 Hz), 8.34 (d, H_d, 1H, $^3J_{(Hd-He)}$ 8.5 Hz), 8.26 - 8.21 (m, $H_{n,j}$ 3H), 8.17 (s, H_t, 1H), 8.07 (d, H_o, 2H, $^3J_{(Ho-Hn)}$ 8.9 Hz), 7.93 (d, H_g, 1H, $^3J_{(Hg-Hf)}$ 8.1 Hz), 7.86 (m, H_e, 1H), 7.72 (m, H_f, 1H), 3.96 (s, H_v, 3H), 3.83 (s, H_u, 3H), 1.28 (s, H_a, 15H). ^{13}C NMR (101 MHz, $CDCl_3$) δ 168.91 (C_l), 160.73(C), 156.61 (C), 153.36 (C), 149.78 (C), 145.14 (C), 139.69 (CH), 133.13 (C), 131.10 (CH), 130.70 (C), 129.80 (CH), 128.93(CH), 128.67 ($C_{o/n}$), 128.62 (CH), 126.83 ($C_{n/o}$), 126.37 (C), 122.41 (CH), 87.16 (C_b), 60.53 (C_v), 54.09 (C_u), 8.62 (C_a). FT-IR (KBr): 1615 cm^{-1} (C=O), 1580 cm^{-1}, 1663 cm^{-1} (shoulder) (C=N_{quin}, C=N_{pyrim}), 488 cm^{-1}, 452 cm^{-1} (Ir-N), 274 cm^{-1} (Ir-Cl). (+)-HR-ESI-MS: *m/z* (%) 792.1824 ([M - Cl]+, 100%), 828.1567 ([M+H]+, 7%). HPLC purity: 98.9%; $t_{r'}$ = 13.61 min.

3.4.8 Synthesis of [IrCl($C_{22}H_{19}N_5O_5S$)($C_{15}H_{17}$)] (**C11**)

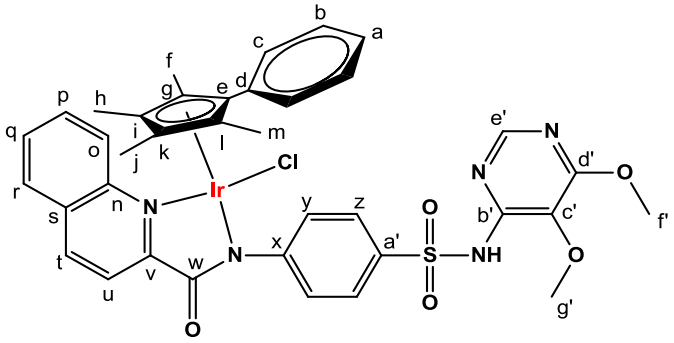

Di-μ-chlorido-(bis(chlorido(tetramethyl-η^5-cyclopentadienylbenzene))iridium(III)) (50.0 mg, 0.054 mmol), **L5** (50.5 mg, 0.109 mmol) and $NaHCO_3$ (9.10 mg, 0.109 mmol) were reacted in MeOH (1.50 mL) to afford an orange powder in 75% yield (73.0 mg). ^{1}H NMR (300 MHz, $CDCl_3$) δ 8.46 (d, H_o, 1H, $^3J_{(Ho\text{-}Hp)}$ 8.8 Hz), 8.34 (d, H_t, 1H, $^3J_{(Ht\text{-}Hu)}$ 8.4 Hz), 8.27 (d, H_u, 1H, $^3J_{(Hu\text{-}Ht)}$ 8.4 Hz), 8.17 (s, $H_{e'}$, 1H), 8.12 (d, H_y, 2H, $^3J_{(Hy\text{-}Hz)}$ 9.0 Hz), 8.06 (d, H_z, 2H, $^3J_{(Hz\text{-}Hy)}$ 9.0 Hz), 7.87 (d, H_r, 1H, $^3J_{(Hr\text{-}Hq)}$ 8.3 Hz), 7.63 - 7.56 (m, H_p, 1H), 7.45 - 7.30 (m, $H_{c,b,a,q}$, 6H), 3.97 (s, $H_{g'}$, 3H), 3.84 (s, $H_{f'}$, 3H), 1.50 (s, H_f, 3H), 1.45 (s, H_m, 3H), 1.41 (s, H_h, 3H), 0.90 (s, H_j, 3H). ^{13}C NMR (75 MHz, $CDCl_3$) δ 169.39 (C_w), 160.89 (C), 156.48 (C), 153.44 (C), 149.92 (C), 145.11 (C), 140.04 (CH), 133.64 (C), 131.16 (C), 131.02 (CH), 130.81 (C), 130.07 (CH), 129.79 ($C_{y/z/b/c}$), 129.07 ($C_{y/z/b/c}$), 128.87 (CH), 128.66 (CH), 128.47 (CH), 127.12 ($C_{y/z/b/c}$), 126.53 (C), 122.66 (CH), 95.98 ($C_{e/g/l/i/k}$), 95.86 ($C_{e/g/l/i/k}$), 87.49 ($C_{e/g/l/i/k}$), 83.49 ($C_{e/g/l/i/k}$), 81.57 ($C_{e/g/l/i/k}$), 60.69 ($C_{g'}$), 54.25 ($C_{f'}$), 10.27 ($C_{f/m}$), 9.71 ($C_{f/m}$), 8.66 ($C_{j/h}$), 8.37 ($C_{j/h}$). FT-IR (KBr): 1622 cm^{-1} (C=O), 1582 cm^{-1}, 1663 cm^{-1} (C=N_{quin}, C=N_{pyrim}). (+)-HR-ESI-MS: *m/z* (%) 854.2007 ([M - Cl]+, 100%), 890.1763 ([M+H]+, 22%). HPLC purity: 97.2%; $t_{r'}$ = 16.24 min.

3.4.9 Synthesis of [IrCl($C_{22}H_{19}N_5O_5S$)($C_{21}H_{21}$)] (**C12**)

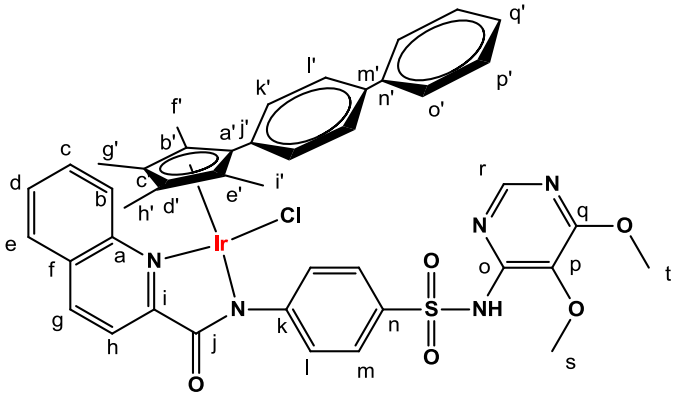

Di-μ-chlorido(bis(chlorido(4-(tetramethyl-η^5-cyclopentadienyl)-1,1'-biphenyl))iridium(III)) (50.0 mg, 0.0470 mmol), **L5** (43.4 mg, 0.0930 mmol) and $NaHCO_3$ (7.80 mg, 0.0930 mmol) were reacted in MeOH (1.50 mL) to afford an orange powder in 56% yield (50.0 mg). ^{1}H NMR (400 MHz, $CDCl_3$) δ 8.47 (d, H_b, 1H, $^3J_{(Hb\text{-}Hc)}$ 8.8 Hz), 8.34 (d, H_g, 1H, $^3J_{(Hg\text{-}Hh)}$ 8.4 Hz), 8.28 (d, H_h, 1H, $^3J_{(Hh\text{-}Hg)}$ 8.4 Hz), 8.17 (s, H_r, 1H), 8.15 (d, H_l, 2H, $^3J_{(Hl\text{-}Hm)}$ 8.9 Hz), 8.07 (d, H_m, 2H, $^3J_{(Hm\text{-}Hl)}$ 8.9 Hz), 7.86 (d, H_e, 1H, $^3J_{(He\text{-}Hd)}$ 8.2 Hz), 7.78 (s, H_{NHSO2}, 1H), 7.65 - 7.54 (m, $H_{k',l',c}$, 5H), 7.51 - 7.44 (m, $H_{p'}$, 2H), 7.44 – 7.35 (m, $H_{o',q',d}$, 4H), 3.97 (s, H_s, 3H), 3.84 (s, H_t, 3H), 1.52 (s, $H_{f'}$, 3H), 1.50 (s, $H_{i'}$, 3H), 1.40 (s, $H_{g'}$, 3H),

0.95 (s, $H_{h'}$, 3H).^{13}C NMR (101 MHz, $CDCl_3$) δ 169.40 (C_j), 160.89 (C), 156.49 (C), 153.44 (C), 149.92 (C), 145.13 (C), 141.16 (C), 140.13 (C), 140.06 (CH), 133.67 (C), 131.02 (CH), 130.83 (C), 130.22 (CH), 130.12 (C), 130.06 (CH), 129.13 (CH), 129.08 (CH), 128.90 (CH), 128.66 (CH), 127.96 (CH), 127.62 (CH), 127.13 (CH), 127.06 (CH), 126.54 (C), 122.68 (CH), 95.93 ($C_{a'/b'/c'/d'/e'}$), 95.73 ($C_{a'/b'/c'/d'/e'}$), 87.82 ($C_{a'/b'/c'/d'/e'}$), 83.37 ($C_{a'/b'/c'/d'/e'}$), 81.39 ($C_{a'/b'/c'/d'/e'}$), 60.69 (C_s), 54.25 (C_t), 10.34 ($C_{f'/i'}$), 9.83 ($C_{f'/i'}$), 8.64 ($C_{g'/h'}$), 8.36 ($C_{g'/h'}$). FT-IR (KBr): 1623 cm^{-1} (C=O), 1579 cm^{-1}, 1661 cm^{-1} (C=N_{quin}, C=N_{pyrim}). (+)-HR-ESI-MS: *m/z* (%) 930.2319 ([M - Cl]+, 100%), 966.2080 ([M+H]+, 18%). HPLC purity: 94.3%; $t_{r'}$ = 20.23 min.

3.4.10 X-Ray crystallographic data collection

Crystals of **L4** were grown by layering a DCM solution of **L4** with hexane and leaving to stand in a sealed vial for several days at room temperature. A single needle like transparent crystal of diffraction quality was selected for analysis and mounted in oil. Low temperature X-ray diffraction data collection for **L4** was performed at 100(2) K on a Bruker APEX II DUO CCD diffractometer using graphite-monochromated Mo Kα radiation (0.71073 Å). An Oxford Cryostream plus, 700 series cryostat that was attached to the diffractometer cooled the sample. Data were collected up to 55.1º. A colourless plate was used of dimensions, 0.118 × 0.073 × 0.048 mm^3, the crystal was triclinic, space group $P\bar{1}$, The asymmetric unit cell had parameters: a = 8.319(2), b = 10.194(3), c = 12.280(3) Å, α = 109.559(4), β = 100.736(4), γ = 103.451(4)°, V = 913.9(4) Å^3, Z = 2, D_c = 1.510 g cm^{-3}, F_{000} = 432. 24537 reflections collected, 4207 unique (R_{int} = 0.0496). Final *GooF* = 1.045, $R1$ = 0.0402, $wR2$ = 0.0970, R indices based on 3483 reflections with $I > 2\sigma(I)$ (refinement on F^2), 272 parameters, 0 restraints. Lp and absorption corrections applied, μ = 0.221 mm^{-1}. Bruker diffraction, SAINT[39] software was used for data reduction and unit cell determinations, while SADABS[40,41] was used for absorption corrections. SHELXT-16[42] and SHELLXT-14[43] was used to refine and solve crystal structures with the X-seed[44,45] graphical user interface. Calculated positions were used to place hydrogen atoms and non-hydrogen atoms were refined anisotropically. Hydrogens on oxygen and nitrogen atoms were located with electron density maps. Figures were generated from the 3D crystal lattice with Mercury 3.7.[46–49]

3.4.11 HPLC method and purity determination

Purity measurements by HPLC were carried out using the Agilent 1220 system with a DAD and 100 µL loop. The column used was a Kinetex® 5 µm C18 100 Å, 150 x 4.6 mm with a 5 µm pore size. The mobile phase was H_2O 0.1% TFA/MeCN 0.1% TFA at gradients of t=0 min 10% B, t=30 min 80% B, t=40 min 80% B, t=41 min 10% B, and t=55 min 10% B over a 55 min period. The flow rate was 1 mL min^{-1}, and the detection wavelength was set at 254 nm and 400 nm with the reference wavelength at 360 nm. Samples were dissolved in 10% MeCN/90% H_2O at ca. 100 µM. Sample injections were half the loop volume (50 µL) with needle washes of MeCN and H_2O between injections. It was assumed that all species in a sample have the same extinction coefficient at 254 nm and 400 nm. All peaks were manually integrated.

3.5 References

(1) OpenStax, Chemistry. OpenStax CNX. Jun 20, 2016 Http://Cnx.Org/Contents/85abf193-2bd2-4908-8563-90b8a7ac8df6@9.311.

(2) Barros, J. *Cutting-Edge Chemistry: Take Green Routes to Amide Formation*; Online, 2016.

(3) Brown, T. L.; LeMay Jr, H. E.; Bursten, B. E.; Murphy, C. J.; Langford, S. J.; Sagatys, D. Nitrogen-Containing Compounds of Biological Relevance. In *Chemistry The Central Science: A Broad Perspective*; Pearson, 2010; pp 1032–1083.

(4) Brown, T. L.; LeMay Jr, H. E.; Bursten, B. E.; Murphy, C. J.; Langford, S. J.; Sagatys, D. Carboxylic Acids and Their Derivatives. In *Chemistry The Central Science: A Broad Perspective*; Pearson, 2010; pp 966–1003.

(5) El-Faham, A.; Albericio, F. Peptide Coupling Reagents, More than a Letter Soup. *Chem. Rev.* **2011**, *111*, 6557 - 6602.

(6) Pattabiraman, V. R.; Bode, J. W. Rethinking Amide Bond Synthesis. *Nature* **2011**, *480*, 471 - 479.

(7) Mishra, A.; Kaushik, N. K.; Verma, A. K.; Gupta, R. Synthesis, Characterization and Antibacterial Activity of Cobalt(III) Complexes with Pyridine-Amide Ligands. *Eur. J. Med. Chem.* **2008**, *43*, 2189–2196.

(8) Gandhi, N.; Kumar, A.; Kumar, C.; Mishra, N.; Chaudhary, P.; Kaushik, N. K.; Singh, R. Synthesis, Characterization, Thermal and Biological Activity of Some Novel Cadmium(II) - Pyridine and Purine Base Complexes. *Main Gr. Chem.* **2016**, *15* (1), 35–46.

(9) Shi, C. Y.; Gao, E. J.; Ma, S.; Wang, M. L.; Liu, Q. T. Synthesis, Crystal Structure, DNA-Binding and Cytotoxicity in Vitro of Novel Cis-Pt(II) and Trans-Pd(II) Pyridine Carboxamide Complexes. *Bioorganic Med. Chem. Lett.* **2010**, *20*, 7250–7254.

(10) Christofis, P.; Katsarou, M.; Papakyriakou, A.; Sanakis, Y.; Katsaros, N.; Psomas, G. Mononuclear Metal Complexes with Piroxicam: Synthesis, Structure and Biological Activity. *J. Inorg. Biochem.* **2005**, *99* (11), 2197–2210.

(11) Montalbetti, C. A. G. N.; Falque, V. Amide Bond Formation and Peptide Coupling. *Tetrahedron* **2005**, *61*, 10827–10852.

(12) Varalakshmi, M.; Nagaraju, C. Synthesis, Spectral Characterization and Biological Activity of N-4-(N-2-(Trifluoromethylphenyl))Sulfamoyl Amide Derivatives. *Org. Commun.* **2016**, *9* (4), 94–101.

(13) Deshmukh, G. K.; Irlapati, N. R.; Jachak, S. M.; Kamboj, R. K.; Karche, V. P.; Palle, V. P.; Sinha, N. Oxazole and Isoxazole Crac Modulators. WO2012056478A1, 2012.

(14) Flaherty, D. P.; Simpson, D. S.; Miller, M.; Maki, B. E.; Zou, B.; Shi, J.; Wu, M.; McManus, O. B.; Aubé, J.; Li, M.; et al. Potent and Selective Inhibitors of the TASK-1 Potassium Channel through Chemical Optimization of a Bis-Amide Scaffold. *Bioorganic Med. Chem. Lett.* **2014**, *24* (16), 3968–3973.

(15) Epsztajn, J.; Bieniek, A.; Kowalska, J. A. Application of Organolithium and Related Reagents in Synthesis. Part 9. Synthesis and Metallation of 4-Chloropicolin- and 2-Chloroisonicotinanilides. A Useful Method for Preparation of 2,3,4-Trisubstituted Pyridines. *Tetrahedron* **1991**, *47* (9), 1697–1706.

(16) Kalusa, A.; Chessum, N.; Jones, K. An Efficient Synthesis of 2,3-Diaryl (3H)-Quinazolin-4-Ones via Imidoyl Chlorides. *Tetrahedron Lett.* **2008**, *49* (41), 5840–5842.

(17) Kalisiak, J.; Piątek, P.; Jurczak, J. A Versatile Approach to the Synthesis of Pendant Benzodiazacoronands. *Synthesis (Stuttg).* **2005**, *13* (13), 2210–2214.

(18) Ihmaid, S. Exploring the Dual Inhibitory Activity of Novel Anthranilic Acid Derivatives towards α-Glucosidase and Glycogen Phosphorylase Antidiabetic Targets: Design, in Vitro Enzyme Assay, and Docking Studies. *Molecules* **2018**, *23* (6), 1304 - 1319.

(19) Schnute, M. E.; Wennerstål, M.; Alley, J.; Bengtsson, M.; Blinn, J. R.; Bolten, C. W.; Braden, T.; Bonn, T.; Carlsson, B.; Caspers, N.; et al. Discovery of 3-Cyano- N-(3-(1-Isobutyrylpiperidin-4-Yl)-1-Methyl-4-(Trifluoromethyl)-1 H-Pyrrolo[2,3- b]Pyridin-5-Yl)Benzamide: A Potent, Selective, and Orally Bioavailable Retinoic Acid Receptor-Related Orphan Receptor C2 Inverse Agonist. *J. Med. Chem.* **2018**, *61* (23), 10415–10439.

(20) Lee, S. J.; Yu, D. T.; Miskowski, T. A.; Riviello, C. M.; Sircar, J. C.; Blazejewski, K. M.; Macina, O. T.; Frierson, M. R.; Konishi, Y.; Kondo, K.; et al. Discovery of Potent Cyclic GMP Phosphodiesterase Inhibitors. 2-Pyridyl- and 2-Imidazolylquinazolines Possessing Cyclic GMP Phosphodiesterase and Thromboxane Synthesis Inhibitory Activities. *J. Med. Chem.* **1995**, *38* (18), 3547–3557.

(21) Aleksanyan, D. V.; Nelyubina, Y. V.; Klemenkova, Z. S.; Kozlov, V. A. Synthesis and Complexing Properties of Phosphorus-Substituted Pyridine-2-Carboxylic Acid Anilides. *Phosphorus, Sulfur Silicon Relat. Elem.* **2014**, *189* (7–8), 1028–1042.

(22) Kil, K. E.; Poutiainen, P.; Zhang, Z.; Zhu, A.; Kuruppu, D.; Prabhakar, S.; Choi, J. K.; Tannous, B. A.; Brownell, A. L. Synthesis and Evaluation of N-(Methylthiophenyl)Picolinamide Derivatives as PET Radioligands for Metabotropic Glutamate Receptor Subtype 4. *Bioorganic Med. Chem. Lett.* **2016**, *26* (1), 133–139.

(23) Özdemir, Ü. Ö.; Güvenç, P.; Şahin, E.; Hamurcu, F. Synthesis, Characterization and Antibacterial Activity of New Sulfonamide Derivatives and Their Nickel(II), Cobalt(II) Complexes. *Inorganica Chim. Acta* **2009**, *362* (8), 2613–2618.

(24) Li, S. N.; Zhai, Q. G.; Hu, M. C.; Jiang, Y. C. Synthesis, Crystal Structures and Characterization of Three Novel Complexes with N-[2-(2-Hydroxybenzylideneamino)Ethyl]-4-Methyl-Benzene-Sulfonamide as Ligand. *Inorganica Chim. Acta* **2009**, *362*, 2217–2221.

(25) Wójcik, G. M. Structural Chemistry of Anilines. In *PATAI'S Chemistry of Functional Groups*; Patai, S., Ed.; Wiley-VCH: Weinheim, 2009.

(26) Sinnokrot, M. O.; Sherrill, C. D. Highly Accurate Coupled Cluster Potential Energy Curves for the Benzene Dimer: Sandwich, T-Shaped, and Parallel-Displaced Configurations. *J. Phys. Chem. A* **2004**, *108* (46), 10200–10207.

(27) McGaughey, G. B.; Gagné, M.; Rappé, A. K. π-Stacking Interactions. Alive and Well in Proteins. *J. Biol. Chem.* **1998**, *273* (25), 15458–15463.

(28) Almodares, Z.; Lucas, S. J.; Crossley, B. D.; Basri, A. M.; Pask, C. M.; Hebden, A. J.; Phillips, R. M.; Mcgowan, P. C. Rhodium, Iridium, and Ruthenium Half-Sandwich Picolinamide Complexes as Anticancer Agents. *Inorg. Chem.* **2014**, *53* (2), 727–736.

(29) Punna, B.; Aradhyula, R.; Kaminsky, W.; Rao, M. Half-Sandwich d_6 Metal Complexes with Bis (Pyridine Carboxamide) Benzene Ligand : Synthesis and Spectral Analysis. *J. Mol. Struct.* **2017**, *1149*, 162–170.

(30) Popescu, A.; Simion, A.; Scozzafava, A.; Briganti, F.; Supuran, C. T. Carbonic Anhydrase Inhibitors. Schiff Bases of Some Aromatic Sulfonamides and Their Metal Complexes: Towards More Selective Inhibitors of Carbonic Anhydrase Isozyme IV. *J. Enzyme Inhib.* **1999**, *14*, 407–423.

(31) Başar, E.; Tunca, E.; Bülbül, M.; Kaya, M. Synthesis of Novel Sulfonamides under Mild Conditions with Effective Inhibitory Activity against the Carbonic Anhydrase Isoforms I and II. *J. Enzyme Inhib. Med. Chem.* **2016**, *31* (6), 1356–1361.

(32) Trans, D.; Lucas, S. J.; Lord, R. M.; Wilson, R. L.; Phillips, R. M.; Mcgowan, P. C. Coordinating Bidentate Ligands as Potential Anti-Cancer Agents. **2012**, *3* (Scheme 2), 13800–13802.

(33) Chohan, Z. H.; Supuran, C. T. Structure and Biological Properties of First Row D-Transition Metal Complexes with N-Substituted Sulfonamides. *J. Enzyme Inhib. Med. Chem.* **2008**, *23* (2), 240–251.

(34) Ferraro, J. R. *Low-Frequency Vibrations of Inorganic and Coordination Compounds.*, 1st ed.; Springer US: New York, 1971.

(35) Adams, D. M. *Metal-Ligand and Related Vibrations: A Critical Survey of the Infrared and Raman Spectra of Metallic and Organometallic Compounds*; St. Martin's Press, 1968.

(36) Nakamoto, K. Applications in Coordination Chemistry. In *Infrared and Raman Spectra of Inorganic and Coordination Compounds: Part B: Applications in Coordination, Organometallic, and Bioinorganic Chemistry*; John Wiley & Sons, Inc: Hoboken, 2008; pp 1–273.

(37) Sigel, H.; Martin, R. B. Coordinating Properties of the Amide Bond. Stability and Structure of Metal Ion Complexes of Peptides and Related Ligands. *Chem. Rev.* **1982**, *82*, 385–426.

(38) Tönnemann, J.; Risse, J.; Grote, Z.; Scopelliti, R.; Severin, K. Efficient and Rapid Synthesis of Chlorido-Bridged Half-Sandwich Complexes of Ruthenium, Rhodium, and Iridium by Microwave Heating. *Eur. J. Inorg. Chem.* **2013**, *2013* (26), 4558–4562.

(39) Bruker AXS Inc. SAINT Data Collection Software, Version V7.99A. Bruker AXS Inc.: Madison, WI 2012.

(40) Bruker AXS Inc. SADABS, Version 2012/1. Bruker AXS Inc.: Madison, WI 2012.

(41) Blessing, R. H.; IUCr. An Empirical Correction for Absorption Anisotropy. *Acta Crystallogr. Sect. A Found. Crystallogr.* **1995**, *51* (1), 33–38.

(42) Sheldrick, G. M.; IUCr. Crystal Structure Refinement with *SHELXL*. *Acta Crystallogr. Sect. C Struct. Chem.* **2015**, *71* (1), 3–8.

(43) Sheldrick, G. M. *SHELXT* – Integrated Space-Group and Crystal-Structure Determination. *Acta Crystallogr. Sect. A Found. Adv.* **2015**, *71* (1), 3–8.

(44) Barbour, L. J. X-Seed — A Software Tool for Supramolecular Crystallography. *J. Supramol. Chem.* **2001**, *1* (4–6), 189–191.

(45) Atwood, J. L.; Barbour, L. J. Molecular Graphics: From Science to Art. *Cryst. Growth Des.* **2003**, *3* (1), 3–8.

(46) Taylor, R.; Macrae, C. F.; IUCr. Rules Governing the Crystal Packing of Mono- and Dialcohols. *Acta Crystallogr. Sect. B Struct. Sci.* **2001**, *57* (6), 815–827.

(47) Macrae, C. F.; Bruno, I. J.; Chisholm, J. A.; Edgington, P. R.; McCabe, P.; Pidcock, E.; Rodriguez-Monge, L.; Taylor, R.; van de Streek, J.; Wood, P. A.; et al. *Mercury CSD 2.0* – New Features for the Visualization and Investigation of Crystal Structures. *J. Appl. Crystallogr.* **2008**, *41* (2), 466–470.

(48) Macrae, C. F.; Edgington, P. R.; McCabe, P.; Pidcock, E.; Shields, G. P.; Taylor, R.; Towler, M.; van de Streek, J.; IUCr. *Mercury* : Visualization and Analysis of Crystal Structures. *J. Appl. Crystallogr.* **2006**, *39* (3), 453–457.

(49) Bruno, I. J.; Cole, J. C.; Edgington, P. R.; Kessler, M.; Macrae, C. F.; McCabe, P.; Pearson, J.; Taylor, R.; IUCr. New Software for Searching the Cambridge Structural Database and Visualizing Crystal Structures. *Acta Crystallogr. Sect. B Struct. Sci.* **2002**, *58* (3), 389–397.

Chapter 4

Biological investigations and activity against *Mycobacterium tuberculosis* and *Plasmodium* parasites

4.1 Introduction

The process of drug discovery is a complicated one, dependant on a multitude of factors for success. It does not only rely on the efficacy of the drug candidate to kill or inhibit the chosen target, as there are many chemical entities able to accomplish this, but rather requires a candidate that will not negatively affect the host and can be safely transported and administered to the target site. The drug candidate should also not have toxic metabolites and needs to be able to be excreted in a safe and expedient manner after it has served its purpose. It has been estimated that the success rate of identifying a hit compound that progresses through clinical trials to the market is only 0.001% and that the cost of its discovery and development is more than $1.75 billion.[1,2] Because the success of a drug candidate depends not only on its potency but also largely on its pharmacological properties, it is vital that potential biological processes that drug candidates will be subjected to upon administration are able to be mimicked and tested.[3,4] There are thus many methods that have been developed to test the most important processes that drugs will undergo in the body, collectively known as their ADMET properties (absorption, distribution, metabolism, excretion and toxicity) or drug-like properties. These tests are routine parts of the drug discovery process and can help eliminate candidates that would otherwise have wasted valuable resources.[4-6]

Whether candidates should be tested for favourable activity against the target or pharmacokinetic properties first is a good question to consider and though it is not currently widely done in industry, Lipinski[7] suggests that the identification of candidates with optimal pharmacokinetic properties would be a more effective and productive approach to drug discovery. The process of drug discovery progresses via the identification of several hit compounds followed by their finetuning into lead compounds and ultimately the selection of a most suitable target.[5,6,8] The optimisation process and selection of a lead compound highly favours promising pharmacokinetic properties and allow for the most stable, active and least toxic molecules to be selected.[5,6,8]

It is thus important that the *in vitro* properties of potential candidates be investigated as far as possible to streamline later target selection and lead optimisation. It is with this purpose that both the solubility of the drug candidates, **C1** – **C12**, which provides important information on bioavailability, and their potential aquation, which can aid in the identification of the potent species, were investigated to identify the most potent and suitable candidates for further testing.

4.2 Results and Discussion

4.2.1 Turbidimetric solubility assays

Aqueous solubility plays an important part of drug discovery given the physiological environment in which medicine is administered in and is thus vital information required to correctly analyse biological data. If the solubility of a drug candidate is below that of the IC_{50} of the compound, then it may be a suspension or solid when administered which has important consequences when the method of administration is being considered.

The aqueous solubility of the first and second libraries, consisting of six imino-sulfadoxine iridium complexes (**C1** – **C6**) and six amido-sulfadoxine iridium complexes (**C7** – **C12**), respectively (Figure 4.1), was investigated by means of a turbidimetric assay.

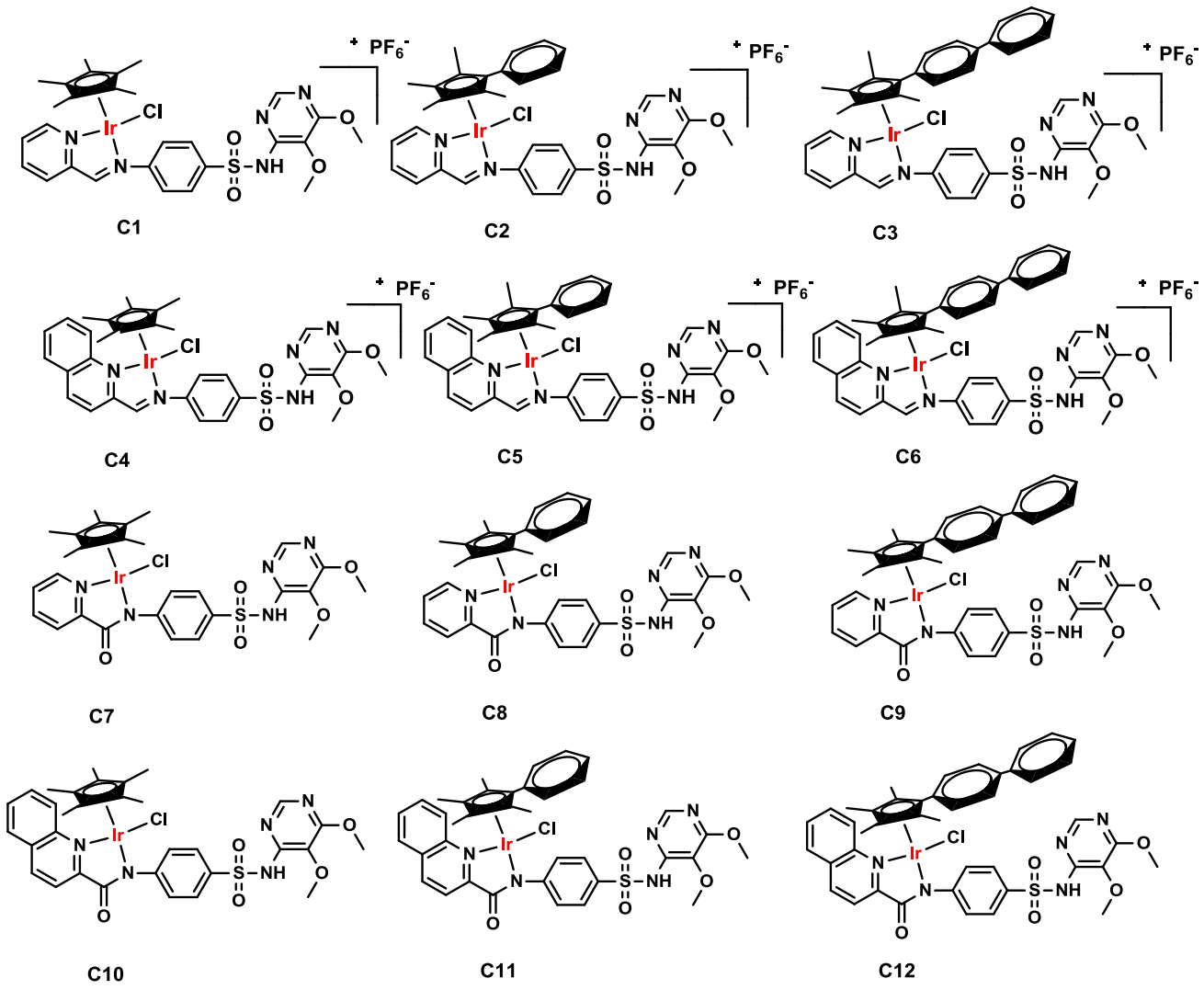

Figure 4.1 - All complexes tested for biological activity against *Mtb* and *P. falciparum*.

The assay analyses the turbidity of the compounds in a solution of 2% DMSO in phosphate buffered saline with a pH of 7.4 at 620 nm. These conditions are chosen with the aim of being applicable to the *in vitro* biological testing that is performed on drug candidates in addition to attempting to

resemble physiological conditions as far as is feasible. The measurements were done in triplicate with two controls, one for soluble species (hydrocortisone, Figure 4.2) and one for less soluble species (reserpine, Figure 4.2).

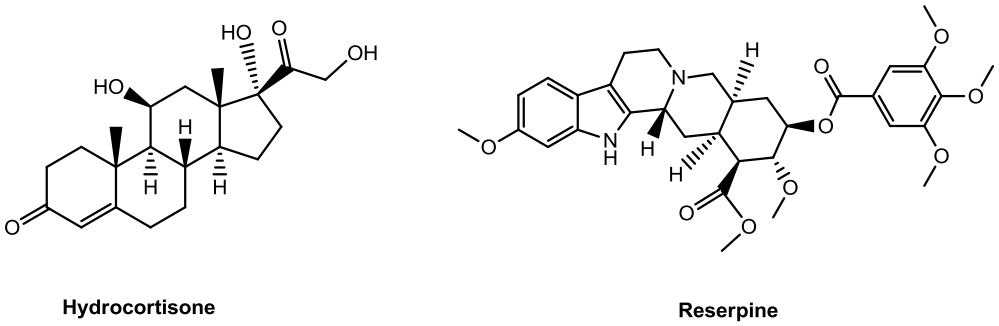

Figure 4.2 - Controls used for turbidimetric assays.

The results are shown in Table 4.1 and an example of the graphical data from which the solubility values are obtained is shown in Figure 4.3.

Table 4.1 - Solubility data of imino complexes, amido ligands and complexes and control drugs

Compound		**C1**	**C2**	**C3**	**Res**	**Hyd**
Solubility (μM)		> 200	> 200	40 - 80		
Compound		**C4**	**C5**	**C6**		
Solubility (μM)		> 160	120 - 160	20 - 40		
Compound	**L6**	**C7**	**C8**	**C9**	40 - 80	> 200
Solubility (μM)	> 200	> 200	> 160	40 - 60		
Compound	**L7**	**C10**	**C11**	**C12**		
Solubility (μM)	> 200	160 - 200	40 - 60	20 - 40		

Of the two controls reserpine is considered insoluble, while hydrocortisone is soluble.

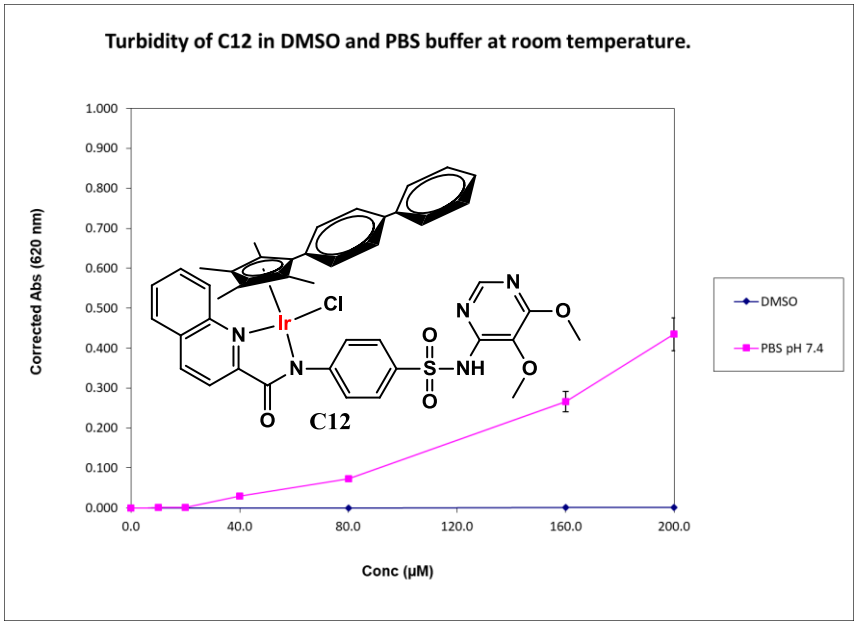

Figure 4.3 - Graph of the turbidity of **C12** in DMSO and PBS at room temperature.

Generally, in the design of a drug candidate, solubility of > 100 µM is the target, however values below this are often obtained.[8,9] To determine whether the solubility is still within the acceptable range other factors such as the potency and the permeability play a large role.[8,9] Most of the drug candidates investigated lie above the target value and those which do not are typically the most effective as is shown later. Thus, these drug candidates are still viable for further investigation. From the data in Table 4.1 it is apparent that as the half-sandwich Cp^x moiety is extended with arene rings, the aqueous solubility of the complexes decreases and conversely the hydrophobicity increases. Furthermore, when comparing the pyridyl complexes to the quinolyl complexes the solubility also decreases. This trend is to be expected as in both cases mentioned, hydrophobic groups are being added to the complex, effectively adding additional hydrophobic character to the complexes. This may be beneficial in assisting the complexes to permeate the cell membranes of the targeted organisms, as a greater hydrophobicity increases the ease with which the molecules can diffuse across the hydrophobic section of the phospholipid bilayer of the relevant cells. The hydrophobicity increasing by too large a margin, however, can lead to the compounds being insoluble under physiological conditions which would complicate administration thereof.

4.2.2 Biological testing against *Mtb*

Testing of the compounds against the *Mycobacterium tuberculosis* strain H37Rv was performed by Audrey Jordaan working under Prof. Digby Warner at the University of Cape Town. The minimum inhibitory concentration that inhibits 90% of cell growth (MIC_{90}) of *Mtb* was determined by growing the cells to an optical density between 0.6 and 0.7 before making a serial dilution with liquid media to appropriate concentrations and incubating. The fluorescence intensity was determined after the addition of alamar blue reagent and the MIC_{90} values calculated from dose response curves that were generated from the raw fluorescent data. A detailed description of the protocol can be found in the experimental section.

The biological data of the complexes and ligands tested against *Mtb* is shown in Table 4.2.

Table 4.2 - Activity of the imino and amido complexes against *Mtb* strain H37Rv.				
Media:	**7H9 CAS GLU Tx[a]**		**7H9 ADC GLU Tw[b]**	
Compound	**Day 7 (μM)**	**Day 14 (μM)**	**Day 7 (μM)**	**Day 14 (μM)**
C1	NA*	35.1	NA*	NA*
C2	79.9	32.4	NA*	NA*
C3	13.8	3.62	NA*	NA*
C4	32.6	16.5	NA*	NA*
C5	8.64	1.73	31.5	61.3
C6	2.78	7.13	14.0	28.6
L6	NA*	NA*	NA*	NA*
L7	NA*	NA*	NA*	NA*
C7	NA*	80.406	NA*	NA*
C8	NA*	NA*	NA*	NA*
C9	68.3	34.3	NA*	NA*
C10	NA*	75.5	NA*	NA*
C11	NA*	NA*	NA*	NA*
C12	NA*	NA*	NA*	NA*
Cp* dimer	78.1	18.6	NA*	NA*
Cp^{xPh} dimer	8.51	4.24	NA*	NA*
Cp^{xbiPh} dimer	2.32	0.455	NA*	NA*
Rifampicin	0.032	0.016	0.004	0.005

*Not active at the highest concentration tested (125 μg/ml).
a – Middlebrook 7H9 media supplemented with casitone, glucose and tyloxapol
b – Middlebrook 7H9 media supplemented with ADC (albumin-dextrose-catalase), glucose and tween 80.

Each measurement was done in duplicate and compounds were tested in two 7H9 media solutions, one enriched with casitone, glucose and tyloxapol and the other with ADC (albumin-dextrose-catalase), glucose and tween 80. A general decrease in the MIC_{90} is seen between day 7 and day 14, except in the case of the quinolyl imino Cp^{xbiPh} complex (**C6**) where an increase in the MIC_{90} is seen. This could be due to the gradual decomposition of the complex in the subsequent 7 days or due to association with other species in solution instead. In addition to this, a drastic decrease in efficacy is seen when the compounds are tested in the media enriched with ADC (Table 4.2, 7H9 ADC GLU Tw). This large decrease in activity could be attributed to serum-albumin binding of the compounds which would prevent them from inhibiting the growth of the infectious cells.[10] If this is the case then administration of these compounds would require some form of protection until they are released within the targeted cells. Figure 4.4 illustrates the results of the testing in the media employing tyloxapol as surfactant.

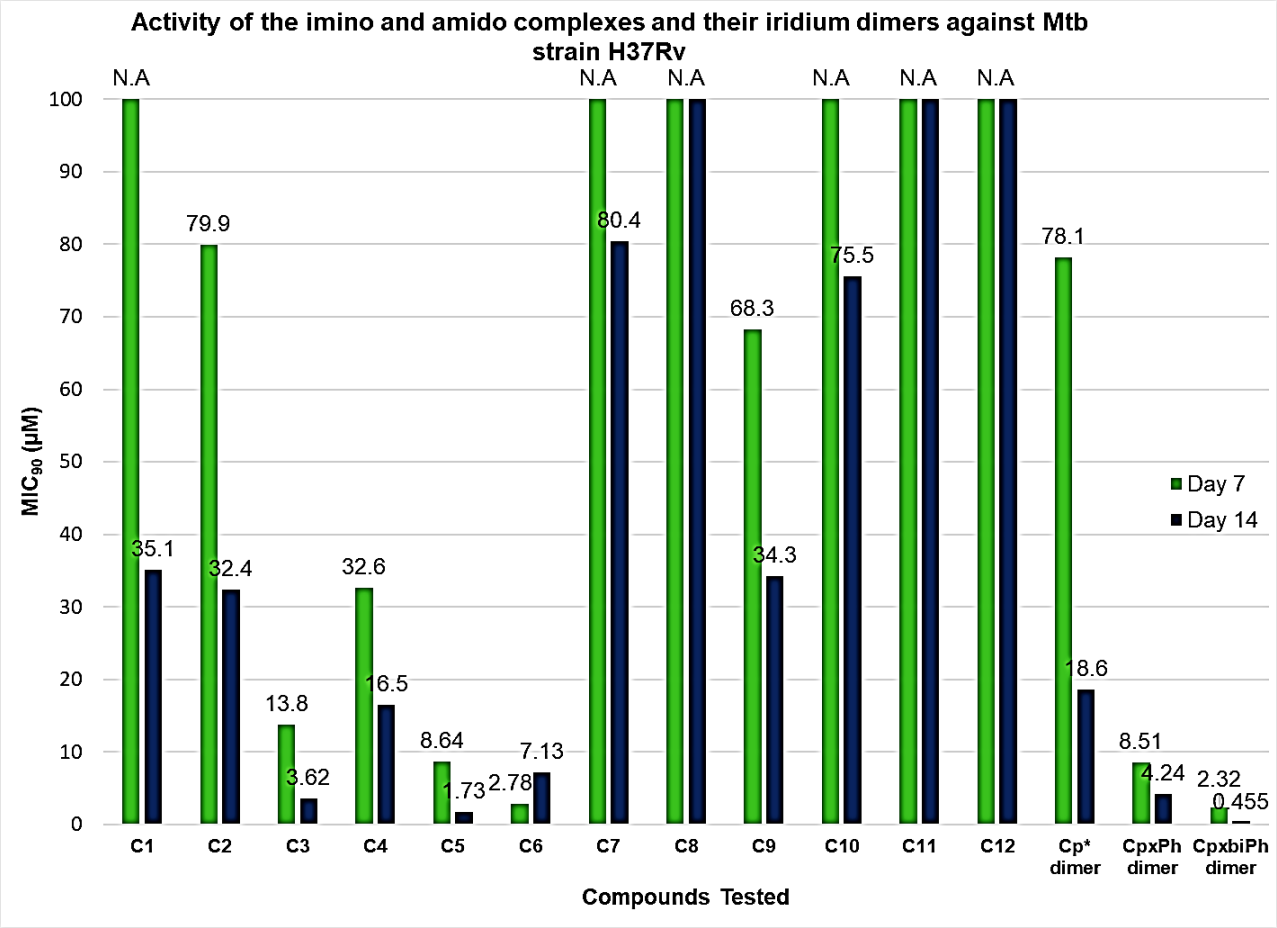

Figure 4.4 – Graph of the activity of the imino and amido complexes and their iridium dimers against *Mtb* strain H37Rv. N.A = Not active at the highest concentration tested.

From this data it is seen that there is a general increase in activity as the half-sandwich moiety is extended (**C1** – **C3**; **C4** – **C6**; **C7** – **C9**; **C10** – **C12**). This is seen particularly clearly when looking at the activity of the iridium chlorido dimers, of which the biphenyl analogue exhibits a sub micromolar activity of 0.455 µM, whereas the Cp* analogue has an activity of 18.6 µM. The trend is seen for the other complexes as well. The apparent exception being **C6** in this data set, however, the activity of **C6** on day 7 was 2.78 µM which is lower than that of **C5** which was 8.64 µM on day 7. As mentioned earlier this discrepancy in activity is likely due to gradual decomposition of the complex after day 7 and is seen in the trends mentioned hereafter as well. Furthermore, when comparing the activity of the pyridyl complexes (**C1** – **C3**; **C7** – **C9**) to that of the quinolyl ones (**C4** – **C6**; **C10** – **C12**) a greater activity is seen for the quinolyl complexes. This is seen especially in the case of the imino Cp* analogues (**C1** and **C4**) in which the quinolyl complex (**C4**) is nearly twice as potent as the pyridyl one (**C1**). Finally, when comparing the amido complexes (**C7** – **C12**) to their imino analogues (**C1** – **C6**), the imino complexes are 2 – 10-fold more active. Purity issues prevented the imino ligands from being tested for activity, while the amido ligands along with complexes **C8**, **C11** and **C12** did not show any activity at the highest concentration tested against *Mtb* strain H37Rv. Additionally, the difference in activity between day 7 and day 14 indicates these drug candidates take some time to effectively inhibit *Mtb*. In summary, the quinolyl Cp^{xbiPh} structure (**C6**) is the most effective in the case

of the imino series whereas the activity for the amido series is significantly lower and does not conform to the trend.

4.2.3 Biological testing against *P. falciparum*

Testing of the compounds against *Plasmodium falciparum* malarial parasite strains 3D7, Dd2 and HB3 and the human epidermal keratinocytes (HEK) cell line was performed by Sandra Duffy working under Prof. Vicky Avery at Griffith University. To summarise the protocol, the compounds were serially diluted to appropriate concentrations in a 384-well imaging plate before cultures of the parasites were added to the wells and the imaging plates were then incubated for 72 hours under the same conditions used to produce the original cultures. The plates were then stained with 4',6-diamidino-2-phenylindole (DAPI) and incubated overnight at room temperature before being imaged on an Opera confocal high content imaging system. Normalized data was used to determine the % inhibition of the compounds and plot the dose response curves from which IC_{50} values were calculated using graph pad prism where appropriate. A detailed description of the protocol can be found in the experimental section.

The complexes, **C1** – **C5**, **C7** – **C12**, and ligands, **L7** and **L8**, were also tested against several strains of the malarial parasite *P. falciparum* as well as to determine the toxicity to healthy cells of these compounds, the results of which are shown in Table 4.3. Unfortunately, there was not enough pure sample available of **C6** to be tested against the malarial strains as well and a full comparison can thus not be made for the quinolyl imino system.

Table 4.3 - Percentage inhibition of metal complexes and their ligands against *Plasmodium* parasitic strains and human skin cells with selected IC_{50} values.																
Strain/Cell line	**3D7A**		**3D7B**		**Dd2A**		**Dd2B**		**HB3A**		**HB3B**		**HEKA**		**HEKB**	
Compound	**IC_{50} µM**	**% inh 80 µM**	**IC_{50} µM**	**% inh 80 µM**	**IC_{50} µM**	**% inh 80 µM**	**IC_{50} µM**	**% inh 80 µM**	**IC_{50} µM**	**% inh 80 µM**	**IC_{50} µM**	**% inh 80 µM**	**IC_{50} µM**	**% inh 80 µM**	**IC_{50} µM**	**% inh 80 µM**
Cp* dimer	> 45	65	> 45	72	> 45	49	> 45	54	> 45	76	> 45	71	> 45	-3	> 45	-1
Cp^{xPh} dimer	13.5	99	14.4	98	N/A	103	16.9	98	19.3	94	20.4	93	> 45	64	> 45	34
Cp^{xbiPh} dimer	9.02	99	5.87	98	6.54	100	10.3	99	8.99	95	9.29	95	> 45	70	> 45	55
C1	> 45	3	> 45	-4	> 45	18	> 45	26	> 45	27	> 45	54	> 45	-8	> 45	-4
C2	> 45	48	> 45	47	> 45	54	> 45	60	> 45	50	> 45	67	> 45	-7	> 45	-2
C3	> 45	77	> 45	68	> 45	88	> 45	86	> 45	75	> 45	93	> 45	-1	> 45	1
C4	> 45	99	> 45	99	> 45	92	> 45	92	> 45	92	> 45	99	> 45	-2	> 45	-2
C5	13.8	98	14.5	99	19.6	98	16.6	98	15.1	96	9.44	85	> 45	7	> 45	14
C7	> 45	50	> 45	39	> 45	38	> 45	51	> 45	32	> 45	28	> 45	-3	> 45	-2
C8	> 45	1	> 45	-4	> 45	13	> 45	23	> 45	7	> 45	21	> 45	-3	> 45	0
C9	> 45	21	> 45	7	> 45	25	> 45	55	> 45	3	> 45	94	> 45	3	> 45	2
C10	> 45	97	> 45	88	> 45	92	> 45	93	> 45	80	> 45	94	> 45	40	> 45	67
C11	> 45	48	> 45	42	> 45	38	> 45	32	> 45	48	> 45	37	> 45	52	> 45	25
C12	0.975	97	0.574	97	1.41	96	0.766	98	0.941	93	0.721	91	> 45	73	> 45	53
L4	> 45	13	> 45	-1	> 45	23	> 45	22	> 45	15	> 45	28	> 45	-3	> 45	-2
L5	> 45	14	> 45	11	> 45	24	> 45	30	> 45	30	> 45	60	> 45	-7	> 45	-5

All IC_{50} values labelled as > 45, did not give a plateau in the graphing data and as such GraphPad prism 4.0 was unable to determine an exact value. Compounds from which the IC_{50} values could be exactly determined have been highlighted in green.

Strain 3D7 is chloroquine sensitive and the standard genomic reference strain[11,12], whereas strain Dd2 is a multidrug resistant strain[13,14] and strain HB3 is a gametocyte forming pyrimethamine resistant and chloroquine sensitive strain.[15,16] Each of the strains were tested in duplicate with two biological replicates (labelled A and B). The percentage inhibition at a compound concentration of 80 µM has been calculated along with the subsequent IC_{50} of the compound where an E_{max} value was able to be determined from the sigmoidal dose response curves (the determination of which required a plateau with minimum two points to be reached in the sigmoidal curve). Compounds which did not give a plateau and for which IC_{50} values could not be determined were given values of > 45 µM. Table 4.3 highlights in green the compounds for which IC_{50} values were calculated.

The percentage inhibition values are generally similar between biological replicates, as would be expected, with several exceptions – in particular for the HB3 strain where there are some drastic differences for compounds **C1**, **C9**, **L4** and **L5**. **C9** also shows a large difference for the strains 3D7 and Dd2 which could indicate that one of these readings was faulty for this compound. There is also a significant difference in the inhibition of the HEK cell line for compounds **C10** – **C12** and the Cp^{xPh} dimer. Figure 4.5 shows the average percentage inhibition between the two biological replicates of each strain and the HEK cell line, and several trends in the activity can be observed through this representation.

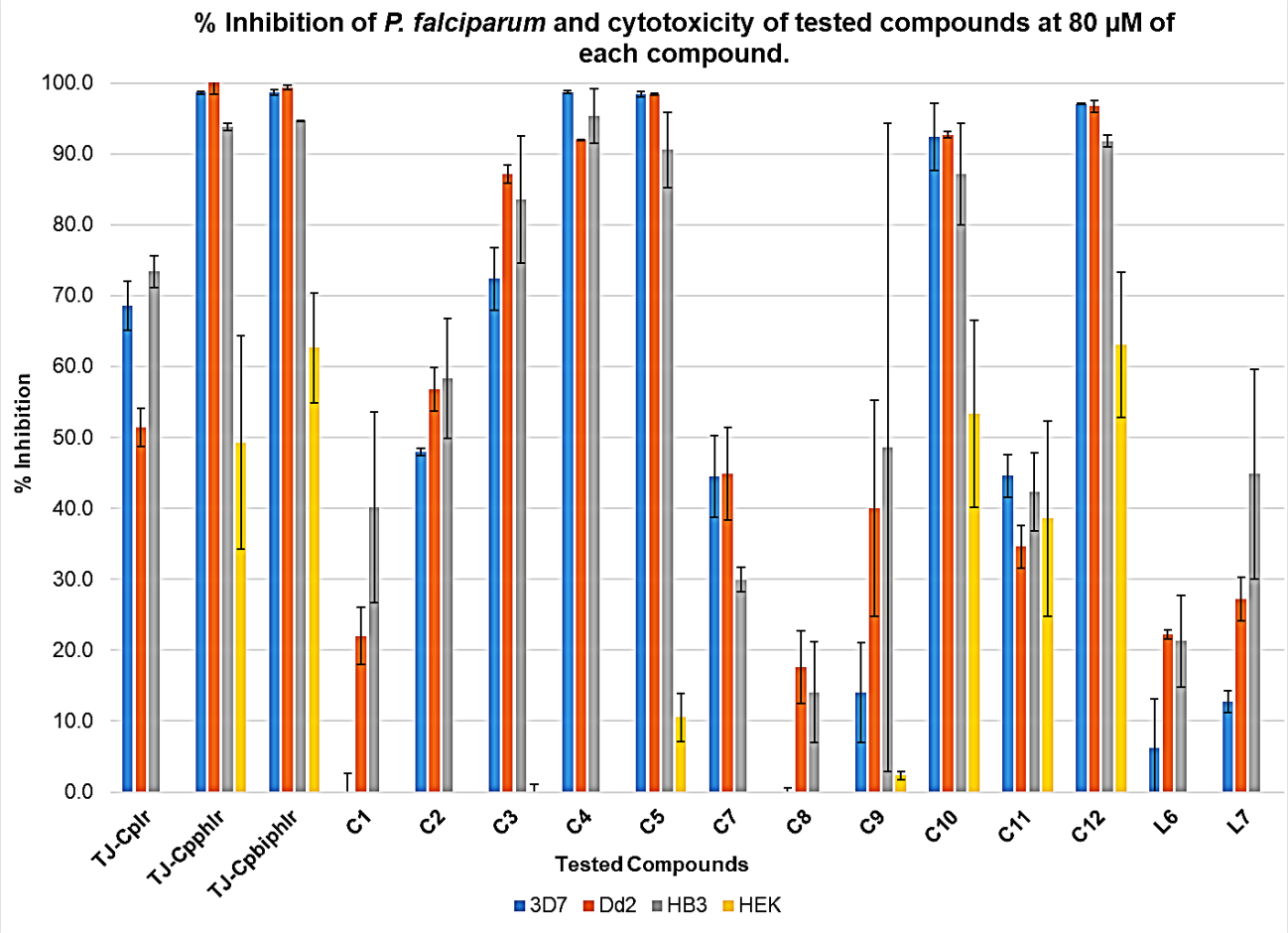

Figure 4.5 – Graph of the inhibition of *P. falciparum* and cytotoxicity of tested compounds.

When looking at the imino pyridyl complexes (**C1** – **C3**), an increase in the percentage inhibition for all the strains is seen as the Cp^{x} moiety is extended, similar to the increase in activity that was seen for *Mtb*. This same trend is observed for the iridium chlorido dimers, though the percentage inhibition of the Cp^{xPh} and Cpx^{biPh} dimers are both near to 100%. The quinolyl imino analogues (**C4** and **C5**) both also have > 90% inhibition for all the strains. Due to this, a further increase in inhibition cannot be seen for these two sets of compounds. The large increase in inhibition seen when moving from the pyridyl (**C1** – **C3**, **C7** – **C9**) to the quinolyl systems (**C4** – **C6**, **C10** – **C12**) for both the imino and the amido complexes, and the earlier trend in increased inhibition as the Cp^{x} moiety is lengthened, indicates that an increase in hydrophobicity can be linked to an increase in inhibition of the malarial strains. This is also observed for the two ligands of the amido series (**L4** and **L5**).

The amido complexes do not fully follow this trend as both the Cp^{xPh} analogues (**C8** and **C11**) have lower percentage inhibition than the rest of the series. Cp^{xbiPh} analogues (**C9** and **C12**) are still more active than their Cp* counterparts (**C7** and **C10**), except in the case of the 3D7 and Dd2 strains, for which **C7** is more active than **C9**. Looking at the cytotoxicity of the tested compounds to the HEK cell line it is clear from the iridium chlorido dimers that an increase in hydrophobicity could also be linked to an increased cytotoxicity. The cytotoxicity is significantly mitigated by the coordination of the ligands as is seen especially in the case of the Cp^{xPh} dimer and compounds **C2**, **C5**, **C8** and for the Cp^{xbiPh} dimer it is seen in compounds **C3** and **C9**. Structurally, when the hydrophobicity is increased by too large a margin, this mitigation of cytotoxicity is no longer as significant, as is seen for compounds **C11** and **C12**. The mitigation of the cytotoxicity is still important in these cases however, as illustrated by the sub-micromolar IC_{50} of compound **C12** which ranges between 0.574 µM and 1.41 µM and was consistently toxic to all strains tested against. This means that even though it is significantly more cytotoxic than the other compounds, given its potency it could be administered in a dose significantly lower than would be detrimental to healthy cells – which illustrates the advantage of such selectivity.

4.2.4 Investigation and monitoring of the aqua species

Given the aqueous environment that drugs are administered and tested in, the aqua species of the metal complexes could be the actual active species *in vivo*. This is due to the possible displacement of the chlorido ligand and substitution by an aqua molecule. Considering that this species would be significantly more soluble and could be easier or more effective to administer, it was thought beneficial to probe the active species. An investigation was consequently undertaken to determine the nature of the potential active species. It was envisioned that generating the aqua species *in situ* and then comparing this species to the chlorido species that had been incubated in deuterium oxide at physiological temperatures would provide some insightful knowledge as to whether this was a facile process or not and thus this route was pursued.

The experiment was designed such that the selected chlorido complex, which was insoluble in deuterium oxide, was stirred at 37 °C in the presence of silver nitrate for 18 hours after which the

solution was filtered through a plug of Celite™ and analysed via ^{1}H NMR spectroscopy. It was assumed that any material that subsequently dissolved in the deuterium oxide had to be the aqua species, where a deuterium molecule was coordinating to the metal centre, forming a doubly charged cationic complex with NO_3^- and PF_6^- acting as the counterions for the imino complexes and a singly charged cationic complex with NO_3^- as the counterion for the amido complexes. This spectrum was then compared to that of the same complex which was incubated under the same conditions in a 25% acetone/deuterium oxide solution without silver nitrate. TMS was added to both samples as an internal standard to compare the relative shifts of the protons. The samples were analysed with mass spectrometry thereafter to further confirm the species in solution. A general scheme for the *in situ* generation of the imino aqua species is shown in Scheme 4.1 to illustrate the process.

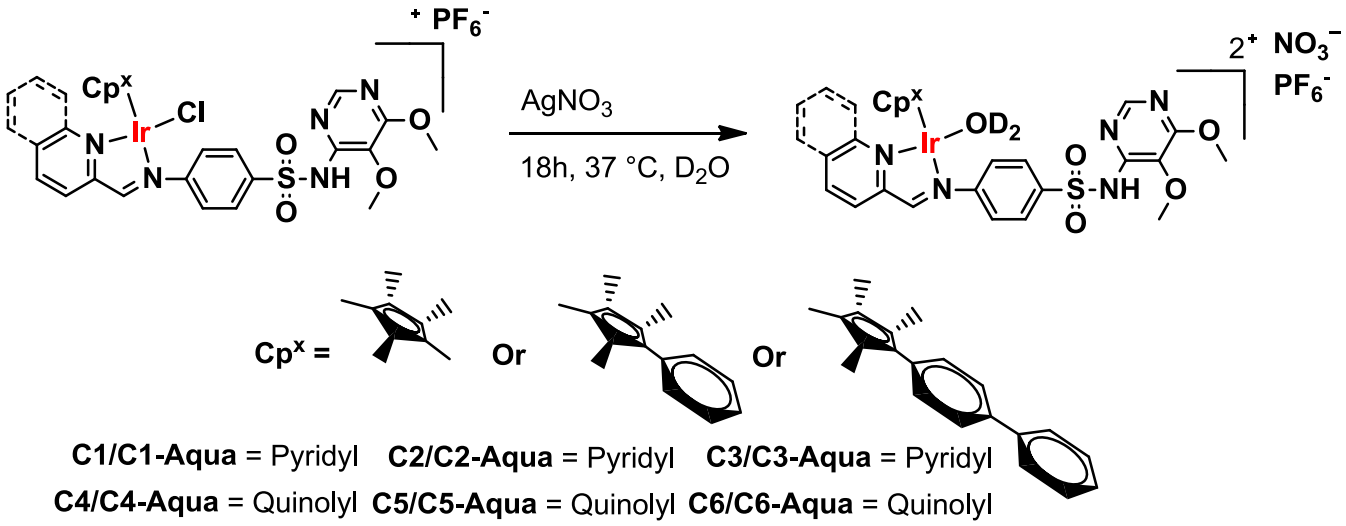

Scheme 4.1 – General scheme for the generation of the imino aqua complexes.

The amido complexes were labelled and generated in the exact same way and thus have not been shown. The complexes **C5** and **C6** were not investigated due to the scarcity of pure material for these complexes and **C12** was not investigated as the increasing hydrophobic character of the metal complexes led to it being extremely insoluble even under the conditions used. The overlaid ^{1}H NMR spectra of the **C1** aqua and incubated chlorido species are shown in Figure 4.6.

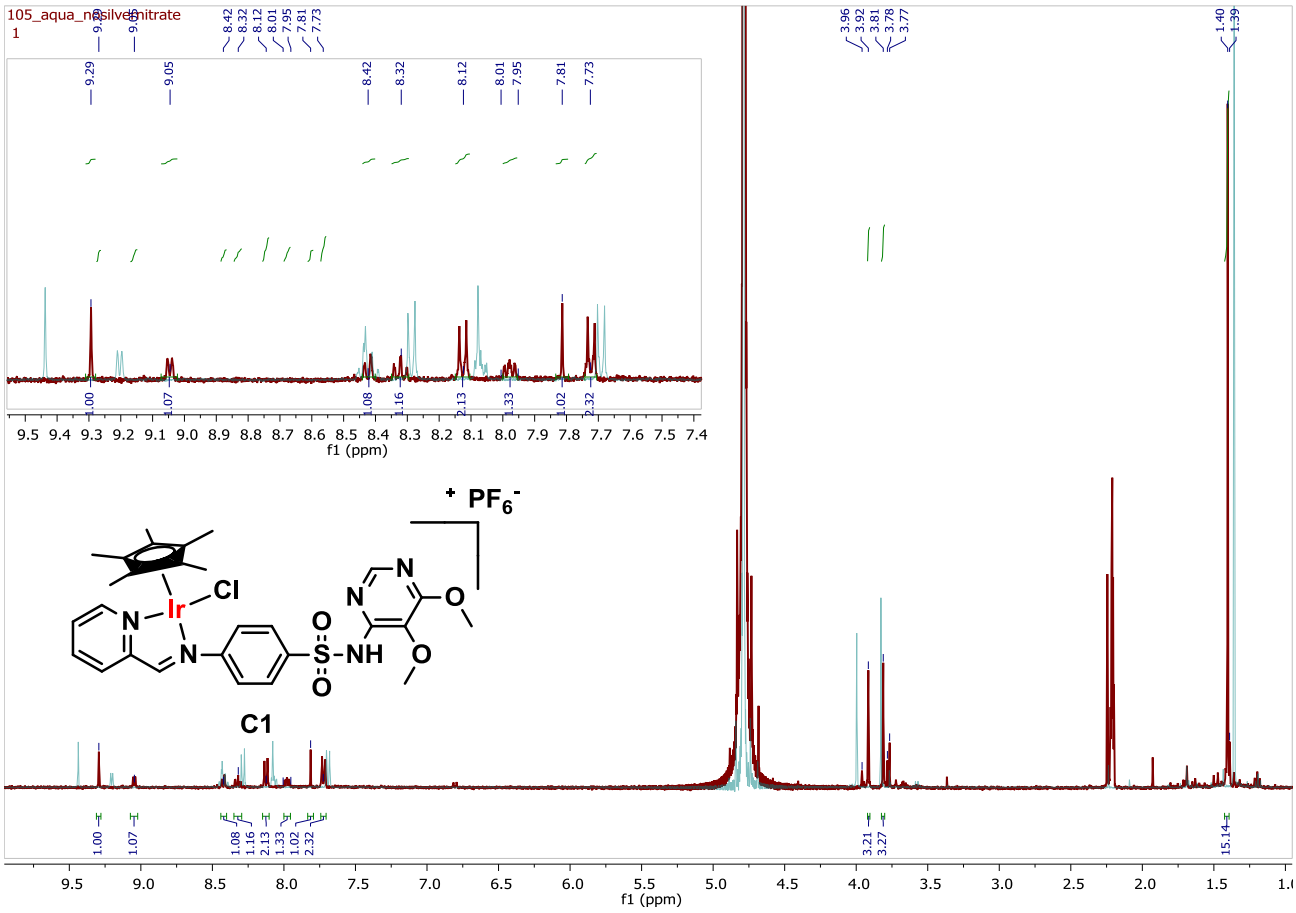

Figure 4.6 - Aqua species of **C1** (Blue), prepared by incubation with silver nitrate, overlaid with the incubated chlorido species of **C1** (Red) with no silver nitrate. Both spectra are referenced to TMS and analysed at 400 MHz.

There is a clear difference in the shift of the aqua species imine proton (9.44 ppm) and that of the incubated species (9.29 ppm). There is also a large difference seen for the proton *ortho* to the nitrogen of the pyridyl ring which is at 9.22 ppm and 9.05 ppm for the aqua and incubated species, respectively. Given that the metal is coordinated to these two functionalities, it is logical that they would experience the greatest shifts when the electron density of the metal is changed. This indicates that for **C1**, the aqua species does not form over a short period of time or in the absence of a moderate coordinating group. The initial plan was to immediately analyse via MS after analysis by ^{1}H NMR, however, the MS analysis is done on a batch to batch basis and as such, samples typically stood for extended periods of time before they were analysed. This allowed for significant breakdown of the original species and subsequent formation of various other species given the mixture present in solution. The MS results of these two solutions both have a base peak at a m/z of 450.1042 which could equate to a $[(M\text{-}D_2O) + TMS + NaNO_3]^{2+}$ fragment, however, it is also likely that hydrolysis occurred and the dimeric species shown in Figure 4.7 is the fragment. Additionally, the $[M\text{-}PF_6]^{+}$ fragment is seen in the incubated chlorido solution at 762.1459 m/z. The $[M\text{-}PF_6\text{-}Cl]^{2+}$ and the $[M\text{-}PF_6\text{-}Cl+4K]^{6+}$ fragments are also observed in the aqua species at 363.5898 and 147.9303 m/z, respectively, providing further support that the proposed species are as stated in the ^{1}H NMR in Figure 4.6.

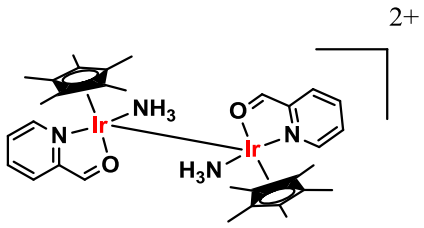

Figure 4.7 - Potential 450 m/z fragment present in **C1** aqua and incubated chlorido solutions.

C2 also shows a significant shift when comparing its aqua and incubated species for the imine, seen at 9.48 ppm in the aqua and 9.35 ppm in the incubated species, and for the proton *ortho* to the nitrogen of the pyridyl ring, at 9.09 ppm in the aqua and 8.83 ppm in the incubated species. Furthermore, the incubated species in this case is seen to form three different species, the smallest of which corresponds to the aqua species and another to the chlorido species. The nature of the third species is not certain at this stage. This indicates gradual aquation of the metal centre. The MS spectrum has the same species present as the base peak as that mentioned for **C1** with a m/z of 512.1201, the difference in weight coinciding exactly with the extension of Cp* to Cp^{xPh}. The $[M\text{-}PF_6]^+$ fragment is still observed in the incubated species of **C2** at 824.1764 m/z, though in this case the $[M\text{-}PF_6\text{-}Cl]^{2+}$ and the $[M\text{-}PF_6\text{-}Cl+4K]^{6+}$ fragments are not observed for the **C2** aqua species. **C3** did not aquate even at increased temperatures of 45 °C – 50 °C, instead only the original chlorido species was obtained when the solid in the suspension of D_2O was analysed. This was also the case for the amido analogue, **C9**, and it is likely that given the large nature of the biphenyl moiety on the metal centre, the removal of the chlorido ligand is prevented by its steric bulk. Only one species was present in the incubated sample, the chlorido species, confirmed with MS by the subsequent identification of the $[M\text{-}PF_6]^+$ fragment seen at 900.1959 m/z and no fragment seen for the species without the chlorido, although a fragment at 333.0628 m/z was identified as the $[M\text{-}Cp^{xbiPh}\text{-}PF_6+D_2O]^{2+}$ ion which likely formed due to the extended time in solution.

The analysis of **C4** showed similar differences as that seen for **C1** and **C2** between its aqua and incubated species with the imine see at 9.72 ppm and 9.59 ppm in the aqua and incubated species, respectively. Additionally, as the hydrophobicity of the compounds increased, the species generally became less soluble and had to be analysed for longer periods of time to obtain a visible spectrum. The $[M\text{-}PF_6]^+$ fragment was identified at 812.1613 m/z in the incubated **C4** species. Unfortunately no significant or realistic fragments could be identified from the aqua solution, likely due to how dilute it was and the length of time it stood before MS analysis.

The amido complexes were investigated in the same fashion as described above and the overlaid spectrum of the aqua and incubated species for **C7**, the pyridyl amido Cp* complex, is shown in Figure 4.8.

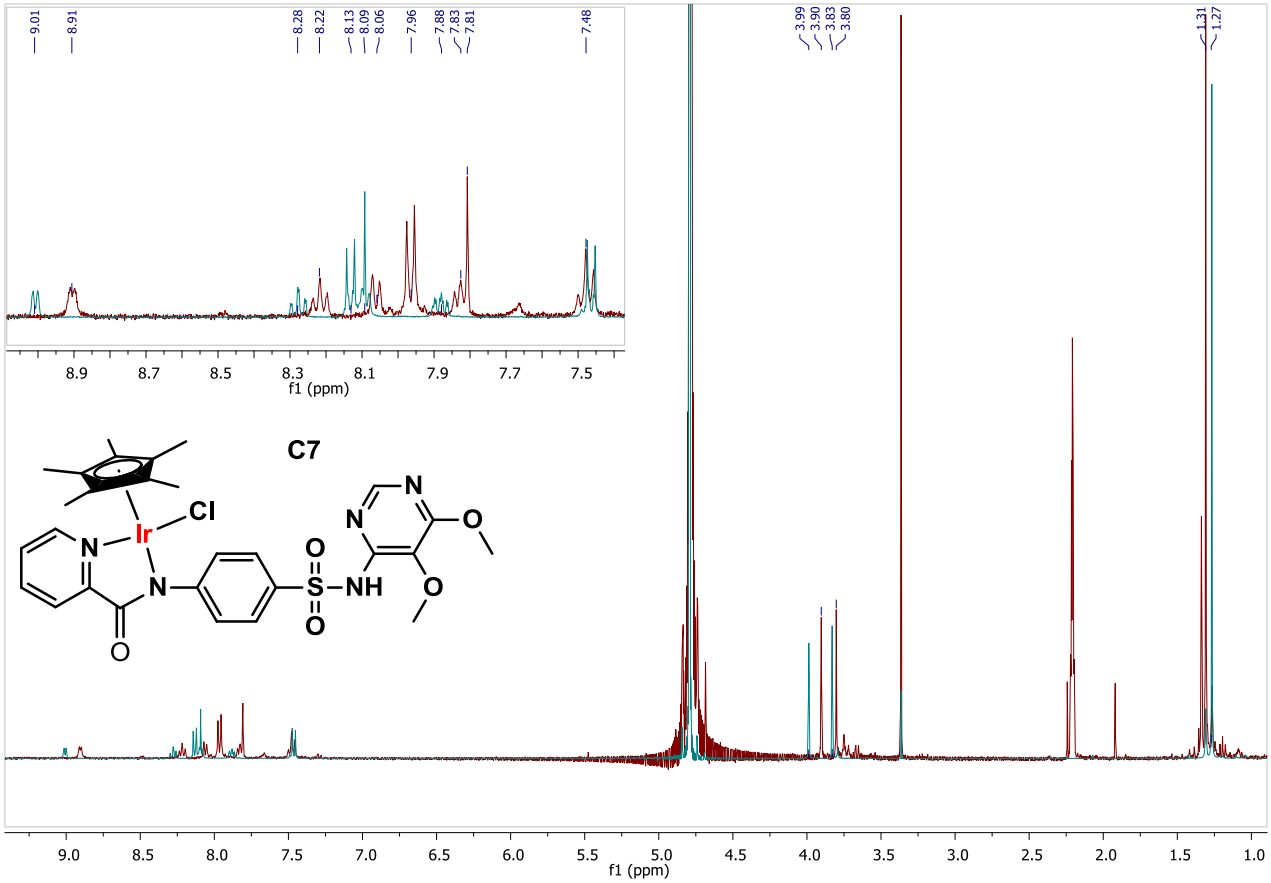

Figure 4.8 - Aqua species of **C7** (Blue), prepared by incubation with silver nitrate, overlaid with the incubated chlorido species of **C7** (Red) with no silver nitrate. Both spectra are referenced to TMS and analysed at 400 MHz.

The proton *ortho* to the nitrogen of the pyridyl ring for the aqua species of **C7** (Figure 4.8, Blue spectrum) is seen at 9.01 ppm, while that of the incubated chlorido complex is at 8.91 ppm. The MS of the amido compounds generally show the base peak as the $[M\text{-}Cl]^+$ fragment and under softer ionisation the $[M+H]^+$ ion can be seen. The MS of the two solutions both show the $[M\text{-}Cl]^+$ ion at 742.1680 m/z, however only the incubated chlorido species shows the $[M+H]^+$ fragment at 778.1426 m/z. The fragment at 764.1522 m/z in the aqua species is proposed to be the $[M\text{-}Cl+D_2O]^+$ ion, with the additional 2 m/z extra being attributed to the lengthy time in deuterated solvent and consequently some exchange between protons on the compound and deuteriums. This fragment is not seen in the original MS of the amido complexes but is observed for the incubated chlorido species of **C7** as well, though it is not the base peak as is the case for the aqua species. Additionally, aggregates for $[M\text{-}Cl]^+$ and $[M\text{-}Cl+D_2O]^+$ at twice the m/z of the aqua species fragments are seen.

The ^1H NMR spectrum for the aqua species of **C8** has the proton *ortho* to the nitrogen of the pyridyl ring appearing at 8.94 ppm; the same proton appears at 8.74 ppm in the incubated chlorido spectrum. This once again confirms two different species and the successful formation of the aqua complex of **C8** in situ. The MS shows the $[M+H]^+$ and $[M\text{-}Cl]^+$ ions for the incubated chlorido complex **C8** at 840.1631 m/z and 804.1835 m/z, respectively. The $[M\text{-}Cl]^+$ ion is seen in the aqua complex of **C8** at 804.1833 m/z but the $[M+H]^+$ ion is not seen. Unlike as was the case for **C7**, the $[M\text{-}Cl+D_2O]^+$

is not seen, although there are aggregates that could be attributed to it, but not conclusively. As discussed earlier, the same results were obtained for **C9** as for **C3**.

Besides the gradual decrease in solubility, the quinolyl amido complexes behaved in similar fashion to the other complexes. The doublets of the quinolyl ring were identified at 8.79, 8.50, 8.23 and 8.17 ppm in the aqua complex of **C10**. The doublets were seen at 8.73, 8.46, 8.16 and 8.10 ppm, respectively, in the incubated chlorido complex, indicating that these were two different species. **C11** was the last compound that was investigated as half an hour of analysis barely gave a visible spectrum and the results of **C3** and **C9** suggested that similar results for **C12** would be obtained. Unfortunately, the species in solution was too dilute and no definitive conclusions could be made from the spectra of **C11**. From the above data it was clear that without a driving force or moderately coordinating group present, the chlorido was either not displaced by H_2O or was extremely slow in being substituted. Wanting to follow the aquation over time, it was decided to select complex **C2** and monitor it with ^1H NMR spectroscopy over time in a solution of 25% acetone-d_6/D_2O in the presence of silver nitrate at 37 °C. The spectra at room temperature showed no difference to that at 37 °C and in the absence of silver nitrate no change was seen in the spectrum. The aquation was followed by means of a pre-acquisition array experiment at 400 MHz. Spectra were acquired every 15 min for 1 hour followed by every 30 min for 3 hours and finally every hour for 6 hours (Figure 4.9).

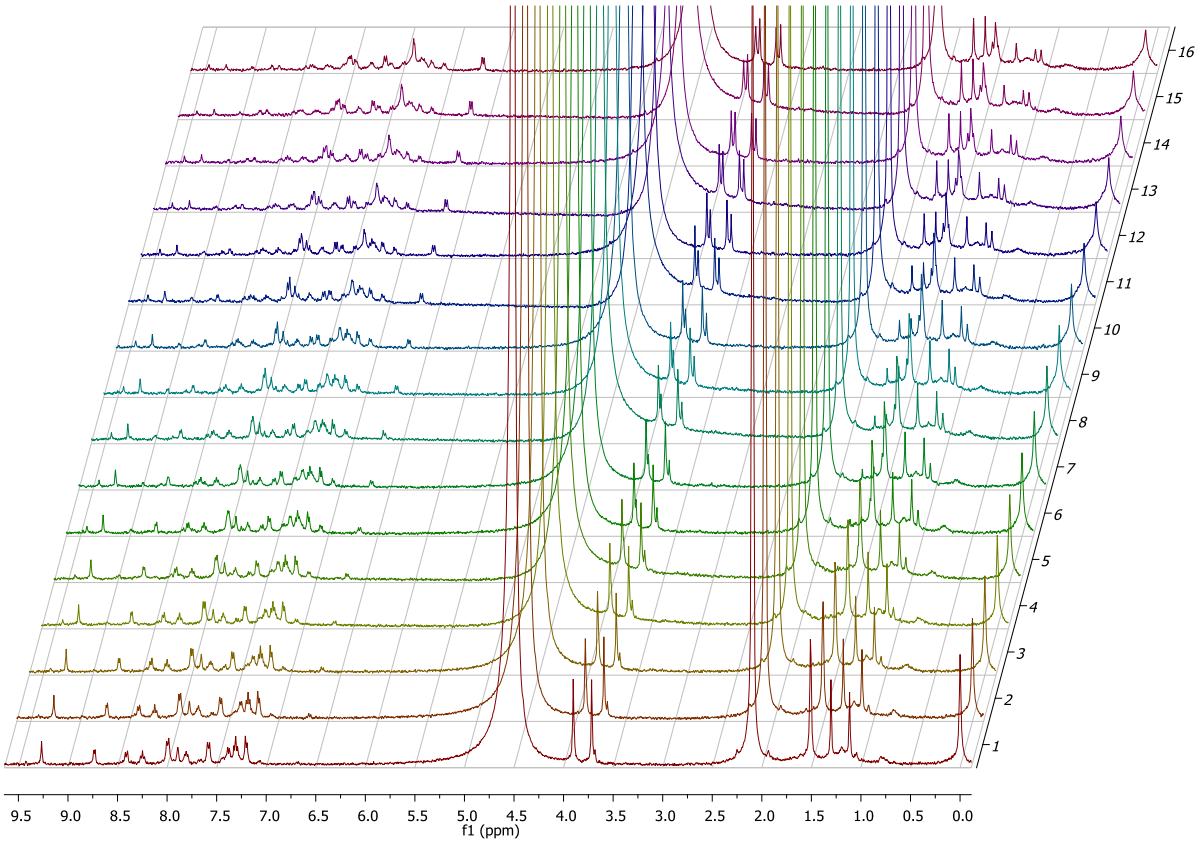

Figure 4.9 - **C2** with an equimolar amount of silver nitrate present in 25% acetone-d_6/D_2O at 37 °C. Spectra were acquired every 15 min for 1 hour followed by every 30 min for 3 hours and finally every hour for 6 hours.

The stacked spectra are shown in Figure 4.9 and two main changes are observed to occur simultaneously. Firstly, some degradation is seen as is evidenced by the formation of the doublet at 6.69 ppm which is indicative of the presence of sulfadoxine. Secondly, the aqua species is observed as a second imine forms downfield at 9.45 ppm compared to the original which is at 9.27 ppm. Further evidence of formation of these species is particularly seen when looking at the signals for the methoxy methyls, between 3.5 ppm and 4.5 ppm, and the Cp^{xPh} methyls, between 1.0 ppm and 2.0 ppm, respectively. Figure 4.10 shows an expanded spectrum of this region for easier discussion.

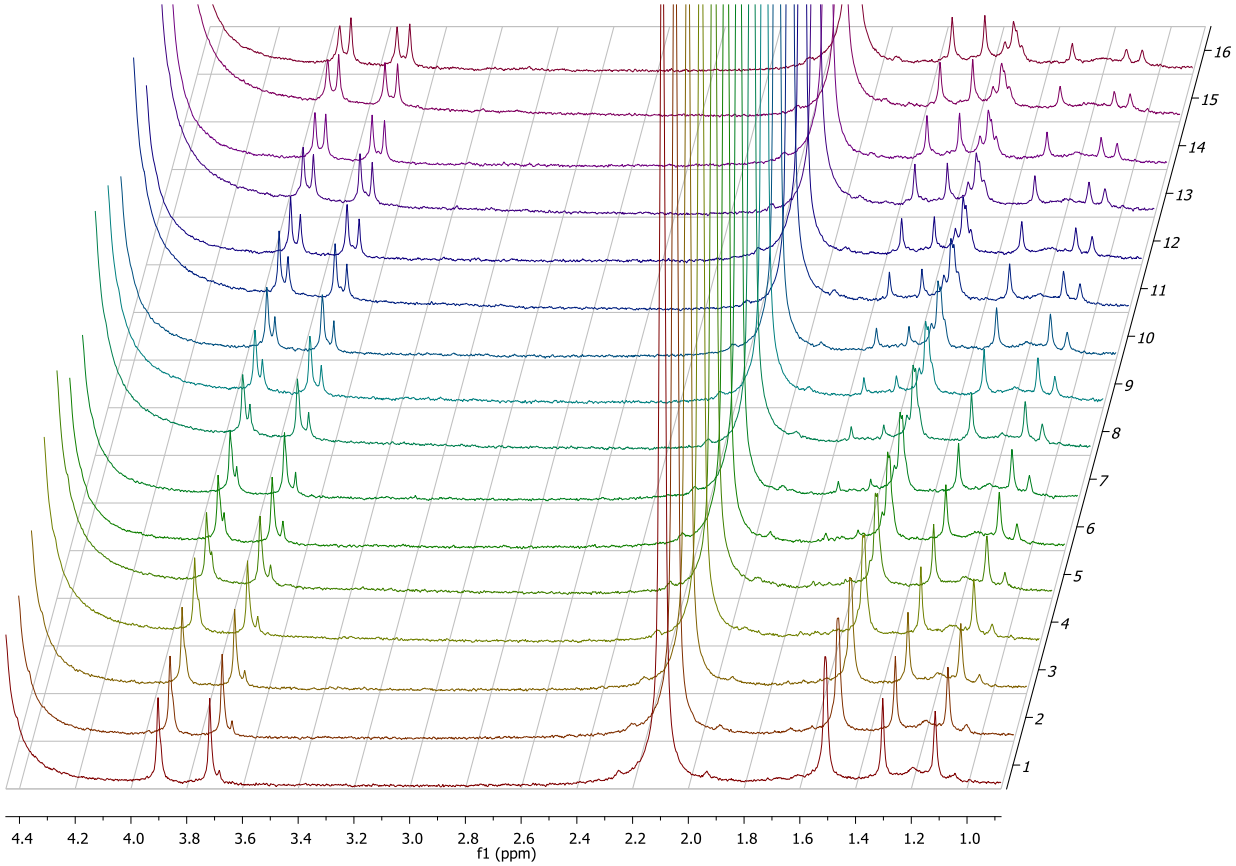

Figure 4.10 - An expansion of the aliphatic region of the spectra that monitored the formation of the aqua species of **C2**.

The original species has the singlets for the methoxy methyls of the pyrimidine ring at 3.72 ppm and 3.90 ppm. Two new singlets appear at 3.90 ppm and 3.69 ppm, upfield from the previous signals. The original species singlet at 3.90 ppm shifts downfield gradually to 3.94 ppm. The increased broadness of these signals is due to the gradual formation of the sulfadoxine as mentioned above, which contributes another set of signals. The methyl singlets of the Cp^{xPh} moiety clearly show the formation of the aqua species with their large downfield shift as the metal centre becomes more cationic. The original chlorido species in the first spectrum shows the singlets at 1.11, 1.30 and 1.51 ppm (representing two methyls). Two new signals appear downfield at 1.62 ppm and 1.74 ppm, each representing two methyls. The original signal becomes rather messy, however, with several new signals appearing around 1.50 ppm, most likely due to the degradation process mentioned earlier. Degradation could be taking place due to the instability of the doubly cationic species, which would

also lend credence to the dimeric species noted during the discussion of the MS of the incubated and aqua species which had stood for a lengthy period before analysis.

4.3 Conclusion

In summary, the decrease in solubility as illustrated by the results of the turbidimetric assays is very clearly linked to an increase in activity for both the *Mtb* and malaria testing performed. This, along with the general increased difficulty in removing of the chlorido ligand as the bulk of the half-sandwich moiety is increased during the investigation of the aqua species, especially for the biphenyl analogues, would seem to indicate that the most active species is the chlorido complex. This species is more likely to reach the target site in tact if protected by a bulky group such as the biphenyl half-sandwich moiety. The imino series of complexes generally exhibits better activity than their amido analogues, especially in the case of *Mtb*, while simultaneously being less toxic. It is unclear whether this increased activity and lower toxicity is due to the imino functionality itself or if the cationic nature of the metal centre also contributes and thus should be investigated further. The trends for the amido complexes against malaria was not as simple but some promising data was obtained for **C12** which exhibited consistent toxicity against all strains.

4.4 Experimental

Chemicals and reagents. Silver nitrate, hydrocortisone, reserpine, phosphate buffered saline and all reagent solvents and deuterated solvents (deuterium oxide and acetone-d_6) were obtained from Sigma Aldrich (Merck).

Instrumentation. NMR data (^{1}H, ^{13}C) were recorded on either a 300 MHz Varian VNMRS or a 400 MHz Varian Unity Inova spectrometer. ^{1}H NMR chemical shifts are reported in ppm and coupling constants in Hertz and were internally referenced to tetramethylsilane (0.00 ppm). Data was processed using MestReNova 11.0.4-18998. Mass spectrometry was performed on a Waters Synapt G2 with an ESI probe in ESI positive mode using a cone voltage of 15 V. Uv-Vis data for the turbidimetric solubility assay were recorded with a Thermo Scientific Multiscan Go plate reader at 620 nm.

4.4.1 General procedure for the preparation of the aqua species

The complex was stirred for 18 hours with an equimolar quantity of $AgNO_3$ in deuterium oxide (1.20 mL) at 37 °C in an oil bath. The liquid was subsequently filtered through a plug of Celite™ and collected in an NMR tube. ^{1}H NMR was run on the samples after 1-2 drops of TMS was added as internal reference and the samples were then submitted for analysis by mass spectrometry.

4.4.2 Synthesis of $[IrD_2O(C_{18}H_{17}N_5O_4S)(C_{10}H_{15})PF_6NO_3]$ (**C1** - aqua)

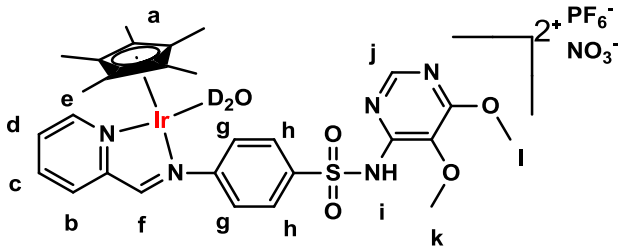

C1 (12.2 mg, 1.30 x 10^{-2} mmol) and $AgNO_3$ (2.30 mg, 1.30 x 10^{-2} mmol) were reacted in D_2O (1.20 mL) and then analysed. ^1H NMR (400 MHz, D_2O) δ 9.44 (s, H_f, 1H), 9.20 (d, H_e, 1H, $^3J_{(He-Hd)}$ 5.4 Hz), 8.47 - 8.38 (m, $H_{b,d}$, 2H), 8.29 (d, H_g, 2H, $^3J_{(Hg-Hh)}$ 8.7 Hz), 8.10 - 8.04 (m, $H_{c,j}$, 2H), 7.69 (d, H_h, 2H, $^3J_{(Hh-Hg)}$ 8.7 Hz), 4.00 (s, H_l, 3H), 3.83 (s, H_k, 3H), 1.36 (s, H_a, 15H).

4.4.3 Synthesis of $[IrD_2O(C_{18}H_{17}N_5O_4S)(C_{15}H_{17})PF_6NO_3]$ (**C2** - aqua)

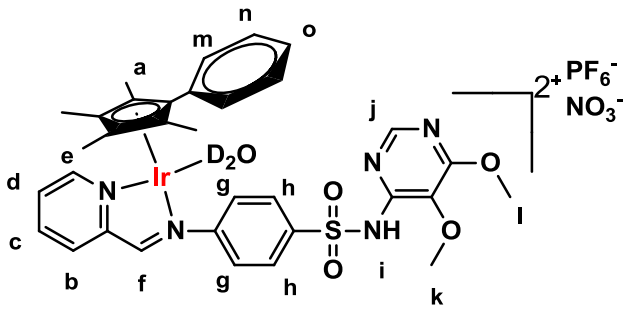

C2 (12.0 mg, 1.20 x 10^{-2} mmol) and $AgNO_3$ (2.10 mg, 1.20 x 10^{-2} mmol) were reacted in D_2O (1.20 mL) and then analysed. ^1H NMR (400 MHz, D_2O) δ 9.50 (s, H_f, 1H), 9.10 (d, H_e, 1H, $^3J_{(He-Hd)}$ 5.4 Hz), 8.51 (d, H_b, 1H, $^3J_{(Hb-Hc)}$ 7.5 Hz), 8.44 (t, H_d, 1H, $^3J_{(Hd-Hc,e)}$ 7.7 Hz), 8.06 – 7.97 (m, $H_{c,g}$, 3H), 7.93 (s, H_j, 1H), 7.51 – 7.43 (m, $H_{h,o}$, 3H), 7.36 (t, H_n, 2H, $^3J_{(Hn-Hm,o)}$7.7 Hz), 7.15 (d, H_m, 2H, $^3J_{(Hm-Hn)}$ 7.7 Hz), 4.03 (s, H_l, 3H), 3.81 (s, H_k, 3H), 1.63 (s, H_a, 3H), 1.55 (s, H_a, 3H), 1.51 (s, H_a, 3H), 1.12 (s, H_a, 3H).

4.4.4 Attempted Synthesis of $[IrD_2O(C_{18}H_{17}N_5O_4S)(C_{15}H_{17})PF_6NO_3]$ (**C3** - aqua)

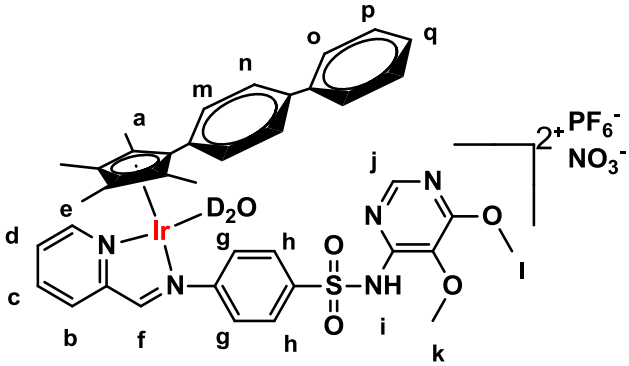

C3 (12.5 mg, 1.20 x 10^{-2} mmol) and $AgNO_3$ (2.00 mg, 1.20 x 10^{-2} mmol) were reacted in D_2O (1.20 mL) and then analysed. The chlorido complex was obtained as a solid; no material was present in the deuterium oxide.

4.4.5 Synthesis of $[IrD_2O(C_{22}H_{21}N_5O_4S)(C_{10}H_{15})PF_6NO_3]$ (**C4** - aqua)

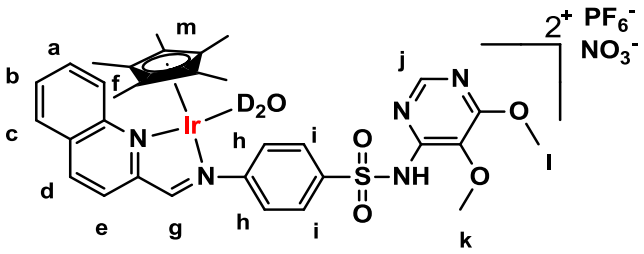

C4 (12.4 mg, 1.30 x 10^{-2} mmol) and $AgNO_3$ (2.30 mg, 1.30 x 10^{-2} mmol) were reacted in D_2O (1.20 mL) and then analysed. ^1H NMR (400 MHz, D_2O) δ 9.72 (s, H_g, 1H), 8.95 (d, H_d, 1H, $^3J_{(Hd-He)}$ 8.4 Hz), 8.49 (d, H_f, 1H, $^3J_{(Hf-Ha)}$ 8.9 Hz), 8.42 (d, H_e, 1H, $^3J_{(He-Hd)}$ 8.4 Hz), 8.37 - 8.32 (m, $H_{h,c}$, 3H), 8.15 (s, H_j, 1H), 8.06 (m, $H_{a/b}$, 1H), 8.00 (m, $H_{a/b}$, 1H), 7.93 (d, H_i, 2H, $^3J_{(Hi-Hh)}$ 8.6 Hz), 4.02 (s, H_l, 3H), 3.84 (s, H_k, 3H), 1.28 (s, H_m, 15H).

4.4.6 Synthesis of $[IrD_2O(C_{18}H_{16}N_5O_5S)(C_{10}H_{15})NO_3]$ (**C7** - aqua)

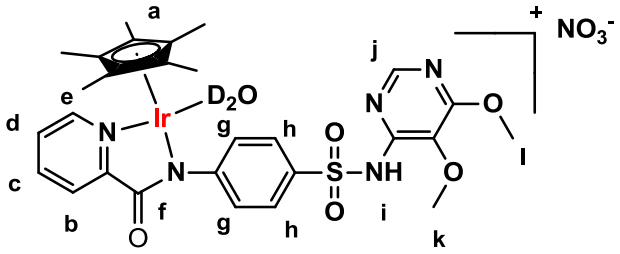

C7 (9.30 mg, 1.20 x 10^{-2} mmol) and $AgNO_3$ (2.10 mg, 1.20 x 10^{-2} mmol) were reacted in D_2O (1.20 mL) and then analysed. ^1H NMR (400 MHz, D_2O) δ 9.01 (d, H_e, 1H, $^3J_{(He-Hd)}$ 5.4 Hz), 8.30 - 8.24 (m, H_c, 1H), 8.16 - 8.06 (m, $H_{b,g,j}$, 4H), 7.91 - 7.85 (m, H_d, 1H), 7.46 (d, H_h, 2H, $^3J_{(Hh-Hg)}$ 8.9 Hz), 3.99 (s, H_l, 3H), 3.83 (s, H_k, 3H), 1.27 (s, H_a, 15H).

4.4.7 Synthesis of $[IrD_2O(C_{18}H_{16}N_5O_5S)(C_{15}H_{17})NO_3]$ (**C8** - aqua)

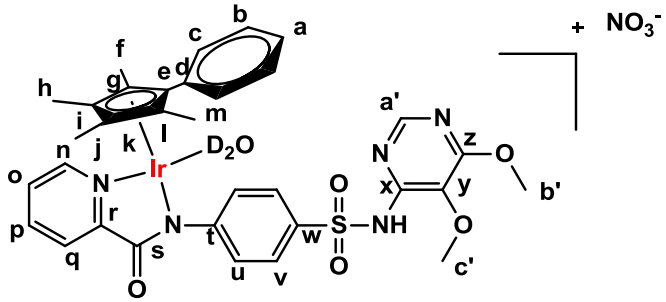

C8 (10.0 mg, 1.20 x 10^{-2} mmol) and $AgNO_3$ (2.10 mg, 1.20 x 10^{-2} mmol) were reacted in D_2O (1.20 mL) and then analysed. ^1H NMR (400 MHz, D_2O) δ 8.94 (d, H_e, 1H, $^3J_{(Hn-Ho)}$ 5.4 Hz), 8.31 (m, H_p, 1H), 8.17 (d, H_q, 1H, $^3J_{(Hq-Hp)}$ 7.6 Hz), 8.04 (s, $H_{a'}$, 1H), 7.92 (d, H_u, 2H, $^3J_{(Hu-Hv)}$ 8.6 Hz), 7.85 (m, H_o, 1H), 7.47 (t, H_a, 1H, $^3J_{(Ha-Hb)}$ 7.7 Hz), 7.36 (t, H_b, 2H, $^3J_{(Hb-Ha,c)}$ 7.7 Hz), 7.18(d, H_v, 2H, $^3J_{(Hv-Hu)}$ 8.6 Hz), 7.12 (d, H_c, 2H, $^3J_{(Hc-Hb)}$ 7.7 Hz), 4.03 (s, $H_{b'}$, 3H), 3.80 (s, $H_{c'}$, 3H), 1.58 (s, $H_{f,m}$, 6H), 1.09 (s, $H_{h,j}$, 6H).

4.4.8 Attempted Synthesis of $[IrD_2O(C_{18}H_{17}N_5O_4S)(C_{15}H_{17})PF_6NO_3]$ (**C9** - aqua)

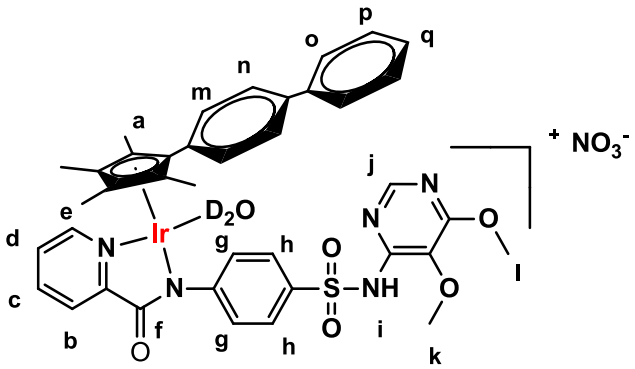

C9 (10.8 mg, 1.20 x 10^{-2} mmol) and $AgNO_3$ (2.00 mg, 1.20 x 10^{-2} mmol) were reacted in D_2O (1.20 mL) and then analysed. The chlorido complex was obtained as a solid; no material was present in the deuterium oxide.

4.4.9 Synthesis of $[IrD_2O(C_{18}H_{16}N_5O_5S)(C_{10}H_{15})NO_3]$ (**C10** - aqua)

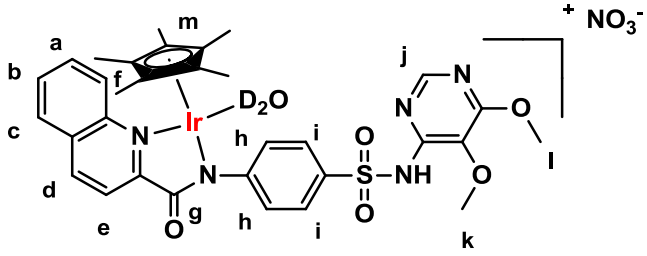

C10 (9.90 mg, 1.20 x 10^{-2} mmol) and $AgNO_3$ (2.00 mg, 1.20 x 10^{-2} mmol) were reacted in D_2O (1.20 mL) and then analysed. ^1H NMR (400 MHz, D_2O) δ 8.79 (d, H_d, 1H, $^3J_{(Hd\text{-}He)}$ 8.6 Hz), 8.50 (d, H_f, 1H, $^3J_{(Hf\text{-}Ha)}$ 9.0 Hz), 8.23 (d, H_c, 1H, $^3J_{(Hc\text{-}Hb)}$ 8.2 Hz) 8.14 - 8.20 (m, $H_{e,b}$, 2H), 8.03 (d, H_h, 2H, $^3J_{(Hh\text{-}Hi)}$ 8.5 Hz), 7.90 - 7.97 (m, $H_{a,j}$, 2H), 7.67 (d, H_i, 2H, $^3J_{(Hi\text{-}Hh)}$ 8.5 Hz), 3.94 (s, H_l, 3H), 3.82 (s, H_k, 3H), 1.19 (s, H_m, 15H).

4.4.10 General procedure for the incubation of the chlorido complexes

The complex was dissolved in deuterated acetone (300 µL) and then mixed with deuterium oxide (900 µL) in a vial for a final solution constitution of 25% deuterated acetone/deuterium oxide (1.20 mL). The resultant mixture was then stirred for 18 hours at 37 °C in an oil bath. The liquid was subsequently filtered through a plug of Celite™ and collected in an NMR tube. ^1H NMR was run on the samples after 1-2 drops of TMS was added as internal reference and the samples were then submitted for mass spectrometry analysis. The ^1H NMR was compared with that of the relevant aquated species generated above, both referenced to TMS, to determine whether aquation readily takes place.

4.4.11 Turbidimetric solubility assays

All compounds including the two positive controls, hydrocortisone (soluble) and reserpine (effectively insoluble), were made up to a 10 mM stock solution in 100% DMSO. All tests were run in duplicate

of triplicate, with the second triplicate run done on a different day. No significant changes in value were observed between the days. The stock solutions were serially diluted with DMSO on a preparatory 96-well plate to concentrations of 8 mM, 4 mM, 2 mM, 1 mM, 0.50 mM, 0.25 mM and 0 mM. These dilutions were then further diluted in DMSO to concentrations of 200 µM, 160 µM, 80 µM, 40 µM, 20 µM, 10 µM, 5 µM and 0 µM. They were also diluted to the same concentrations in 0.01 M phosphate buffered saline at a pH of 7.4 to yield a 2% DMSO/buffer solution. The 96-well plates were then incubated for 2 hours in the dark at room temperature. Thereafter, the absorbance was measured at 620 nm and the data analysed using Microsoft Excel 2016.

4.4.12 Antitubercular testing

The minimum inhibitory concentration that inhibits 90% of cell growth (MIC_{90}) of *Mtb* strain H37Rv[17] of the synthesized compounds was determined through the broth micro dilution method.[18] A 10 mL culture of this strain was grown to an optical density between 0.6 and 0.7 and diluted 1:500 in Middlebrook 7H9 media (Difco) supplemented with 0.2% glucose, Middlebrook albumin-dextrose-catalase (ADC) enrichment (Difco) and 0.05% Tween 80.[19] A second 1:500 dilution was prepared with Middlebrook 7H9 media (Difco) supplemented with 0.03% casitone, 0.4% glucose and 0.05% tyloxapol.[20] Stock solutions of the compounds to be tested were made up in DMSO and the compounds were then diluted to appropriate concentrations in the 7H9 media. A serial dilution was prepared in duplicate across 10 wells in a 96-well micro titre plate with volumes of 50 µL in each well. The diluted mycobacterial cultures were then added to the wells to make up a final volume of 100 µL. The plate layout was a modification of a previously described method.[21] The controls used were a minimum growth control with rifampicin at twice its known MIC (0.150 µM), a maximum growth control with DMSO, the final concentration of which was equal to that of its concentration used in the dose response assay for the test material, and a rifampicin dose response control ranging between 0.15 µM and 0.0002 µM. The micro titre plate was then sealed in a secondary container and incubated at 37 °C with 5% CO_2 and humidification. Twenty-four hours before the assay data was to be collected alamar blue reagent was added to each well and the assay plate was reincubated for the remaining 24 hours. After 7 days the assay was scored visually and the MIC_{90} allocated to the lowest concentration of material that did not display visible growth. The relative fluorescence was then measured using a SpecraMax i3x plate reader (excitation 540 nm; emission 590 nm) and the raw fluorescent data analysed with Softmax® Pro 6 software version 6.5.1. The 4-parameter curve fit protocol was used to generate the calculated MIC_{90}. The raw fluorescent data was normalised to the minimum and maximum inhibition controls from which a dose response curve was generated through the Levenberg-Marquardt damped least-squares method from which the MIC_{90} was subsequently calculated. All procedures requiring the handling of pathogenic mycobacterial strains were performed in a biosafety level III certified and compliant facility. MIC_{90} values were also determined after 14 days.

4.4.13 Antiplasmodial testing[22]

Stock solutions in DMSO of 20 mM of the compounds to be tested were prepared. The stock solutions were further diluted in 384-well polypropylene micro titre plates to produce 3 doses per log dose response with final assay concentrations of the compounds ranging between 80 µM and 0.8 nM. A 1:25 dilution was then made of the compound plates with sterile water in a 384-well polystyrene plate and 5 µL of these wells were then transferred into a 384-well imaging plate. 4% DMSO and 50 µM Puromycin were used as controls under the same conditions and dilutions as that of the compounds.

A Plasmodium falciparum standard genomic reference strain (3D7), multidrug resistant strain (Dd2) and gametocyte forming pyrimethamine resistant and chloroquine sensitive strain (HB3) were cultured within the medium RPMI-1640 which was supplemented with 10 mM HEPES, 25 µg/mL hypoxanthine, 5% human serum and 2.5 mg/mL Albumax while being incubated at 37 °C under 5% CO_2, 5% O_2 and 90% N_2. Sorbitol synchronization was performed twice, consecutively, during the intra-erythrocytic lifecycles to provide ring-stage parasites for the assays.[23] The ring stage parasite culture had its percentage parasitaemia and percentage haematocrit adjusted to 2% and 0.3%, respectively, and thereafter 45 µL of the adjusted parasite culture was added to compound containing imaging plates prepared as described earlier. The imaging plates were then incubated for 72 hours under the same conditions as described for the original cultures. The plates were then stained with 4',6-diamidino-2-phenylindole (DAPI) and incubated overnight at room temperature before being imaged on an Opera confocal high content imaging system. Accapella scripting software was used to determine the number of classified parasites which was subsequently normalized to obtain the percentage inhibition with regards to the two plate controls, 0.4% DMSO and 5 µM puromycin. The normalized inhibition data was then plotted against the log concentration of the compounds using GraphPad Prism 4.0, and the non-linear regression, sigmoidal dose response variable slope and the IC_{50} determined (where two or more points formed a plateau in the software). The data was generated from two biological replicates in duplicate of the three strains used.

4.5 References

(1) Blass, B. E. Drug Discovery and Development: An Overview of Modern Methods and Principles. In *Basic Principles of Drug Discovery and Development*; Academic Press: Amsterdam, 2015; pp 1–33.

(2) Paul, S. M.; Mytelka, D. S.; Dunwiddie, C. T.; Persinger, C. C.; Munos, B. H.; Lindborg, S. R.; Schacht, A. L. How to Improve RD Productivity: The Pharmaceutical Industry's Grand Challenge. *Nat. Rev. Drug Discov.* **2010**, *9*, 203–214.

(3) Sittampalam, G. S.; Coussens, N. P. Preface. In *Assay Guidance Manual*; Eli Lilly & Company and the National Center for Advancing Translational Sciences: Bethesda (MD), 2004; pp xiii–xix.

(4) Li, A. P. Preclinical in Vitro Screening Assays for Drug-like Properties. *Drug Discov. Today Technol.* **2005**, *2* (2), 179–185.

(5) Wan, H. What ADME Tests Should Be Conducted for Preclinical Studies? *ADMET DMPK* **2013**, *1* (3), 19–28.

(6) Chung, T. D. Y.; Terry, D. B.; Smith, L. H. *In Vitro and In Vivo Assessment of ADME and PK Properties During Lead Selection and Lead Optimization – Guidelines, Benchmarks and Rules of Thumb*; Eli Lilly & Company and the National Center for Advancing Translational Sciences: Bethesda (MD), 2004.

(7) Lipinski, C. A. Drug-like Properties and the Causes of Poor Solubility and Poor Permeability. *J. Pharmacol. Toxicol. Methods* **2000**, *44*, 235–249.

(8) Hughes, J. P.; Rees, S. S.; Kalindjian, S. B.; Philpott, K. L. Principles of Early Drug Discovery. *Br. J. Pharmacol.* **2011**, *162*, 1239–1249.

(9) Kerns, E. H.; Di, L. Solubility. In *Drug-like Properties: Concepts, Structure Design and Methods*; Academic Press, 2008; pp 56–85.

(10) Zsila, F.; Bikadi, Z.; Malik, D.; Hari, P.; Pechan, I.; Berces, A.; Hazai, E. Evaluation of Drug–human Serum Albumin Binding Interactions with Support Vector Machine Aided Online Automated Docking. *Bioinformatics* **2011**, *27* (13), 1806–1813.

(11) Walliker, D.; Quakyi, I. A.; Wellems, T. E.; McCutchan, T. F.; Szarfman, A.; London, W. T.; Corcoran, L. M.; Burkot, T. R.; Carter, R. Genetic Analysis of the Human Malaria Parasite Plasmodium Falciparum. *Science (80-.).* **1987**, *236* (4809), 1661–1666.

(12) Chellan, P.; Avery, V. M.; Duffy, S.; Triccas, J. A.; Nagalingam, G.; Tam, C.; Cheng, L. W.; Liu, J.; Land, K. M.; Clarkson, G. J.; et al. Organometallic Conjugates of the Drug Sulfadoxine for Combatting Antimicrobial Resistance. *Chem. - A Eur. J.* **2018**, *24* (40), 10078–10090.

(13) Oduola, A. M. J.; Milhous, W. K.; Weatherly, N. F.; Bowdre, J. H.; Desjardins, R. E. Plasmodium Falciparum: Induction of Resistance to Mefloquine in Cloned Strains by Continuous Drug Exposure in Vitro. *Exp. Parasitol.* **1988**, *67* (2), 354–360.

(14) Wellems, T. E.; Oduola, A. M. J.; Fenton, B.; Desjardins, R.; Panton, L. J.; Rosario, V. E. do. Chromosome Size Variation Occurs in Cloned Plasmodium Falciparum on in Vitro Cultivation. *Rev. bras. genét* **1988**, *11*, 813–825.

(15) Bhasin, V. K.; Trager, W. Gametocyte-Forming and Non-Gametocyte-Forming Clones of Plasmodium Falciparum. *Am. J. Trop. Med. Hyg.* **1984**, *33* (4), 534–537.

(16) Wellems, T. E.; Panton, L. J.; Gluzman, I. Y.; Do Rosario, V. E.; Gwadz, R. W.; Walker-Jonah, A.; Krogstad, D. J. Chloroquine Resistance Not Linked to Mdr-like Genes in a Plasmodium Falciparum Cross. *Nature* **1990**, *345* (6272), 253–255.

(17) Ioerger, T. R.; Feng, Y.; Ganesula, K.; Chen, X.; Dobos, K. M.; Fortune, S.; Jacobs, W. R.; Mizrahi, V.; Parish, T.; Rubin, E.; et al. Variation among Genome Sequences of H37Rv Strains of Mycobacterium Tuberculosis from Multiple Laboratories. *J. Bacteriol.* **2010**, *192*, 3645–3653.

(18) Jorgensen, J.; Turnidge, J. Antibacterial Susceptibility Tests: Dilution and Disk Diffusion Methods. In *Manual of clinical microbiology*; Murray, P., Baron, E., Jorgensen, J., Landry, M., Pfaller, M., Eds.; American society for microbiology: Washington, DC, 2007; pp 1152–1172.

(19) Franzblau, S. G.; Degroote, M. A.; Cho, S. H.; Andries, K.; Nuermberger, E.; Orme, I. M.; Mdluli, K.; Angulo-Barturen, I.; Dick, T.; Dartois, V.; et al. Comprehensive Analysis of Methods Used for the Evaluation of Compounds against Mycobacterium Tuberculosis. *Tuberculosis* **2012**, *92* (6), 453–488.

(20) Tang, Y. J.; Shui, W.; Myers, S.; Feng, X.; Bertozzi, C.; Keasling, J. D. Central Metabolism in Mycobacterium Smegmatis during the Transition from O2-Rich to O2-Poor Conditions as Studied by Isotopomer-Assisted Metabolite Analysis. *Biotechnol. Lett.* **2009**, *31*, 1223–1240.

(21) Ollinger, J.; Bailey, M. A.; Moraski, G. C.; Casey, A.; Florio, S.; Alling, T.; Miller, M. J.; Parish, T. A Dual Read-Out Assay to Evaluate the Potency of Compounds Active against Mycobacterium Tuberculosis. *PLoS One* **2013**, *8* (4), 60531.

(22) Duffy, S.; Avery, V. M. Development and Optimization of a Novel 384-Well Anti-Malarial Imaging Assay Validated for High-Throughput Screening. *Am. J. Trop. Med. Hyg.* **2012**, *86* (1), 84–92.

(23) Lambros, C.; Vanderberg, J. P. Synchronization of Plasmodium Falciparum Erythrocytic Stages in Culture. *J. Parasitol.* **1979**, *65* (3), 418–420.

Chapter 5
Conclusions and future work

5.1 Summary and conclusions

The imino ligands (**L1** and **L3**) and complexes (**C1** – **C6**) had been synthesized before by Chellan et al.[1] A new synthetic method was developed for the synthesis of **L1** which achieved a percentage composition as analysed by ^{1}H NMR of 78%, a great success given the equilibrium nature of imine formation. From this point, recrystallisation no longer posed a problem as had previously been the case and several recrystallisations could be used for further purification. The same method was used for the synthesis of **L3**, however it was found to be lacking and gave product conversion of ca. 30%. Various synthetic methods were investigated until a product conversion of 50% was achieved, before other aspects of the project had to be focussed on. The iridium chlorido dimers were synthesized in generally good yields according to a method from literature[2] and their isolation was a facile process. The crude nature of **L1** did not prevent the isolation of the pure metal complexes **C1** – **C3**, however complexes **C4** – **C6** proved significantly more challenging. This was likely due to the much greater impurity of the crude of **L3** as compared to **L1**.

After the successful synthesis of the imino sulfadoxine iridium complexes, a second library of iridium conjugates was investigated which had not been synthesized before, as determined by a literature search. This library focussed on the incorporation of the amide moiety instead of the imine. The pyridyl and quinolyl amido sulfadoxine ligands, **L4** and **L5**, were successfully synthesized via the *in situ* generation of an acid chloride from the parent carboxylic acid and gave moderate yields of 73% and 60%, respectively. Transparent needle-like crystals were obtained for **L4** which were found to crystallise in the triclinic, $P\bar{1}$ space group. A facile microwave synthetic procedure was discovered in literature[3] for the synthesis of the subsequent complexes, **C7** – **C12**, after the initial synthetic route gave low yields and employed long reaction times. This new method used significantly shorter reaction times and gave moderate to excellent yields, 56% - 84%, for the complexes **C7** – **C12**. The successful generation of the amido iridium complexes were characterised by the disappearance of the amide NH in both FTIR and ^{1}H NMR spectra. Furthermore, the phenylene carbons overlapped with an additional CH carbon signal, as there was consistently one signal less in the ^{13}C NMR spectra of both the ligands and complexes than would be expected after symmetry has been taken into account. The MS spectra generally gave the $[M\text{-}Cl]^{+}$ ion as the base peak, though the $[M+H]^{+}$ ion was observed as base peak under softer ionisation conditions. Unfortunately, crystal structures were unable to be obtained of the complexes as the crystals were consistently too small for analysis. Confirming whether the coordination took place between the nitrogen of the amide and of the pyridyl or quinolyl moiety thus required investigation with Far-IR spectroscopy. **C10** was investigated as a

representative with caesium iodide pellets and iridium-nitrogen absorption bands were successfully identified at 488 cm^{-1} and 452 cm^{-1} for the amide and quinolyl nitrogens, respectively. It was thus concluded that all the complexes coordinated in *N, N* fashion as was determined for **C10**.

Following the synthesis of the two small libraries of complexes, **C1** – **C12**, some of their physico-chemical properties were determined. Turbidimetric assays were run in triplicate to determine the range of solubility of the compounds. The results determined that as the Cp^x moiety was extended a general decrease in solubility was observed. There were also decreases in solubility going from a pyridyl to a quinolyl system and from an imine to an amide. Following this the nature of the active species was probed by investigating the substitution of the chlorido on the metal centre with an aqua group. To do this, the in situ generated analogues of **C1** – **C12** were compared to their parent complexes which had been incubated under similar conditions. This was to determine if the substitution of the chlorido was a facile process or not. It was found that as the bulk of the half-sandwich moiety was increased it was increasingly difficult to remove the chlorido, especially seen for **C3** and **C9**, in which it could not be removed under the conditions used. This data suggests that the actual active species is likely the chlorido complex. The complexes were sent for biological testing against *Mtb* strain H37Rv and *P. falciparum* strains 3D7, Dd2 and HB3. The imino series of complexes generally exhibited better activity than their amido analogues, especially in the case of *Mtb*, while simultaneously being less toxic. It is unclear whether this increased activity and lower toxicity is due to the imino functionality itself or if the cationic nature of the metal centre also contributes and should be investigated further. The complex found to be most active against *Mtb* was **C6**, which after 7 days displayed an MIC_{90} of 2.78 µM. Regarding the IC_{50}'s that were determined against *P. falciparum* strains, **C12** was found to be the most active with an IC_{50} of 0.975 µM. The biological data showed that as the solubility decreased there was a general increase in the activity against the strains tested. Furthermore, the intact chlorido species is more likely to reach the target site if protected by a bulky group such as the biphenyl half-sandwich moiety, which could explain the increased activity of these analogues.

These results have aided in further investigating the properties of an existing set of biologically active complexes and identifying a new set of biologically active complexes and several of their relevant drug-like properties, from which more detailed lead compounds can be identified.

5.2 Future work

There are a variety of investigations that can still be done on the current system. One of these would be to continue exploring the conditions for the formation of the aqua analogues of the complexes. This could be done with UV spectroscopy which gives more sensitive measurements than could be achieved with an NMR spectrometer. Additionally, the NMR aquation experiments detailed in chapter 4 could be repeated with immediate detection of the species in solution. LC-MS could be employed to provide a much greater breadth of knowledge on the species present.

The aqua analogues of **C1** – **C12** can also be isolated and themselves tested for biological activity to determine any difference in activity that might occur between these species. This could also confirm the previous hypothesis of the active species being the chlorido complexes. The lipophilicity of these compounds should be investigated to find whether the data follows the same trends that were determined for the solubility as this could give insight into part of the mechanism by which these drug candidates reach the target cells. This can be done via octanol water studies to determine the Log P, by determining Log D which accounts for the ionized and non-ionized forms, or through *in silico* methods.[4] All complexes were isolated as chiral mixtures and tested without further separation. Given that there can be activity difference between enantiomers, the enantiomers of the iridium complexes should be investigated to identify whether they are separable and if there is a difference in activity or cytotoxicity between them.

A decrease larger than four-fold in activity was seen for the complexes during testing against *Mtb* when a medium containing serum albumin was used. It is thus important that incubation tests be done with the compounds to ascertain whether they undergo serum-albumin binding as this could lead to their inefficacy in a biological system if this was the case. A variety of other biological assays could also be investigated to further determine the drug-like character (ADMET) of these complexes if they warranted further investigation.

To identify a specific lead compound for potential clinical evaluation, a series of further analogues should be synthesized focussing on the Cp^{xbiPh} half sandwich moiety, as these complexes have proved the most active. This series can involve the investigation of both *C, N* coordination systems as well as *N, O* coordination by varying the aldehyde or acid used to derivatise sulfadoxine. Additionally, several different sulfonamides (Figure 5.1), such as sulfadiazine, sulfasalazine and sulfamethoxazole, which have all found clinical application,[5] can be employed to investigate the difference in efficacy between derivatised species.

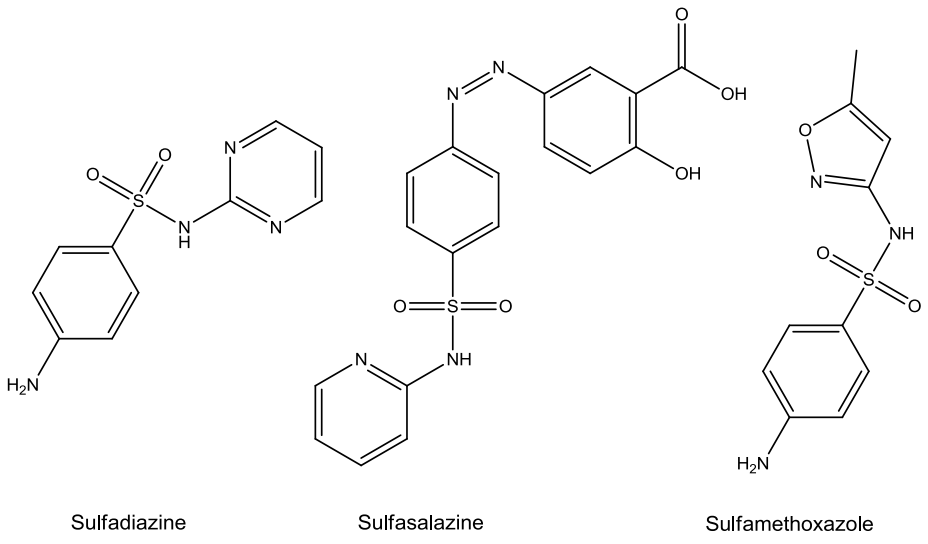

Figure 5.1 - The clinically used sulfonamides, sulfadiazine, sulfasalazine and sulfamethoxazole.

A variety of different metal centres with varying oxidation potentials and coordination numbers could also be incorporated, as it has already been shown that the type of metal used influences the activity.[1] One other approach would be to identify clinical drugs that have synergistic effects, such as sulfamethoxazole and trimethoprim[6] and synthesize their respective complexes to investigate whether this synergism is still present and if their efficacy is greatly improved. Finally, **C1** – **C12** and the various analogues mentioned should be tested against a variety of other diseases to determine potential selectivity or pronounced activity against them. Particularly testing against cancer cell lines could prove successful as many similar half-sandwich complexes have shown good activity against cancers.[7]

5.3 References

(1) Chellan, P.; Avery, V. M.; Duffy, S.; Triccas, J. A.; Nagalingam, G.; Tam, C.; Cheng, L. W.; Liu, J.; Land, K. M.; Clarkson, G. J.; et al. Organometallic Conjugates of the Drug Sulfadoxine for Combatting Antimicrobial Resistance. *Chem. - A Eur. J.* **2018**, *24* (40), 10078–10090.

(2) Tönnemann, J.; Risse, J.; Grote, Z.; Scopelliti, R.; Severin, K. Efficient and Rapid Synthesis of Chlorido-Bridged Half-Sandwich Complexes of Ruthenium, Rhodium, and Iridium by Microwave Heating. *Eur. J. Inorg. Chem.* **2013**, *2013* (26), 4558–4562.

(3) Almodares, Z.; Lucas, S. J.; Crossley, B. D.; Basri, A. M.; Pask, C. M.; Hebden, A. J.; Phillips, R. M.; Mcgowan, P. C. Rhodium, Iridium, and Ruthenium Half-Sandwich Picolinamide Complexes as Anticancer Agents. *Inorg. Chem.* **2014**, *53* (2), 727–736.

(4) Chung, T. D. Y.; Terry, D. B.; Smith, L. H. *In Vitro and In Vivo Assessment of ADME and PK Properties During Lead Selection and Lead Optimization – Guidelines, Benchmarks and Rules of Thumb*; Eli Lilly & Company and the National Center for Advancing Translational Sciences: Bethesda (MD), 2004.

(5) World Health Organization. *WHO Model Formulary 2008*; Couper, M. R., Mehta, D. K., Eds.; World Health Organization, 2008.

(6) Forgacs, P.; Wengenack, N. L.; Hall, L.; Zimmerman, S. K.; Silverman, M. L.; Roberts, G. D. Tuberculosis and Trimethoprim-Sulfamethoxazole. *Antimicrob. Agents Chemother.* **2009**, *53* (11), 4789–4793.

(7) Bruijnincx, P. C.; Sadler, P. J. New Trends for Metal Complexes with Anticancer Activity. *Curr. Opin. Chem. Biol.* **2008**, *12* (2), 197–206.